HEAT AND MASS TRANSFER STUDIES

I. Transfer of Heat and Momentum in Uniform Turbulent Air Streams

II. Evaporation of Water Drops in a Turbulent Air Stream

Thesis by

Stuart Donald Cavers

In Partial Fulfillment of the Requirements

for the degree of

Doctor of Philosophy

California Institute of Technology

Pasadena, California

1951

Table of Contents

Acknowledgment

Abstract

Part I. Transfer of Heat and Momentum in Uniform Turbulent Air Streams

Introduction....1

Equipment....5

Experimental Methods....13

Experimental Results....23

Analysis of Results

Pressure Gradients....29

Velocity Correlations....31

Calorimetric Data....35

Variation of the Eddy Quantities with Position....39

Variation of the Ratio of Total Conductivity to Total Viscosity....50

The Effect of Natural Convection on the Thermal Flux and on the Eddy Properties....52

Conclusion....54

Nomenclature....56

References....59

Figures....62

Tables....115

Part II. Evaporation of Water Drops in a Turbulent Air Stream

Introduction.....141

Apparatus.....142

Experimental Methods.....145

Experimental Results

Primary Data.....151

Derived Data.....153

Analysis of Results.....164

Conclusion.....168

Nomenclature.....170

References.....172

Figures.....174

Tables.....186

Propositions.....208

Acknowledgment

The research reported in this thesis was done under the direction of Professor B. H. Sage. His guidance and many helpful suggestions are deeply appreciated. The author is indebted to his co-worker, Franklin Page, Jr., for a considerable portion of the design of the calorimeters described in the first portion of the thesis, and to D. M. Mason for checking the magnitude of the eddy diffusivities reported in the second portion. The assistance of Darlton K. Breaux and H. Hollis Reamer with design work and experimental measurements, and the assistance of Virgil J. Berry, Bert H. Golding, John L. Mason, and Frederick D. Parker with experimental measurements is also gratefully acknowledged.

Thanks are also due to Katharine Schlinger who typed the manuscript, and to Ann Jarvis who prepared many of the figures.

The work described in the second portion of this thesis was made possible by a grant of funds by the Essick Manufacturing Company.

Abstract

Part I

Measurements have been made of temperature, velocity, and pressure as functions of position in an air stream flowing in a uniform, two-dimensional manner between horizontal parallel plates maintained at different temperatures. Reynolds numbers ranged from 8,000 to 55,000. Calorimeters have been designed to measure the thermal flux entering or leaving the stream at the upper plate. The data obtained have permitted the calculation of eddy viscosity and eddy conductivity, and total viscosity and total conductivity as functions of position. Correlations of the data have been devised to permit the prediction of the total quantities in other situations of engineering interest.

The thermal flux determined from calorimetric data is compared with that obtained from the slope of the temperature profile in the laminar layer. The effect of gross velocity and the resulting point velocities on the thermal flux is considered, and the results are compared with those obtainable from macroscopic considerations.

The effect of natural convection on the eddy quantities has been determined for one Reynolds number.

Part II

Water drops were dispersed by means of a nozzle in a turbulent air stream flowing in a tube. Apparent temperatures, velocities, compositions, and drop size distributions were obtained as a function of position in the stream. Apparent eddy conductivities and eddy diffusivities were calculated. It appears that the eddy diffusivity is approximately double the eddy conductivity for this case of nonuniform flow.

Part I

Transfer of Heat and Momentum in Uniform Turbulent Air Streams

Introduction

The research to be described is part of a comprehensive experimental program now in progress in the Chemical Engineering Laboratory of the California Institute of Technology. This program involves the study of the transfer of momentum, thermal energy, and material from the microscopic point of view, and has as its objective the gathering of data to facilitate the prediction of velocity, temperature, and concentration at any location of interest in engineering equipment. The point concept is being emphasized in this study since the microscopic viewpoint has been inadequately investigated as compared with its macroscopic counterpart and knowledge of point conditions in industrial equipment is of increasing interest to designers. It is evident that the development and testing of analogies between the various types of transfer should perceptibly shorten the task at hand since data obtained for one type of transfer could then be applied to the others without further experimental work. In the present paper the author has concerned himself with the analogy between the transfer of heat and the transfer of momentum first suggested by O. Reynolds (1) and extended through the efforts of G. I. Taylor (2), L. Prandtl (3), Th. von Kármán (4), L. M. K. Boelter (5), and R. C. Martinelli (6).

The analogy between the transfer of momentum and the transfer of heat may be developed in the following elementary manner. Consider the case of uniform, two-dimensional flow between parallel horizontal

plates. Transfer of momentum in the flowing stream is brought about by the action of the shear force which may be related to the velocity gradient by the following equation:

$$\tau = \rho (\nu + \epsilon_m) \, du/dy \qquad (1)$$

Equation 1 replaces, for the case of turbulent flow, the relation

$$\tau = \rho \nu \, du/dy \qquad (2)$$

which applies to laminar flow and is often used to define viscosity. In Equation 1 the eddy viscosity, ϵ_m, arises from the effective increase in viscosity resulting from the presence of eddies in the flowing stream. Suppose that because of an eddy w pounds of fluid per square foot pass in time $d\theta$ from an elevation y to an elevation y + dy in the fluid stream. Because of the existence of a velocity gradient the fluid undergoing the change of elevation will also undergo an acceleration or deceleration corresponding to a transfer of momentum. If the change of elevation of the fluid corresponds to a change of time average velocity of du, then by Newton's second law of motion,

$$\tau = w/g \, du/d\theta \qquad (3)$$

Combining Equations 1 and 3 and noting that

$$\rho = \sigma/g \qquad (4)$$

we obtain:

$$w/g \, du/d\theta = \sigma/g \, (\nu + \epsilon_m) \, du/dy \qquad (5)$$

---

* A nomenclature listing the various symbols employed will be found on pages 59 and 60.

or

$$w \frac{dy}{d\theta} = \sigma(\nu + \epsilon_m) \tag{5}$$

Now if it is assumed that a temperature gradient exists in the stream, and if it is recalled that w pounds of fluid were transferred in time $d\theta$ between the levels dy apart, the rate of thermal transfer is given by the equation:

$$\dot{Q} = w c_p \, dt/d\theta \tag{7}$$

where dt is the difference in temperature between the two levels. But from Equation 6

$$w = \sigma(\nu + \epsilon_m) \, d\theta/dy \tag{8}$$

Substitution in Equation 7 produces:

$$\dot{Q} = c_p \sigma (\nu + \epsilon_m) \, dt/dy \tag{9}$$

Now the Fourier equation for the transfer of heat may be written for the turbulent case (4) as

$$\dot{q} = c_p \sigma (K + \epsilon_c) \, dt/dy \tag{10}$$

where the eddy conductivity ϵ_c takes into account the thermal transfers resulting from turbulence. The $\dot{q}$ from Equation 10 may now be equated to that given by Equation 9 based on the mechanism assumed for the transfer of momentum. The result is

$$\nu + \epsilon_m = K + \epsilon_c \tag{11}$$

or

$$w \frac{dy}{d\theta} = \sigma(\nu + \epsilon_m) \tag{6}$$

Now if it is assumed that a temperature gradient exists in the stream, and if it is recalled that w pounds of fluid were transferred in time $d\theta$ between the levels dy apart, the rate of thermal transfer is given by the equation,

$$\dot{Q} = w C_p \frac{dt}{d\theta} \tag{7}$$

where dt is the difference in temperature between the two levels. But from Equation 6

$$w = \sigma(\nu + \epsilon_m) \frac{d\theta}{dy} \tag{8}$$

Substitution in Equation 7 produces:

$$\dot{Q} = C_p \sigma(\nu + \epsilon_m) \frac{dt}{dy} \tag{9}$$

Now the Fourier equation for the transfer of heat may be written for the turbulent case (4) as

$$\dot{Q} = C_p \sigma(K + \epsilon_c) \frac{dt}{dy} \tag{10}$$

where the eddy conductivity ϵ_c takes into account the thermal transfers resulting from turbulence. The $\dot{Q}$ from Equation 10 may now be equated to that given by Equation 9 based on the mechanism assumed for the transfer of momentum. The result is

$$\nu + \epsilon_m = K + \epsilon_c \tag{11}$$

If transfer of momentum is strictly analogous to transfer of heat, Equation 11 must hold. If for the moment the equality of ϵ_m and ϵ_c is assumed, it is evident that the analogy holds if

$$\nu = K \tag{12}$$

or the Prandtl number, $\frac{\nu}{K}$, equals 1. Equation 12 is approximately true for gases, for which an approximate average Prandtl number is 0.7. In the case of liquids, however, ν is much larger than K. It is found also (7) that ϵ_m does not equal ϵ_c but that these two parameters bear a relationship to one another which is a function of position.

In this investigation the primary emphasis has been on the phenomena of the boundary and buffer zones, and the outer portion of the turbulent core. For theoretical reasons which will become apparent as the discussion progresses, the attention of the writer has been focused on the mode of variation of the sum of the eddy and molecular quantities rather than on that of the eddy quantities alone. This method of treating the problem is convenient also because near the wall both are important in their respective transfer processes. Equations 1 and 10 may be solved for the total quantities and written as follows:

$$\epsilon_m + \nu = \frac{\frac{\tau}{\rho}}{\frac{du}{dy}} \tag{13}$$

$$\epsilon_c + K = \frac{\frac{\dot{Q}}{c_p \sigma}}{\frac{dt}{dy}} \tag{14}$$

The variables on the right-hand sides of these equations have been measured in this research to permit the calculation of the total viscosity and total conductivity, and, by subtracting the molecular properties from these, the eddy viscosity and the eddy conductivity. Correlations have been devised for predicting the total quantities in circular pipes as well as between parallel plates. These correlations apply to fluids and at velocities other than those for which measurements have been made. The thermal flux has been determined calorimetrically and in some cases also by measuring the limiting slope of the temperature profile at the wall. Velocity distributions near the boundary have been determined and have been compared with the results of previous workers. Secondary emphasis in the investigation has been placed on determining the effect of natural convection on the eddy quantities for which data have been obtained at one Reynolds number. All measurements have been made in a two-dimensional channel. The flow was essentially uniform. In the natural convection work the lower boundary was kept hotter than the upper one, this situation being the reverse of that obtaining in the bulk of the measurements.

Equipment

With the exception of the calorimeters the apparatus used for the investigation has been described very completely by S. W. Billman (8) and W. F. Corcoran (9). For this reason the equipment as a whole will be considered in broad outline only. The calorimeters, on the other hand, will be described in some detail.

Figure 1 is a view of the equipment as a whole. The essential parts of the apparatus are shown in plan and elevation in Figure 2. It consists of a closed-circuit wind tunnel formed by two copper plates (A and B in Figure 1), 15 feet 6 inches long and 12 3/8 inches wide, oriented in horizontal planes with 0.7 inch between their inner polished surfaces. A blower C with speedtrol unit promotes the passage of air between the plates at cross velocities ranging from 2 to 180 feet per second. The flow is two-dimensional down the midlines of the plates. Heaters D and refrigeration coils are provided in the air circuit so that the temperature of the air may be controlled over a wide range. The temperature of each copper plate is maintained at a predetermined value by means of an oil bath provided with heaters, refrigerating coils, and a circulating pump. The oil baths and plates are shown in cross section in Figure 3 in which A and B are the oil baths whereas F and I are the copper plates. Thermocouples are imbedded in the latter so that the temperature of their air-side surfaces may be determined. Fine control of oil bath and air temperatures is obtained by the use of thyratron-controlled heaters immersed directly in the fluid being heated so as to be almost without lag.

A combination hot wire anemometer (10) and platinum resistance thermometer (11) is mounted on piano wires supported by a traversing mechanism in such a manner that point values of velocity and temperature may be measured in the air stream between the plates.

A pitot tube and static pressure tap are mounted on the piano wires in parallel with the hot wire anemometer to permit calibration of the latter device. The type of micromanometer used with the pitot tube is shown in Figure 4. The combination hot wire anemometer and platinum resistance thermometer will be designated for the sake of brevity by the term thermanemometer (7). This instrument and the pitot tube are shown in a perspective sketch inset in Figure 6, which shows also a cross section view of the oil baths, plates, and traversing mechanism. The cathetometer J mounted on the traversing gear is used to determine the vertical position of the thermanemometer in the channel. At the beginning of a set of measurements the thermanemometer is moved to a point 0.002 to 0.003 inch from the upper plate and is then located exactly by a measurement of the distance between the wire and its image in the polished copper surface. The thermanemometer may be moved to a new location in the channel by means of the traversing mechanism. The new location is determined in relation to the first location near a plate by means of the cathetometer and a dial gauge with interlocked motions.

The working section of the equipment and one of the venturi meters used for measuring the weight rate of flow are shown in Figure 6. The side walls of the channel are closed by sliding blocks provided with felt contact pads as shown in Figure 7.

Pressure measurements in the channel are obtained by reading kerosene levels in several glass manometers connected respectively to piezometer bars in the upper copper plate, and to static taps in

the side walls of the working section. The manometer bank and the cathetometer used for these readings are shown in Figure 8.

Thermocouple, resistance thermometer, and hot wire readings are obtained at the structure shown in Figure 9. This "temperature bench" is equipped with two Mueller bridges, a type K potentiometer, a White double potentiometer, and the electronic equipment used in control of the oil bath and air temperatures.

Two calorimeters are used to measure the rate of heat transfer between the upper copper plate and the air stream. These instruments are placed in openings cut in the upper oil bath and the copper plate which forms its lower boundary. The center of the upstream calorimeter is 100.1 inches from the channel entrance. The centers of the calorimeters are 52.6 inches apart. Reasonable agreement is obtained between the thermal flux measurements made with the two instruments under the conditions studied so that uniform flow seems to have been established at a point upstream from the first calorimeter.

Figure 10 shows a cross section of one of the calorimeters and its relation to the adjacent parts of the heat transfer apparatus. A copper block E is supported in the opening in the copper plate B so that an air gap of only 0.002 inch exists between the edge of the block and the edge of the hole in the plate. The above measurement applies at the channel side of the block and plate which therefore present an almost unbroken surface to the air flow. An outer jacket C is attached by machine screws D to the upper plate, and serves with the oil seals at M and N to prevent leakage from the upper oil bath.

The seals at M and N are arranged to permit lateral and longitudinal motion of the calorimeter in the oil bath opening as the apparatus is heated or cooled. The stainless steel inner jacket H of the calorimeter and the copper block E to which it is attached at its lower end, are supported by the copper plate B. Air is kept from passing into the channel by way of the space between the inner and outer jackets by means of an O-ring between jackets C and H. A pancake heater F of manganin wire is wound on the upper surface of the copper block. This heater is of the four-lead type. A copper pad G containing cooling coils is situated above the heater. The associated equipment for providing cooled liquid to these coils has been designed and built, but has not, as yet, been assembled and put into operation.

In principle the operation of either calorimeter consists of measuring the energy passing through the calorimeter block and into the air stream when the block and the nearby copper plate are at the same temperature. A multi-junction, copper-constantan thermocouple L is used in adjusting the plate-block temperature difference to zero. Four junctions of this thermocouple are located in wells around the circumference of the calorimeter block, and four are located in similar wells in the copper plate. The electrical input to the heater is varied until an equilibrium temperature difference of 0.005°F or less is maintained between the block and the plate. The electrical energy input to the heater is then measured and the thermal

flux determined. It is evident that losses of heat from the block to the room and to the oil baths must be kept to a minimum. The parts of the apparatus which function to achieve this objective will now be described.

The region of contact between the copper plate and the block-jacket assembly is shown in Figure 11. The jacket is joined to the block by means of the stainless steel ring A. The latter rests on a stainless steel supporting washer B* which fits into a recess in the copper plate C. Circular grooves are cut in ring A, and radial grooves in the supporting washer B, to decrease the contact area between the block-jacket assembly and the supporting washer. Holes drilled in the supporting washer further decrease this area which is approximately 5% of the nominal area of the parts and represents a minimum beyond which there would be danger of local yielding of the metal. Plastics and other insulators were ruled out for use in the rings and washers because of their low yield points. The calorimeters are supported by springs hung from an I-beam located vertically above the apparatus. These springs decrease the load on the grooved contact surfaces and therefore not only decrease heat loss from the block to the plate, but also lessen deflection of the plate at the calorimeter openings.

The product hA, of the heat transfer coefficient and the area of contact, has been measured for the path from the block to the plate and was found to be 0.000284 B.T.U./°F sec. for the upstream calorimeter and 0.000178 B.T.U./°F sec. for the downstream

* The stainless steel washer is shown in Figure 19 also.

calorimeter. The difference in these figures was probably a result of slightly different tensions in the springs supporting the calorimeters. If a temperature difference of 0.01°F is assumed between the plate and the block, the rate of heat transfer would be of the order of 0.000002 B.T.U./sec. This loss would in fact amount to less than 0.1% of the energy input to the calorimeters under almost all conditions of operation.

To prevent losses of heat from the block to the room by conduction through the jacket walls H in Figure 10, auxiliary cooling coils and heaters K are provided on the horizontal surface resulting from the decrease in diameter of the jacket between H and Q. Figure 12 shows these parts before assembly. The part at the far left with the auxiliary heater grooves at its base corresponds to jacket Q of Figure 10. It fits into the top of the next part to the right in the photograph which corresponds to jacket H of Figure 10. The jacket cooling coils also are shown in Figure 12. Another eight-junction differential thermocouple is employed to indicate whether or not the desired zero temperature gradient along the jacket wall is being maintained when the calorimeter is in operation. Adjustments to the heater or to the rate of flow of coolant are made from time to time to insure such a zero gradient. Radiation shields J in Figure 10 are so situated as to decrease greatly possible losses from the block by radiation. The radiation shields which are gold plated are shown before assembly in Figure 13. Oil from the upper oil bath is circulated through an oil jacket, fitted around jacket Q of

Figure 10. In this way there is provided for the upper part of the calorimeter walls a constant thermal environment of approximately the same temperature as the calorimeter block. The oil jacket is shown before assembly at the right of Figure 12. Its relation to the calorimeter jackets after assembly is shown in Figure 14 and in Figure 10 at P.

In order to decrease further the heat transfer from the block other than to the air stream, an absolute pressure of less than one micron of mercury is maintained within the walls of the calorimeter jackets, (H and Q of Figure 10), by means of the usual laboratory vacuum pump and an oil diffusion pump. The latter is connected into the system through a sylphon bellows, the function of which is to provide a flexible connection between the calorimeter and the diffusion pump. The assembled calorimeter is shown installed in the upper plate in Figure 15. The oil diffusion pump is at the right of the calorimeter. The block heater leads and the thermocouple leads pass upward through the vacuum jacket and leave the equipment through a conventional wax seal.

The equipment for supplying the cold fluid to the coils of the cooling pad of the calorimeter block is shown in Figures 16 through 21. It is intended that this equipment will be connected to the calorimeter by means of the sylphon bellows opposite to the one used with the oil diffusion pump (Figure 15). In principle the cooling system consists of a gear pump drawing oil from the upper oil bath and passing it to a constant head device from which it flows

by gravity to a small freon cooler located in the calorimeter vacuum system. The temperature of the oil is lowered below that of the calorimeter block and the oil then passes to the block cooling pad. However, of the oil supplied to the constant head device by the pump, only a small fraction follows the route just described. The remainder overflows at the constant head device and is returned to the upper oil bath. The small oil lines to the calorimeters are jacketed by means of the oil lines from the pump to the constant head device and the comparatively large flow of oil in these insures that the temperature of the oil passing to the calorimeters will not be greatly affected by changes in room temperature.

Figure 16 shows a front and a side elevation of the cooling system. Oil from the gear pump is passed through the oil filter at A, a Cuno Micro-Klean filter which removes all particles larger than 10 microns. The stream is then divided into two parts and used to jacket the gravity flows from the constant head device B to the coolers C. Overflow from the constant head device is returned to the upper oil bath through line D. The copper tubes carrying the oil from the pump to the constant head device and from the latter to the coolers are to be soft-soldered together in a bundle during assembly and protected in part from variations in temperature and air circulation in the room by the inverted T shape system of laboratory gutter shown in Figure 16 at E.

The constant head device is shown in Figure 17. The filtered oil from the pump enters through the 3/16-inch lines at A. The two

streams impinge on one another in the space B and the velocity of the oil in the vertical direction is reduced. The oil then passes upward through the inlet port C and is deflected in a horizontal direction through the openings D into the annular space E. The oil being fed to the calorimeter cooling system then passes downward through the 100-mesh brass screen F and into the outlet ports G. The oil exit is raised above the bottom of space E and is horizontal in order to lessen the chance of foreign particles being carried into the calorimeters, should any of these escape the filter and screen. In the constant head device the excess oil from the pump flows over the weir H and into the outer annular space J whence it is returned by gravity in a 1/2-inch line to a tank connected directly to the upper oil bath. The rings K support the screen which is soft-soldered between them. The screen assembly makes a slip fit with the walls of space E and may be removed by hooks L when cleaning becomes necessary.

The freon cooler is shown in Figure 18. The oil from the constant head device enters it at A. The oil then passes through the heat exchanger B where it is cooled by freon from the laboratory refrigeration system. The oil next passes through a section of tubing C, wound with an 18 ohm, 60 watt nichrome heating element, where it is brought to the proper temperature for removing heat from the calorimeter block. A thermocouple D is provided between the cooler and the heater for control purposes. The space E around the oil lines and freon cooler is evacuated since it is directly connected to the calorimeter vacuum jacket through the sylphon bellows. For

this reason, when the oil has been brought to the proper temperature, it cannot perceptibly lose or gain heat from the room. The oil passes from the heated section of tube C into the calorimeter. A wax seal F is provided for the thermocouple and heater leads. The liquid freon is treated in a silica gel drier and is filtered in standard refrigerant filters by felt held in place by bronze screens. The freon enters the cooling device at G. The rate of flow of freon is controlled by the valve H. The evaporating freon passes around the oil tube in the baffled heat exchanger J and leaves the apparatus at K.

The cooled oil flows from the freon cooler into the calorimeter vacuum jacket through a small copper tube which is coupled to a similar stainless steel tube within the calorimeter. The stainless steel tube conveys the oil to the block cooling pad. A similar tube takes away the warmed oil. Portions of the stainless steel lines entering and leaving the cooling pad are shown in Figures 19 and 20, which also show the lower part of the calorimeter vacuum jacket. In the preassembly photograph (Figure 19) the top of the calorimeter block can be glimpsed within the jacket. In Figure 20 the cooling pad has been placed in its operating location on top of the block. Thermocouples are located in wells provided in the lines entering and leaving the cooling pad so that the change in temperature of the oil may be measured. The locations of the wells are considered to be optimum with respect to possible errors which could be caused by heat flowing from the block up the stainless steel tubes. The thermocouple wells can be seen in Figures 19 and 20 and are shown in more

detail in Figure 21. The wells, and the tubes above and below them, are protected by radiation shields shown before assembly in Figure 22. These radiation shields are gold plated. In Figure 10 the thermocouple wells are located at S and the radiation shields at T.

The oil from the calorimeter cooling coil leaves the equipment through tube LL of Figure 10 and is then weighed. The rate of removal of heat from the calorimeter block is obtained from the weight rate of oil flow, the specific heat of the oil, and the readings of the thermocouples in the wells described above.

Experimental Methods

Maintenance of constant temperatures of the copper plates and of the entering air stream was, of course, fundamental to the making of uniform flow measurements. Thyratron circuits were used in both the air and oil temperature control. These circuits were actuated by copper resistance thermometers. However, each fluid had immersed in it, in addition to the copper thermometer, a standard, four-lead platinum resistance thermometer which could be used to determine the temperature of the fluid. Temperature readings were made with the assistance of Mueller bridges to within 0.01°F relative to the international platinum scale. The temperatures of the oil baths were controlled to within 0.02°F and the temperature of the air to within 0.10°F of specified values.

In all the measurements, each plate was set to the proper temperature by adjustment of the oil bath temperature until the

plate thermocouples gave the desired reading. The oil bath then controlled the plate temperature at this value to within approximately 0.02°F. However since the thermocouples were read only to the nearest 0.03°F, the control of the plate temperatures was actually to within approximately 0.05°F of the specified value. Some difficulty was experienced in the first uniform flow measurements in that slight temperature gradients were found to exist along the copper plates. Although resulting variations in the uniformity of the air flow were believed to be negligible, advantage was taken of an opportunity to lower the viscosity of the oil in the baths with kerosene. The temperature gradients were markedly reduced by the change.

The weight rate of flow was determined by measurements of the pressure difference between the throat of a venturi meter and a point immediately upstream from the meter. The piezometer rings at these points were connected to a kerosene-in-glass manometer. The heights of the kerosene columns were read to within 0.1 millimeter with the cathetometer shown in Figure 8. Readings of these manometers and adjustment of the blower speed by means of the speedtrol unit permitted the maintenance of a weight rate of flow constant within 0.2%.

Point temperature values were measured with the same short length of 0.0005-inch diameter platinum wire which formed the sensing element of the hot wire anemometer. Both velocity and temperature readings could therefore be made at exactly the same location in the channel. Platinum was chosen as the best material available for the

wire because of its excellent resistance characteristics in the thermometer application. The thermanemometer circuit is shown in Figure 23. With the six-pole switch in the upward position, the four leads of the platinum wire were connected into one of the Mueller bridges. Platinum leads were carried from the ends of the wire to a point on the traversing gear, where they were connected to copper leads in a junction box. Thermocouple effects were therefore negligible. The thermanemometer was calibrated as a temperature measuring device by setting it in a horizontal position in the channel and placing beside it the laboratory standard platinum resistance thermometer. With stagnant air between the plates the oil baths were set to identical temperatures. After sufficient time had elapsed for equilibrium to be reached, the two thermometers were read. Repetition of the procedure at various temperatures gave the resistance of the small platinum wire as a linear function of temperature. Calibrations were repeated at frequent intervals since some drift in the calibration with time was noted. It was found that in regions of low temperature gradient the uncertainty of temperature measurement was approximately $\pm 0.02^{\circ}F$, whereas in regions of high temperature gradient it was approximately $\pm 0.1^{\circ}F$. The difficulty here was to a large extent one of positioning the wire. In midstream, temperatures were correct to approximately $0.1^{\circ}F$ relative to the international platinum scale.

Measurements of the position of the wire were probably accurate to ± 0.001 inch, and in regions of high temperature gradient an error

of 0.001 inch in the position of the wire would result in a temperature error of the order of magnitude of 0.1°F. Furthermore, readings were made more difficult near the walls by much larger fluctuations in temperature than those which were experienced in midchannel. The position of the wire was determined by sighting on one of its supports. It is possible that at times the wire may have been moving slightly in the air stream although the support appeared to be steady. The resultant fluctuations in the temperature of the wire were, of course, comparatively large in the large temperature gradients near the wall.

With the six-pole switch of Figure 23 in the downward position the thermanemometer became a velocity measuring device. The platinum wire then formed one leg of a Wheatstone bridge. A gross velocity of 30 ft./sec. was established in the channel with the oil baths and air at 100°F. The resistance of the platinum wire corresponding to 250°F was determined from the temperature calibration line. The wire was brought to this resistance by adjusting the current from the battery by means of variable resistance R2 of Figure 23. The Wheatstone bridge was then balanced by means of variable resistance R1. In making velocity measurements the constant resistance method was used, R1 being left set and the current being varied in the hot wire by means of R2 until the bridge was balanced. The equation of King (12) in one of the forms given by Willis (10) was used for the velocity determinations. In terms of the nomenclature of this paper it is:

$$\frac{i^2 R_{h.w.}}{R_{h.w.} - R_a} = a + b\sqrt{u} \qquad (15)$$

Quantities a and b were found to vary with time, probably as a result of the accumulation of dust on the hot wire. The shift in the calibration curve was in a direction corresponding to a decrease in the heat transfer coefficient so that the above explanation for the phenomenon is a plausible one. In further support of the above conclusion it was found that heating the wire to a high temperature restored a and b approximately to their original values. After the heating process the wire was observed under a microscope and a few particles of charred matter were noted dangling from the wire. Quantities a and b were plotted as functions of the time during which the blower had been in operation since a burn-off, and all values of velocity were calculated by using the proper a and b values for the time at which the velocity determination was made.

Some difficulty was experienced with measurements very close to the wall in the work at low velocity. The heat loss from the wire was found to be abnormally large for the estimated velocity obtaining at such locations. Probably the effect was caused by conduction from the wire to the wall becoming appreciable as compared with heat losses from the wire to the air. Little information is available regarding the corrections to be applied and Dryden (13) recommends that no correction be made if the speed is greater than 3 ft./sec. The writer found, however, that his velocities seemed to be correct when greater in magnitude than about 2 ft./sec. Velocities above this magnitude in the laminar layer were consistent with the values calculated from the equation:

$$\tau/\rho = \nu \, du/dy \qquad (13)$$

by the graphical integration which may be expressed as follows:

$$(u)_{y/y_o} = y_o \int_1^{y/y_o} \frac{\tau}{\eta} d(y/y_o) \qquad (17)$$

where

$$\eta = \nu\rho \qquad (18)$$

It is estimated that the uncertainty of velocity measurement in the turbulent core of the stream was approximately ±0.05 ft./sec. As with temperature measurement, the uncertainty increased in regions of higher velocity gradient, and near the wall the uncertainty was about ±0.25 ft./sec. except in regions where the velocity was less than 2 ft./sec as noted above. The absolute accuracy of the velocity measurements increased with velocity, since larger pitot readings were involved in the calibration. An average value of the deviation from the true velocity would be of the order of ±0.5 ft./sec.

It should be emphasized that the "velocity" which has been considered above is really the time average velocity at the point under consideration in the turbulent stream. The hot wire as it was used in this research measured the time average square root of the velocity. In the present work the intensity of turbulence was found to be 3%. The difference between the time average velocity, and the square of the time average square root velocity, was obviously negligible.

Measurements of pressure difference by means of the kerosene-in-glass manometers and the cathetometer of Figure 8 were certain to within approximately 0.2 millimeter of kerosene. The deviation of these measurements from the true value was of approximately the same magnitude.

Thermal flux measurements were made by maintaining an equilibrium temperature difference between the calorimeter plate and block of 0.005°F or less by use of the block heater. The electrical energy input rate was then measured. The current was determined potentiometrically by a measurement of the voltage drop across a manganin resistor calibrated against a standard resistor. The voltage across the heater was determined with the aid of a potentiometer and a voltage divider. The calibrations of the manganin resistor and of the voltage divider were accurate to better than 0.1%.

The calorimeters were calibrated, with no air flowing, for losses to the room. The oil baths were brought to the temperature to be assumed by the upper plate in the uniform flow thermal flux tests, and the plate-block differential temperature was adjusted to the equilibrium value noted above. The room temperature was measured and the electrical power input to the calorimeter was determined. The calibration was repeated at various room temperatures and a correction curve for the uniform flow energy inputs to the calorimeters was obtained.

The uncertainty of measurement of the thermal flux by means of the calorimeters was approximately ±10%. This figure at first glance seems somewhat high, but when it is realized that the power input to the calorimeter block was of the order of 1 watt, it becomes evident that the task under consideration was a very difficult one. It is believed that the mean of perhaps four calorimetric

measurements would give a value for the thermal flux within ±5% of the true value.

Experimental Results

The results of two explorations of the temperature and velocity fields between the parallel plates are presented in Tables I and II. Table I lists the point values of temperature and velocity for a traverse (Test 60) in which the upper plate of the apparatus was maintained at 115°F, the lower plate at 85°F, and the temperature of the inlet air at 100°F. The average velocity across the test section was 13.31 ft./sec. and the Reynolds number was 8198. The average velocity and Reynolds number were calculated from the following equations:

$$U = \int_0^1 u \, d(y/y_0) \tag{19}$$

$$Re = \frac{2 y_0 U}{(\nu)_{y/y_0 = 0.5}} \tag{20}$$

Table II lists the point values of temperature and velocity for a traverse (Test 61) in which the upper plate was maintained at 85°F, the lower plate at 115°F, and the temperature of the inlet air at 100°F. The average velocity was 13.13 ft./sec. and the Reynolds number 8039. Tests 60 and 61 were, in fact, as identical as they could be made except that the plate temperatures were interchanged for the second test. The temperatures listed were corrected for the

heating effect of the bridge current on the thermanemometer wire. The applicability of Equation 15 was assumed. Corrections for the impact of the moving air on the thermanemometer wire were negligible at the velocities involved.

Further data for conditions of uniform flow are listed in the Ph.D. thesis of co-worker Franklin Page, Jr. (7). The primary concern of the latter author was the behavior of the eddy quantities in the turbulent core, while the writer was responsible for the study of their behavior near the walls of the channel. Reference to the body of data in (7) will be made from time to time and derived quantities used in this thesis will be tabulated. However the primary data will not be relisted here.

The traverses of Tests 60 and 61 described above were made in very great detail near the upper wall in order that a very definite understanding of the behavior of the eddy quantities in this region of the channel could be obtained. It would have been desirable to obtain data in great detail at the lower wall also. However the thermanemometer wire was soldered to the upper surface of the needles which support it. As a result it was impossible to approach the lower wall more closely than some 0.015 inch. For this reason attention was focused on the upper wall in the experimental work. The traverses of Tests 60 and 61 were taken under identical conditions except for the interchange of plate temperatures in order that the effect of natural convection on the eddy properties could be studied.

The temperature fields for Tests 60 and 61 are shown in Figure 24. The linearity of temperature as a function of distance

in the laminar layer at the upper wall is evident. The plot for Test 60 shows definite evidence near the center of a slight displacement of the curve. Other tests showed this displacement also. It is quite noticeable in Figure 25 which shows the temperature field for Test 40 where the average velocity was 28.13 ft./sec. As the velocity is increased the displacement occurs over a larger y/y_o range. In Test 61, however, no such displacement of the temperature curve can be observed. The reason for the lack of the displacement is not understood.

In taking the data the operators began the traverses at the upper plate and proceeded to the lower plate. They then moved the thermanemometer in an upward direction and filled in the profiles of temperature and velocity with several additional points. Those taken when the thermanemometer was being moved downward and those taken when it was being moved upward are designated by different symbols in the plots of temperature and in the plots of velocity now to be described.

The velocity profile for Test 60 is shown graphically in Figure 26. The corresponding profile for Test 61 is shown in Figure 27. The three points nearest to $y/y_o = 1$ in each figure were those referred to in a previous section as being in error because of the effect of the proximity of the wall on the thermanemometer readings. In drawing the velocity curves these three points were disregarded in each traverse. It is evident from Figures 26 and 27 that the curves extrapolate nicely to zero velocity at the wall when

the points in question are omitted. Both plots show the near linearity of the velocity profile near the walls.

Various miscellaneous data including the pressure gradient, the distance between the plates, and the rate of heat transfer are listed in Table III.

Table IV lists the eddy properties for Test 60 and 61, calculated by means of Equations 13 and 14 of the Introduction. These equations are repeated below in slightly different form:

$$\epsilon_m = \left(\frac{\tau}{\rho}\right)\left(\frac{1}{\frac{du}{dy}}\right) - \nu \tag{21}$$

$$\epsilon_c = \left(\frac{\dot{Q}}{c_p \sigma}\right)\left(\frac{1}{\frac{dt}{dy}}\right) - K \tag{22}$$

The shear was calculated by means of the relationship:

$$\tau = -y_o \frac{dP}{dx}\left[\frac{y}{y_o} - \left(\frac{y}{y_o}\right)_{u\,max.}\right] \tag{23}$$

This equation was obtained by integrating the expression:

$$\frac{d\tau}{dy} = -\frac{dP}{dx} \tag{24}$$

which may be derived from a simple force balance on an element of the uniform stream. The velocity and temperature gradients of Equations 21 and 22 were obtained graphically from large plots of the temperature and velocity distributions. The velocity gradient did not become zero exactly at the mid-point of the stream since a small amount of asymmetry was present in the velocity profiles. This fact was taken

into account in Equation 23. Near each wall the temperature and velocity gradients were weighted averages obtained from the plots mentioned above and from enlarged plots of temperature and velocity for the regions within 0.2 y/y_o units of either wall. For calculating the eddy conductivity the thermal flux was obtained from the slope of the temperature profile at the wall. In other words,

$$\dot{Q} = \lim_{\frac{y}{y_o} \to 1} \left\{ k \frac{dt}{dy} \right\} \tag{25}$$

The above method of determining $\dot{Q}$ was used since the writer wished to treat Tests 60 and 61 in a consistent manner. No calorimetric data were available for Test 61 with the result that Equation 25 had to be used for Test 61 in any case. In Test 60 the average of the calorimetric determinations of $\dot{Q}$ was 3.7% less than the $\dot{Q}$ calculated from Equation 25. Quantities ρ and σ in Equations 21 and 22 were obtained by use of the expressions:

$$\frac{P}{\sigma} = ZBT \tag{26}$$

$$\rho = \frac{\sigma}{g} \tag{27}$$

In Equations 21 and 22 ν and K were obtained by means of the relationships:

$$\nu = \frac{\eta}{\rho} \tag{28}$$

and

$$K = \frac{k}{C_p \sigma} \tag{29}$$

C_p, η , and k were assumed to be linear functions of the temperature, and independent of the small amounts of moisture present in the air. These properties are listed in Table V at three different temperatures. This table is the result of a critical survey of the literature by members of the Chemical Engineering Department of the California Institute of Technology. The value of the eddy viscosity at the mid-point of the channel was obtained by applying l'Hospital's rule to the eddy viscosity equation. Thus,

$$(\epsilon_m + \nu)_{y/y_o = 0.5} = \frac{\frac{1}{\rho} \frac{d\tau}{dy}}{d^2u/dy^2} \qquad (30)$$

The eddy quantities of Tests 60 and 61 have been plotted as functions of position in Figures 28 and 29. The reader should give more weight to the values in close proximity to the upper wall ($y/y_o = 1$) than to those near the lower wall, since the slopes of the temperature and velocity curves at the lower wall were smoothed to make them approximately symmetrical with those obtaining at the upper wall where experimental points in the laminar layer were available. The calculated eddy viscosity has a small apparent value in the laminar layers mainly as a result of the difficulty of measuring the slopes of the steep velocity profiles obtaining in the regions of the stream near the walls. In Figures 28 and 29 it is interesting to note the steep rise of the eddy properties from zero in the laminar layer to the value obtaining at the turbulent edge of the buffer zone. This behavior is apparently quite characteristic. The reason

for the asymmetry evident in the plots is not well understood. Care was taken during the experimental work to see that the operating variables remained constant within the limits described earlier. It seems likely that the asymmetry in the plots is more apparent than real and that it is a result of minor departures from uniformity in the stream which would have a much larger effect on the derivatives of velocity and temperature than on the velocity and temperature themselves.

Analysis of Results

Pressure Gradients

The values of the pressure gradients listed in Table III for Tests 60 and 61 are larger than those measured experimentally. A plot was prepared showing the variation of the logarithm of the measured pressure gradient with the logarithm of the average velocity at the traversing point. The average velocities ranged from 11 to 90 ft./sec. This plot has been reproduced as Figure 30. The data on which it was based are listed in Table VI. Examination of Table VI and Figure 30 shows that the measured pressure gradient was lower than would be expected for Tests 60 and 61, and for Test 49. In calculating the results of Tests 60 and 61 the pressure gradients were obtained from the plot of Figure 30 by reading off the pressure gradient corresponding to the average velocity for the respective test.

The main reason for the low values of the measured pressure gradient at the low velocities was that during these tests the pressure in the channel was below atmospheric. The flow was therefore not strictly uniform and the average velocity increased gradually down the channel as a result of leakage. The measured pressure gradient was obtained upstream from the traversing point and therefore related to an average velocity lower than that obtaining where the traverse was taken. Since the pressure gradient depends on the square of the average velocity a noticeable effect was obtained. The points at 15 ft./sec. and higher in Figure 30 lie on a smooth curve since in the tests at 15 ft./sec. the average channel pressure was approximately atmosphoric, and at the higher average velocities leakage was not a significant percentage of the total flow.

It is noteworthy also that uncertainties of pressure gradient measurement and of velocity measurement were considerably larger at the low velocities than at the high ones. The pressure differences measured in Tests 60 and 61 were of the order of 1 millimeter of kerosene. Since the uncertainty of measurement of such differences was approximately 0.2 millimeter of kerosene, some of the deviation of the low velocity pressure gradients may have been the result of the uncertainty being a significant fraction of the reading. Errors in velocity measurement would be more significant than at higher Reynolds numbers because of the greater percentage uncertainty in the readings of the pitot tube used in calibration. It is believed,

however, that the resulting errors in the average velocities would not be as important as leakage or as uncertainties in pressure difference measurements in causing displacement of the Test 49, Test 60 and Test 61 points from the smooth curve of Figure 30.

H. Ludwieg (14) has recently developed an instrument for measuring wall shearing stresses. This instrument consists of a small heated block forming part of the channel wall but insulated from it as much as possible. The heat transfer from the block is shown to be a measure of the shearing stress at the wall. From the latter the pressure gradient is obtainable at once by an application of Equation 24. Such an instrument might be useful in the wind tunnel described in this thesis for making pressure gradient determinations at low Reynolds numbers.

Velocity Correlations

Before proceeding further it is convenient to define the friction velocity, u^*, the dimensionless velocity parameter, u^+, and the dimensionless distance parameter, y^+, by means of the following equations:

$$u^* = \sqrt{\frac{y_o}{2(\rho)_{\frac{y}{y_o}=0.5}}\left(-\frac{dP}{dx}\right)} \tag{31}$$

$$u^+ = \frac{u}{u^*} \tag{32}$$

$$y^+ = \frac{u^* \, y_o}{(\nu)_{\frac{y}{y_o}=0.5}} \, \frac{y_d}{y_o} \tag{33}$$

The quantities u* and y^+ have usually in the past been defined in situations where the properties ρ and ν have been essentially constant. It would have been possible to define y^+ as a point function of ν as well as of y_d, but the problem of assigning a value to ρ in the u^+ equation is not so easily solved, since u* is customarily treated as a constant for a given boundary and flow situation. With a temperature difference of 30°F between the plates the deviation of the ρ and ν values from the value at the center is less than 5% for all points between the plates. In certain of the runs at constant temperature where only the transfer of momentum has been studied, the problem of definition of u* and y^+ is simplified because of the constancy of ρ and ν.

Previous workers have shown from experimental and theoretical considerations that near a smooth wall the dimensionless velocity parameter u^+ is a universal function of the dimensionless distance parameter y^+. The theoretical background for this statement is ably summarized by Bakhmeteff (15). Experimental evidence to support it has been obtained by Nikuradse (16) for round pipes and by Reichardt (17) for flat plates. Martinelli (6) shows a plot of these experimental results.

The universal velocity distribution may be approximated as follows in the laminar sublayer, the buffer layer, and in the turbulent core respectively:

$$u^+ = y^+ \qquad (0 < y^+ < 5) \tag{34}$$

$$u^+ = -3.05 + 11.5 \log y^+, (5 < y^+ < 30) \tag{35}$$

$$u^+ = 5.5 + 5.75 \log y^+, (30 < y^+) \tag{36}$$

The boundaries of the various layers are somewhat arbitrary and a gradual shading of one zone into another is to be expected.

The velocity distributions obtained in the course of this research follow reasonably closely the universal distribution equations given above. These results therefore confirm the data of Reichardt (17) that the velocity distribution laws apply to flow between smooth parallel plates as well as to flow in circular pipes. The plates of the heat transfer equipment are hydraulically smooth, the average root mean square depth of the scratches on the surfaces being 16 microinches. Figure 31 shows u^+ as a function of $\log y^+$ for Test 60. The displacement of the lower and upper wall curves is probably the result of a certain amount of asymmetry in the velocity traverse of Test 60. In order to check the effect of somewhat different definitions of u* and y^+ on the plot, these quantities were redefined for this single application as:

$$u^* = \sqrt{\frac{\tau_o}{\rho'}} \tag{37}$$

and

$$y^+ = \frac{y_o\, u^*}{\nu} \quad \frac{y_d}{y_o} \tag{38}$$

Where τ_o is the shear at the wall under consideration, ρ' is the average of the density at the center and at the wall, and ν is the viscosity at the point. The plot which resulted is shown as Figure 32. The curves for the two walls are displaced in the turbulent core as a result of different values of u* having been used for the two walls.

Figure 33 shows u^+ plotted versus log y^+ for Test 61 in which the temperature gradient was inverted but essentially the same average velocity used as in Test 60. The velocity profile of Test 61 was more symmetrical than that of Test 60 and it is interesting to note the near coincidence of the upper and lower wall curves in Figure 33.

The velocity distribution curves described above afford further experimental confirmation of the correctness of the adjustment applied to the pressure gradients of Tests 60 and 61 as described in the previous subsection. The $u^+ - y^+$ curves corresponding to the measured pressure gradients were found to be considerably displaced from the universal distribution lines particularly in the turbulent core.

In Figure 34 is shown the variation of u^+ with log y^+ for an isothermal run at an average velocity of 30.0 ft./sec.: Test 39. An adjustment in the pressure gradient of only 1% was indicated by Figure 30 for this test, and it was decided to use the experimentally measured pressure gradient for this figure. Again the experimental data follow the universal distribution quite closely.

It should be noted that in all the $u^+ - y^+$ plots, unsmoothed experimental values of the point velocity were used. Measurements taken with the gear moving downward are indicated by symbols different from those used for points taken with the gear moving upward.

Calorimetric Data

It seems advisable to review briefly the history of thermal flux measurements with the calorimeters of the heat transfer project, in order that some of the results obtained may be better understood. The flux determinations which have been made fall into three distinct groups. The first group consists of measurements made at Reynolds numbers ranging from 6,000 to 50,000 and with an average temperature gradient of approximately 1000°F./ft. between the upper and lower plates, which were maintained at 130°F. and 70°F. respectively. The entering air was at 100°F. After this first group of runs was concluded the calorimeters were removed from the apparatus for minor repairs. At the same time the distance between the plates was decreased approximately 8% to the present separation of 0.7 inch. After the calorimeters had been reinstalled the second group of measurements was obtained. These cover the same range of Reynolds number but were made with an average temperature gradient of one sixth of that obtaining in the first set of tests. The upper plate was maintained at 105°F. and the lower at 95°F. The inlet air temperature was controlled at 100°F. In one test only of this group the upper plate and lower plate were maintained at 115°F. and 85°F. respectively. In this test the air entered at the usual 100°F. and

the Reynolds number was 9370. At the conclusion of the second group of tests the calorimeters were removed from the apparatus and subjected to extensive alterations, the main purpose of which was to reduce the thickness of the calorimeter block. At the same time cooling loads were installed in the block cooling pad. Figure 35 shows one of the calorimeters before these changes were made. Figure 10 shows the instrument afterward. The decrease in block thickness permitted more rapid attainment of equilibrium. The third group of measurements was made with the calorimeter of Figure 10. This group consists of only one test, a run made with the inlet air at 100°F., with the upper plate at 115°F., and with the lower plate at 85°F. The Reynolds number was 8198.

The calorimetric data for the three groups of tests have been listed in Table VII. Table VII shows also the rate of heat transfer per degree difference in temperature between the plates calculated from the slope of the temperature curve at the wall by the application of Equation 25. In many of the tests the laminar layer was very thin and insufficient experimental points were taken within it to establish the slope of the temperature profile at the wall. For such tests the thermal flux could not, of course, be computed from Equation 25. The agreement of the available data obtained from the temperature slopes, with the data from the calorimeters, leaves something to be desired. However Column 8 of Table VII shows increased agreement with the passage of time, indicating a marked improvement in technique during the year of experimental work which the table represents.

The calorimetric data have also been compared in Table VII with the heat transfer coefficient calculated from the relationship:

$$\frac{hD}{k} = 0.023 (Re)^{0.8} (P_r)^{0.4} \qquad (39)$$

which is recommended by McAdams (18). The calculated h from Equation 39 has been divided by 2 for purposes of comparison with $\dot{Q}/\Delta t$ in Table VII, Δt being the difference in temperature between the plates. The heat transfer coefficient is defined by the equation:

$$\dot{Q} = h (t_{wall} - t_{bulk}) \qquad (40)$$

For the situation under consideration the bulk temperature* is within 0.2% of the average of the two wall temperatures, and Equation 40 may be written as:

$$\dot{Q} = h \, \Delta t/2 \qquad (41)$$

or

$$h/2 = \dot{Q}/\Delta t \qquad (42)$$

In applying Equation 39 the properties of the fluid were evaluated at 100°F, which temperature differs by approximately 0.2°F. from the bulk temperature in the channel for which Equation 39 applies. An equivalent diameter of 2 y_o was used.

In every case the value of $\frac{h}{2}$ is larger than that of $\frac{\dot{Q}}{\Delta t}$ obtained calorimetrically or from the slope of the temperature curve. However Equation 39 was derived for nonuniform flow situations and

---

* The bulk value of any property G is defined as follows: $\frac{\int_o^{y_o} u \sigma G \, d(y/y_o)}{\int_o^{y_o} u \sigma \, d(y/y_o)}$

considerable deviation might be expected in the present approximately uniform case.

The logarithm of the calorimetrically determined ratio $\frac{\dot{Q}}{\Delta t}$ has been plotted versus the logarithm of the corresponding Reynolds number in Figure 36. Included also are the calculated heat transfer coefficients. It is evident that the readings of each of the first two groups of measurements are consistent within the group. The third group includes only a single determination of the thermal flux. However a trend is apparent in that with each improvement in calorimeter design and reinstallation of the calorimeters in the equipment, lower $\frac{\dot{Q}}{\Delta t}$ readings were obtained. It is believed that future work will probably show that the early values were high.

The shift of the $\frac{\dot{Q}}{\Delta t}$ curves in Figure 35 is too large to be explained by the change in temperature gradient between the plates. The displacement between the first and second groups of determinations is in the wrong direction to be explained by the change in y_o. The shift after each reinstallation of the calorimeters indicates probably that the orientation of the calorimeter in the plate is very important. It is difficult to line up the calorimeter block and the plate exactly and it would seem advisable to investigate the possibility of filling in the gap between the calorimeter and plate with a thin, smooth annulus of plastic to prevent possible disturbance of the smooth flow of the laminar layer. Ludwieg (14) found a similar course advisable in building his instrument for measuring shearing stresses at walls. Before the comprehensive altering of the calorimeters at the conclusion of the second group of measurements some leakage of air into the

channel may have occurred between the vacuum jacket and the outer jacket of the calorimeters. This path was closed by the O-ring mentioned in the description of the calorimeters. High values of $\dot{Q}$ would result from such leakage or from interference with the streamlines by a surface discontinuity at the plate-block junction. The measured values of the thermal flux have been used in this thesis except in the two succeeding subsections. There the $\dot{Q}$ of Test 60 has been adjusted to make it consistent with the second group of calorimetric measurements, in order that the tests considered may be compared on an equal basis.

Variation of the Eddy Quantities with Position

In his extension of Reynolds' analogy to liquids, von Kármán (4) showed that ϵ was a universal function of y^+ in regions near the wall where the shear could be considered constant. Von Kármán represented by ϵ a quantity which he called the coefficient of turbulent exchange, and which replaced in his paper the eddy viscosity and eddy conductivity used in this thesis. Von Kármán thus treated the eddy conductivity and the eddy viscosity as equal. If the equality of these two quantities is not assumed it is necessary to deal with one or the other. Eddy viscosity will be considered first. Furthermore, shear is in reality a variable and it is profitable to consider it as such.. The treatment of von Kármán may then be modified and extended as shown below.

The universality of the velocity distribution referred to in a previous subsection is taken to have been sufficiently established. Thus

$$u^+ = f(y^+) \tag{43}$$

or,

$$u = u^* f(y^+) = \sqrt{\frac{\tau_o}{\rho}}\ f(y^+) \tag{44}$$

where the variation of the density of the fluid is to be neglected and where $f(y^+)$ represents a universal function. Differentiation of Equation 44 then produces:

$$\frac{du}{dy_d} = \sqrt{\frac{\tau_o}{\rho}}\ f'(y^+)\ \frac{dy^+}{dy_d} \tag{45}$$

However

$$y^+ = \frac{u^* y_d}{\nu} \tag{46}$$

Neglecting the small variations in ν and ρ with position as a result of temperature gradients,

$$\frac{dy^+}{dy_d} = \frac{u^*}{\nu} = \sqrt{\frac{\tau_o}{\rho}}\ \frac{1}{\nu} \tag{47}$$

Therefore by substitution of Equation 47 into Equation 45

$$\frac{du}{dy_d} = \sqrt{\frac{\tau_o}{\rho}}\ f'(y^+) \sqrt{\frac{\tau_o}{\rho}}\ \frac{1}{\nu}$$

or

$$\frac{du}{dy_d} = \frac{\tau_o}{\rho \nu}\ f'(y^+) \tag{48}$$

However by Equation 1,

$$\frac{du}{dy} = \frac{\tau}{\rho(\epsilon_m + \nu)} = \frac{du}{dy_d} \tag{49}$$

where y and y_d are really one variable: the distance from the wall. The sign of τ_o is then positive in Equation 44 and consistent with the sign of τ in Equation 49. Equating the right sides of Equations 48 and 49,

$$\frac{\tau_o}{\rho\nu} f'(y^+) = \frac{\tau}{\rho(\epsilon_m + \nu)} \tag{50}$$

and

$$\frac{\epsilon_m + \nu}{\nu} = \frac{\tau}{\tau_o} \frac{1}{f'(y^+)} \tag{51}$$

Now

$$\frac{\tau}{\tau_o} = \frac{\frac{y_o}{2} - y_d}{\frac{y_o}{2}} = 1 - \frac{2y_d}{y_o} \tag{52}$$

Substitution of Equation 52 into Equation 51 produces the result:

$$\left(\frac{\epsilon_m + \nu}{\nu}\right)\left(\frac{1}{1 - \frac{2y_d}{y_o}}\right) = \frac{1}{f'(y^+)} \tag{53}$$

In other words the ratio $\frac{\epsilon_m + \nu}{\nu}$ when multiplied by the dimensionless correction factor $\frac{1}{1 - \frac{2y_d}{y_o}}$ is a universal function of y^+. The function is independent of the average velocity of flow and of whether the stream is in a circular pipe or between parallel plates. The kind of fluid is immaterial except that the properties must not change very rapidly with temperature or else the temperature gradients in the stream must be small, as otherwise Equation 43 would be invalid

as pointed out by McAdams (18), and also considerable error would be introduced into the derivation at the step taken in Equation 47. Equation 53 should apply to all parts of the channel where the universality of Equation 43 has been demonstrated. For circular conduits Equation 53 becomes:

$$\left(\frac{\epsilon_m + \nu}{\nu}\right)\left(\frac{1}{1 - \frac{r_d}{r_o}}\right) = \frac{1}{f'(y^+)} \tag{54}$$

It is of interest to consider the specific forms which the universal function may assume. In the laminar layer by Equation 34,

$$u^+ = y^+ \tag{55}$$

However, in deriving this equation constant shear is assumed whereas in deriving Equation 53 such as approximation was not made. Equation 55 may be revised to allow for shear variations. Equation 1 written for the laminar layer reduces to:

$$\frac{\tau}{\rho} = \nu \frac{du}{dy_d} \tag{56}$$

Then

$$\int_0^u du = \int_0^{y_d} \frac{\tau}{\rho \nu}\, dy_d \tag{57}$$

But Equation 52 may be rewritten as

$$\tau = \left(1 - \frac{2y_d}{y_o}\right)\tau_o \tag{58}$$

Substitution of Equation 58 in Equation 57 produces:

$$u = \frac{\tau_o}{\rho \nu}\int_0^{y_d} \left(1 - \frac{2y_d}{y_o}\right) dy_d \tag{59}$$

or

$$\frac{u}{u^*} = \frac{u^*}{\nu}\left(y_d - \frac{y_d^2}{y_o}\right) \tag{60}$$

Thus

$$u^+ = y^+ - \frac{(y^+)^2 \nu}{y_o u^*} \tag{61}$$

is the revised equation for the laminar layer. Then differentiation with respect to y^+ produces:

$$f'(y^+) = 1 - \frac{2 y^+ \nu}{y_o u^*} \tag{62}$$

or

$$f'(y^+) = 1 - \frac{2 y_d}{y_o} \tag{63}$$

Then in the laminar layer Equation 58 reduces to:

$$\left(\frac{\epsilon_m + \nu}{\nu}\right)\left(\frac{1}{1 - \frac{2y_d}{y_o}}\right) = \frac{1}{1 - \frac{2y_d}{y_o}} \tag{64}$$

or

$$\frac{\epsilon_m + \nu}{\nu} = 1 \tag{65}$$

as one would expect.

In the buffer zone by Equation 36

$$f(y^+) = -3.05 + 11.5 \log y^+ \tag{66}$$

Then

$$f'(y^+) = \frac{11.5}{(y^+)(2.30)} = \frac{5}{y^+} \tag{67}$$

Thus in the buffer layer Equation 53 reduces to

$$\left(\frac{\epsilon_m + \nu}{\nu}\right)\left(\frac{1}{1 - \frac{2y_d}{y_o}}\right) = \frac{y^+}{5} \tag{68}$$

However as Equation 35 is not a particularly good fit for the data in the buffer zone as shown by Figures 33 and 34, one would not expect Equation 68 to be a very exact representation of fact.

In the turbulent core by Equation 36 the universal function has the form:

$$f(y^+) = 5.5 + 5.75 \log y^+ \tag{69}$$

and

$$f'(y^+) = \frac{2.5}{y^+} \tag{70}$$

Substitution in Equation 53 gives the result:

$$\left(\frac{\epsilon_m + \nu}{\nu}\right)\left(\frac{1}{1 - \frac{2y_d}{y_o}}\right) = \frac{y^+}{2.5} \tag{71}$$

The experimental results would be expected to fit Equation 71 reasonably well in the turbulent core since Equation 36 agrees quite closely with the velocity data. However some comment is in order with respect to the behavior of the universal velocity distribution as the center of the channel is approached.

It may be shown that a universal distribution of velocities does not obtain in the central portion of a channel in which there is

turbulent flow. In any channel the velocity distribution follows quite closely the logarithmic velocity distribution equation for the turbulent core, as the observer proceeds outward from the edge of the buffer zone. However as the center of the channel is reached the velocity increases less rapidly than the logarithmic equation requires. This statement may be verified by examining Figures 31 and 33 at large y^+ values. This lowered rate of increase of velocity is necessary in order that the velocity profile be rounded at the center of the conduit, rather than sharply pointed as the logarithmic equation would imply. Figure 37 shows this feature of the logarithmic expression for the universal velocity distribution. As the average velocity of the stream is increased the departure of the experimental u^+ points from the logarithmic equation occurs at larger y^+ values as shown in the sketch below:

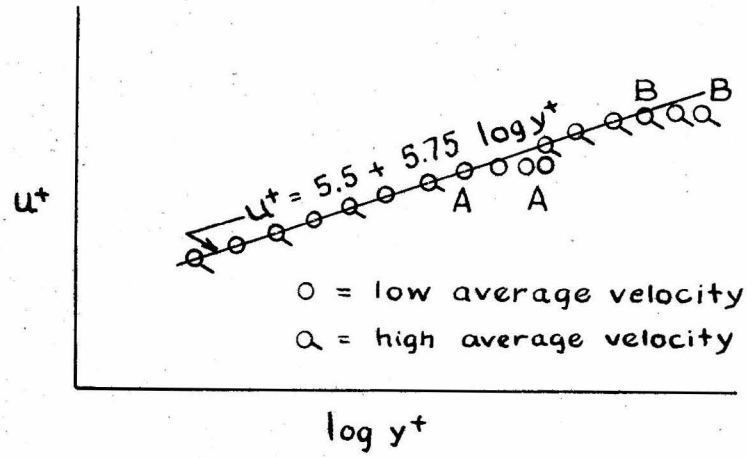

It is apparent that the portions A-A and B-B of the velocity distributions shown in the sketch are nonuniversal. Equation 33 which is

repeated below for convenience, also would be expected to become nonuniversal in the y^+ ranges corresponding to A-A and B-B in the sketch.

$$\left(\frac{\epsilon_m + \nu}{\nu}\right)\left(\frac{1}{1 - \frac{2y_d}{y_o}}\right) = \frac{1}{f'(y^+)} \tag{53}$$

In particular, in regions A-A and B-B the value of $f'(y^+)$* decreases more rapidly than it did before the velocities began to deviate from the logarithmic equation. The rate of increase of the left side of Equation 53 therefore becomes more rapid and nonuniversal in nature. When the left side of Equation 53 is plotted as a function of y^+ this lack of universality is evident as the y^+ values approach those of the middle of the channel. The left side of Equation 53, of course, is infinite at $y/y_o = 0.5$.

The function $\left(\frac{\epsilon_m}{(\nu)_{\frac{y}{y_o}=0.5}}\right)\left(\frac{1}{1-\frac{2y_d}{y_o}}\right)$ where

$$\epsilon_m = \epsilon_m + \nu \tag{72}$$

has been plotted as a function of y^+ in Figure 38 and again in Figure 39 where the scale of the abscissa has been changed to focus attention on the low velocity tests. Equations 68 and 71 for the buffer zone and for the turbulent core, respectively, have been shown on each figure. Agreement between the experimental results and the prediction of the existence of a universal relation is seen to be satisfactory. The predicted departures from universality are evident as the channel center is approached by each curve. Data of Nikuradse (16) for the

---

* In regions A-A and B-B $f'(y^+)$ is simply the derivative of the velocity distribution obtaining.

flow of water in smooth pipes have been included in Figures 38 and 39. The ratio $\frac{\epsilon_m}{\nu}$ was multiplied by the factor $\left(\frac{1}{1-\frac{r_a}{r_o}}\right)$ and was plotted for a pipe 1.0 centimeter in diameter where the Reynolds number was 16,700, and for a pipe 3.0 centimeters in diameter where the Reynolds number was 105,000. Agreement is satisfactory with the data of the present research except in the laminar and buffer regions where the data of Nikuradse fall somewhat above those reported in this paper.

It is believed that the experimental curves of Figures 38 and 39 may be used to predict the total viscosity* as a function of position in a fully developed turbulent stream in a pipe or between parallel plates. The curves apply to any fluid with properties reasonably insensible to temperature changes. The values apply specifically to uniform flow but probably apply at least approximately in nonuniform cases. However, the curves should not be used at larger y^+ values than the one where departure of the u^+-log y^+ curve from universality begins. Equation 71 appears to be satisfactory as an analytical expression for the universal relationship between $\left(\frac{\epsilon_m}{(\nu)_{y/y_o=0.5}}\right)\left(\frac{1}{1-\frac{2y_d}{y_o}}\right)$ and y^+ in the turbulent core beyond a y^+ value of approximately 45.

Figures 38 and 39 are based on the data of Table VIII. In this table the total viscosity and the total conductivity are listed at various positions in the channel for several tests. The data as presented have been averaged between the two sides of the middle line

---

* The total viscosity is defined as the sum of the eddy and molecular viscosities. The total conductivity is defined analogously.

of the stream to remove asymmetry. Included in the table are the values of y^+ corresponding to these data and the values of the molecular viscosity and of the molecular conductivity at the middle of the channel. These are equal to the respective bulk values within 0.2%. The ordinates of Figures 38 and 39 contain the above value of the molecular viscosity in the denominator. The total viscosities listed were calculated from pressure gradient values obtained from Figure 30.

It was assumed by analogy that the function $\left(\frac{\epsilon_c}{(K)_{\frac{y}{y_0}=0.5}}\right)\left(\frac{1}{1-\frac{2y_d}{y_0}}\right)$ might be a universal function of y^+. The function was therefore plotted as ordinate versus y^+ as abscissa. Figures 40 and 41 show the results of this work and confirm that a universal function is probably involved. It is believed that the curves of Figures 40 and 41 may be used to predict the total conductivity in channels where fully developed uniform turbulent flow exists and natural convection is absent. The remarks made above in the discussion of the use of the total viscosity curves near the middle of the stream apply here also as do the remarks made previously concerning variation of the properties of the fluid with temperature. The values of the total conductivity obtainable from the correlation apply primarily to uniform flow but probably approximate those obtaining in nonuniform flow. The following equation represents closely the universal total conductivity function in the turbulent core:

$$\left(\frac{\epsilon_c}{K_{\frac{y}{y_0}=0.5}}\right)\left(\frac{1}{1-\frac{2y_d}{y_0}}\right) = 0.372\,y^+ - 2.9 \qquad (73)$$

Figures 40 and 41 were plotted from the data of Table VIII.

In order to magnify the region near the wall the logarithms of the functions plotted in Figures 38 to 41 were replotted against the logarithm of y^+ in Figures 42 and 43. For both the conductivity and the viscosity the resulting universal curves may be approximated by straight lines between y^+ values of 10 and 40, the part of the stream usually classed as the buffer zone and the outer edge of the turbulent core. The universal viscosity function may be represented by the equation:

$$\log \left\{ \left(\frac{\epsilon_m}{(\nu)_{\frac{y}{y_o}=0.5}} \right) \left(\frac{1}{1 - \frac{2y_d}{y_o}} \right) \right\} = -1.6384 + 1.7439 \log y^+ \qquad (74)$$

The universal conductivity function may be approximated by the equation:

$$\log \left\{ \left(\frac{\epsilon_c}{(K)_{\frac{y}{y_o}=0.5}} \right) \left(\frac{1}{1 - \frac{2y_d}{y_o}} \right) \right\} = -1.3182 + 1.5099 \log y^+ \qquad (75)$$

It is important to note that the scattering of experimental points at low values of y^+ in Figures 42 and 43 is the result of the difficulty of measuring the slopes of the temperature and velocity profiles very close to the walls. At y^+ values above 40 in Figure 42 the points follow a line inclined at 45 degrees to the bottom of the page. This line corresponds to Equation 71.

In addition to the above correlations of the eddy properties it was found empirically that on log-log paper the ratios $\frac{\epsilon_m}{(\nu)_{\frac{y}{y_o}=0.5}}$ and $\frac{\epsilon_c}{(K)_{\frac{y}{y_o}=0.5}}$

plotted against y^+ gave straight lines. Figures 44 and 45 are examples of those plots and refer to Test 69. The straight lines extend through the buffer zone and into the turbulent core to a y^+ value of 40. However, from the arguments given above it is evident that the functions determined by these plots are not universal unless the variation in shear may be neglected. In Test 69 the decrease in shear from the wall to the edge of the turbulent core amounted to about 25% of the shear at the wall. However, the plots of the type under discussion may be useful for smoothing the total conductivity and the total viscosity from the edge of the laminar sublayer to a point within the turbulent core.

Variation of the Ratio of Total Conductivity to Total Viscosity

It has been shown analytically and verified experimentally that the quantity $\left(\frac{\epsilon_m}{\nu}\right)\left(\frac{1}{1-\frac{2y_d}{y_o}}\right)$ is a universal function of y^+. It has been indicated experimentally that $\left(\frac{\epsilon_c}{K}\right)\left(\frac{1}{1-\frac{2y_d}{y_o}}\right)$ is also a universal function of y^+. The above statements apply except near the center of the conduit. Division of the total conductivity universal function by the total viscosity universal function results in the relationship given below:

$$\frac{\epsilon_c}{\epsilon_m}\,\frac{\nu}{K} = \phi(y^+) \tag{76}$$

where ϕ represents another universal function. Since $\frac{\nu}{K}$ is the Prandtl number, one may write:

$$\frac{\epsilon_c}{\epsilon_m}\,P_r = \phi(y^+) \tag{77}$$

The form of the function ϕ was determined by obtaining the quotient

of corresponding ordinates read from the plots of $\left(\frac{\epsilon_m}{(\nu)_{\frac{y}{y_o}=.05}}\right)\left(\frac{1}{1-\frac{2y_d}{y_o}}\right)$ and $\left(\frac{\epsilon_c}{(K)_{\frac{y}{y_o}=0.5}}\right)\left(\frac{1}{1-\frac{2y_d}{y_o}}\right)$ versus y^+. The function is shown in Figure 46. The restrictions on the use of this plot are the same as those already noted for the plots on which it is based.

Following a suggestion by W. G. Schlinger the ratio $\frac{\epsilon_c}{\epsilon_m}$ was determined as a function of position from plots of temperature versus velocity for Test 46 and for Test 60. Equation 10 may be divided by Equation 1 to give the result:

$$\frac{\dot{Q}}{T} = \frac{C_p \sigma}{\rho} \frac{\epsilon_c}{\epsilon_m} \frac{dt}{du} \tag{78}$$

Solving for $\frac{\epsilon_c}{\epsilon_m}$ gives the relationship:

$$\frac{\epsilon_c}{\epsilon_m} = \frac{\dot{Q}\rho}{T C_p \sigma} \frac{1}{\frac{dt}{du}} \tag{79}$$

But by Equation 4:

$$\frac{\rho}{\sigma} = \frac{1}{g} \tag{80}$$

Substitution of Equation 80 into Equation 79 simplifies the latter slightly:

$$\frac{\epsilon_c}{\epsilon_m} = \frac{\dot{Q}}{T C_p g} \frac{1}{\frac{dt}{du}} \tag{81}$$

Slopes were obtained from temperature versus velocity plots and substitution of these into Equation 81 produced values of $\frac{\epsilon_c}{\epsilon_m}$ as a function of position. These ratios were multiplied by the Prandtl number for air and plotted versus y^+. The plots have been reproduced as Figures 47 and 48 which refer to Tests 46 and 60 respectively. Figures 47 and 48 should be compared with Figure 46. The

agreement is not outstanding but the curves have the same general form. It must be remembered that in the preparation of the curve of Figure 46 considerable smoothing took place. Furthermore small shifts in the location of the curves on which Figure 46 is based produce very large changes in the latter.

The Effect of Natural Convection on the Thermal Flux and on the Eddy Properties

One of the reasons for making the measurements of Tests 60 and 61 was to obtain an indication of the effect of natural convection on the transfer of heat and on the transfer of momentum. It is evident from Table III that Tests 60 and 61 were made under identical conditions except that the upper and lower plate temperatures of Test 60 were interchanged in Test 61. The effect of this interchange on the heat transfer rate may be seen by consulting Table III. The conductivities and viscosities, both eddy and total, may be compared in Table IV where they are listed as functions of position in the channel. The total quantities may be compared also in Table VIII where they are presented as averages of the values experimentally determined on each side of the middle line of the channel.

The increase in the heat transfer rate from Test 60 to Test 61 as a result of natural convection amounted to 4.2% of the heat transfer rate of Test 60. Few natural convection data are

available in the literature dealing with the horizontal plate case. The measurements of Saunders (19) indicate that the heat loss by natural convection from a horizontal plate facing upward in still air would amount to 0.0027 B.T.U./sec.ft.^{2} with the plate 15°F above the temperature of the surrounding air. This heat transfer rate is 27.3% of that of Test 60. The experiments of Saunders are far from being directly comparable with those reported in this thesis. However his results probably indicate that those obtained in this research are of the correct order of magnitude. The situation reported on by Saunders differed from that studied here in that his plate was not enclosed by side walls and forced convection was absent. Enclosing the heat transfer surface and superimposing forced convection as was done in this research would probably tend to reduce the contribution of natural convection to the heat transfer rate. The results obtained are therefore approximately what would be expected.

The total viscosities and the total conductivities for Tests 60 and 61 are compared in Figures 49 and 50. In Figure 49 $\log \frac{\epsilon_m}{(\nu)_{\frac{y}{y_o}=0.5}}$ is plotted as a function of $\log y^+$. In Figure 50 $\log \frac{\epsilon_c}{(k)_{\frac{y}{y_o}=0.5}}$ is shown plotted against the same abscissa. Little difference in total viscosity resulted from the interchange of the plate temperatures except over part of the turbulent core where there was apparently a small decrease in total viscosity. The total conductivities show a small increase, the magnitude of which varies with y^+ in Figure 50. However the apparent mode of variation is probably not significant because of experimental uncertainty.

Conclusion

The correlations which have been developed in the research described in this thesis should be of definite practical value for predicting the total viscosity and the total conductivity in other situations of engineering interest. The correlations do not apply near the middle of a channel but the situation there has been dealt with by F. Page, Jr. (7). A few data have been obtained concerning the effect of natural convection on the total viscosity and the total conductivity, and further data were obtained concerning the analogy between the transfer of momentum and the transfer of heat.

A few further remarks concerning the analogy are in order. These remarks apply to a fluid with a Prandtl number near that of air. At large values of y^+ the molecular properties may be neglected as compared with the eddy quantities. The curve of Figure 46 indicates that in such regions the transfer of momentum and the transfer of heat are approximately analogous, with the eddy conductivity somewhat larger than the eddy viscosity. In the buffer zone where both the eddy and molecular quantities are important, the analogy is not as exact, the total conductivity being of considerably greater magnitude than the total viscosity. This difference increases as the laminar layer is approached.

If one considers fluids of widely varying Prandtl numbers it is evident by Equation 76 that the form of the function ϕ and the value of the Prandtl number determine the extent to which Reynolds' analogy will obtain. The function ϕ has been determined approximately by this research. Knowing the Prandtl number for a particular

fluid one may estimate from Equation 76 the extent to which Reynolds' analogy, as expressed by Equation 11, will hold at various values of the dimensionless distance parameter y^+ except near the middle of a stream.

In closing the writer would like to recommend the study of a fluid with a different Prandtl number from that of air with a view to checking in particular the universality of the relationship between total conductivity and the dimensionless distance parameter.

Nomenclature

A	area of surface, ft.^{2}
a	intercept term of hot wire equation, dimensionless.
B	specific gas constant, ft./$^\circ$R.
b	slope factor of hot wire equation, dimensionless.
C_p	specific heat at constant pressure, B.T.U./lb. $^\circ$F.
D	diameter or equivalent diameter, ft.
$f(\ )$	a function of
$f'(\ )$	the derivative of a function with respect to its argument.
G	any property
g	gravitational acceleration, ft./sec.^{2}
h	heat transfer coefficient, B.T.U./sec.ft.^{2} $^\circ$F.
i	current, amps.
K	thermometric conductivity, ft.^{2}/sec.
$(K)_{\frac{y}{y_o}=0.5}$	thermometric conductivity at middle of channel, ft.^{2}/sec.
k	thermal conductivity, B.T.U. ft./sec.ft.^{2} $^\circ$F.
P	pressure, lb./ft.^{2}
Pr	Prandtl number, dimensionless. (For this paper a constant =0.709 to within 0.2%)
$\dot{Q}$	rate of heat transfer per unit area, B.T.U./ft.^{2} sec.
R_a	electrical resistance of the thermanemometer when used as a temperature measuring device, ohms.
R_{hw}	electrical resistance of the thermanemometer when used as a velocity measuring device, ohms.
Re	Reynolds number, dimensionless.
r	radial distance, ft.

r_o radius of a pipe, ft.

T time average temperature at a point, $^{\circ}R$.

t time average temperature at a point, $^{\circ}F$.

t_{bulk} bulk temperature, $^{\circ}F$, defined as follows:

$$\frac{\int_0^1 u \sigma t \, d\frac{y}{y_o}}{\int_0^1 u \sigma \, d\frac{y}{y_o}}$$

t_{wall} wall temperature, $^{\circ}F$.

Δt temperature difference, $^{\circ}F$.

U average velocity, ft./sec., defined as follows:

$$\int_0^1 u \, d\frac{y}{y_o}$$

u time average velocity at a point, ft./sec.

u^* friction velocity, ft./sec., defined as follows:

$$\sqrt{\frac{y_o}{2(\rho)_{\frac{y}{y_o}=0.5}}\left(-\frac{dP}{dx}\right)}$$

u^+ dimensionless velocity parameter, defined as follows:

$$\frac{u}{u^*}$$

$u_{max.}$ u_m maximum time average velocity, ft./sec.

V specific volume, $ft.^3/lb.$

w weight of fluid per unit of area which passes per unit of time between elevations dy apart in the two-dimensional channel, $lb./sec.ft.^2$

x longitudinal distance downstream from piezometer number two, ft.

y distance above lower plate, ft.

y_d distance from nearer wall, ft.

y_o height of channel, ft.

y^+ dimensionless distance parameter, defined as follows:

$$\left(\frac{u^* y_o}{(\nu)_{\frac{y}{y_o}=0.5}}\right)\left(\frac{y_d}{y_o}\right)$$

Z compressibility factor, dimensionless, defined as follows:

$$Z = \frac{PV}{BT}$$

Δ a difference

ϵ von Kármán's coefficient of turbulent exchange

ϵ_c eddy conductivity, ft.^{2}/sec.

ϵ_o sum of ϵ_c and K, total conductivity, ft.^{2}/sec.

ϵ_m eddy viscosity, ft.^{2}/sec.

ϵ_m sum of ϵ_m and ν, total viscosity, ft.^{2}/sec.

η absolute viscosity, lb.sec./ft.^{2}

θ time, sec.

ν kinematic viscosity, ft.^{2}/sec.

$(\nu)_{\frac{y}{y_o}=0.5}$ kinematic viscosity, at middle of channel, ft.^{2}/sec.

ρ density, lb.sec.^{2}/ft.^{4} = slugs/ft.^{3}

$(\rho)_{\frac{y}{y_o}=0.5}$ density, at middle of channel, lb.sec.^{2}/ft.^{4} = slugs/ft.^{3}

ρ' average of density at center and at wall.

σ specific weight, lb./ft.^{3}

τ shear, lb./ft.^{2}

τ_o shear at a wall, lb./ft.^{2}

$\phi(\ )$ a function of

References

(1) Reynolds, O., Proceedings of the Manchester Literary and Philosophical Society, 14, 7 (1874). Also: O. Reynolds, Papers on Mechanical and Physical Subjects, 1, 81-85, Cambridge (1890).

(2) Taylor, G. I., Great Britain Advisory Committee for Aeronautics, Reports and Memoranda No. 272, 2, 423-429 (1916-1917).

(3) Prandtl, L., Phys. Z., 29, 487-489 (1928).

(4) von Kármán, Th., Trans. A.S.M.E., 61, 705-710 (1939).

(5) Boelter, L. M. K., Martinelli, R. C., and Jonasson, F., Trans. A.S.M.E., 63, 447-455 (1941).

(6) Martinelli, R. C., Trans. A.S.M.E., 69, 947-959 (1947).

(7) Page, F., Jr., Ph.D. Thesis, California Institute of Technology (1950).

(8) Billman, G. W., Ph.D. Thesis, California Institute of Technology (1948).

(9) Corcoran, W. H., Ph.D. Thesis, California Institute of Technology (1948).

(10) Willis, J. B., Australian Council for Aeronautics Report No. ACA-19 (1945).

(11) American Institute of Physics, Temperature, Its Measurement and Control, Reinhold (1941).

(12) King, L. V., Phil. Trans. Roy. Soc., A116, 170-397 (1927).

(13) Dryden, H. L., N.A.C.A. Technical Report No. 562 (1936).

(14) Ludwieg, H., N.A.C.A. Technical Memorandum No. 1284 (1950).

(15) Baldmotoff, B. A., The Mechanics of Turbulent Flow, Princeton University Press (1936).

(16) Nikuradse, J., V.D.I., Forschungsheft 356 (1932).

(17) Reichardt, H., N.A.C.A. Technical Memorandum No. 1047 (1943).

(18) McAdams, W. H., Heat Transmission, McGraw-Hill (1942).

(19) Saunders, O. A., Fishenden, M., and Mansion, H. D., Engineering, 139, 483 (1935).

List of Figures

1. The Equipment as a Whole.

2. The Essential Parts of the Apparatus.

3. A Cross Section of Oil Baths and Plates.

4. A Micromanometer.

5. The Thermanemometer and a Cross Section of the Oil Baths and the Traversing Gear.

6. The Working Section of the Equipment.

7. The Sliding Blocks Used as Side Walls.

8. The Manometer Bank and the Cathetometer.

9. The Temperature Bench.

10. A Cross Section of One of the Calorimeters.

11. The Region of Contact Between the Copper Plate and the Block-Jacket Assembly.

12. The Calorimeter Vacuum Jackets, Sylphon Bellows, Jacket Cooling Coils, and Oil Jacket.

13. The Calorimeter Radiation Shields.

14. The Assembled Calorimeter Vacuum Jackets, Jacket Cooling Coils, Oil Jacket, and Sylphon Bellows.

15. The Assembled Calorimeter Installed in the Upper Plate.

16. The Calorimeter Cooling System.

17. The Constant Head Device.

18. The Freon Cooler.

19. The Calorimeter Cooling Pad and Liquid Lines. The Lower Part of the Vacuum Jacket. The Stainless Steel Grooved Ring.

20. The Assembled Cooling Pad and the Lower Vacuum Jacket.

21. The Cooling Liquid Thermocouple Wells.

22. The Cooling Line Radiation Shields.

23. The Thermanemometer Circuit.

24. The Temperature Fields of Tests 60 and 61.

25. The Temperature Field of Test 40.

26. The Velocity Profile of Test 60.

27. The Velocity Profile of Test 61.

28. The Eddy Quantities as Functions of y/y_o for Test 60.

29. The Eddy Quantities as Functions of y/y_o for Test 61.

30. Log Pressure Gradient as a Function of Log Average Velocity.

31. u^+ as a Function of Log y^+, Test 60.

32. u^+ as a Function of Log y^+, Test 60. (Revised Definitions of u^* and y^+ Used)

33. u^+ as a Function of Log y^+, Test 61.

34. u^+ as a Function of Log y^+, Test 39.

35. A Cross Section of One of the Calorimeters before the Block Thickness Was Decreased.

36. Log $\frac{\dot{Q}}{\Delta t}$ as a Function of Log Re.

37. Von Kármán's Universal Velocity Distribution.

38. $\left(\frac{\epsilon_m}{(\gamma)_{\frac{y}{y_o}=0.5}}\right)\left(\frac{1}{1-\frac{2y_d}{y_o}}\right)$ as a Function of y^+.

39. $\left(\frac{\epsilon_m}{(\gamma)_{\frac{y}{y_o}=0.5}}\right)\left(\frac{1}{1-\frac{2y_d}{y_o}}\right)$ as a Function of y^+.

40. $\left(\frac{\epsilon_c}{(K)_{\frac{y}{y_o}=0.5}}\right)\left(\frac{1}{1-\frac{2y_d}{y_o}}\right)$ as a Function of y^+.

41. $\left(\frac{\epsilon_c}{(K)_{\frac{y}{y_o}=0.5}}\right)\left(\frac{1}{1-\frac{2y_d}{y_o}}\right)$ as a Function of y^+.

42. $\text{Log}\left\{\left(\frac{\epsilon_m}{(\nu)_{\frac{y}{y_o}=0.5}}\right)\left(\frac{1}{1-\frac{2y_d}{y_o}}\right)\right\}$ as a Function of $\text{Log } y^+$.

43. $\text{Log}\left\{\left(\frac{\epsilon_c}{(K)_{\frac{y}{y_o}=0.5}}\right)\left(\frac{1}{1-\frac{2y_d}{y_o}}\right)\right\}$ as a Function of $\text{Log } y^+$.

44. $\text{Log}\ \frac{\epsilon_m}{(\nu)_{y/y_o=0.5}}$ as a Function of $\text{Log } y^+$ for Test 60.

45. $\text{Log}\ \frac{\epsilon_c}{(K)_{y/y_o=0.5}}$ as a Function of $\text{Log } y^+$ for Test 60.

46. $\frac{\epsilon_c}{\epsilon_m}\ P_r$ as a Function of y^+.

47. $\frac{\epsilon_c}{\epsilon_m}\ P_r$ as a Function of y^+, Test 46.

48. $\frac{\epsilon_c}{\epsilon_m}\ P_r$ as a Function of y^+, Test 60.

49. Comparison of Total Viscosities of Tests 60 and 61.

50. Comparison of Total Conductivities of Tests 60 and 61.



Figure 1. The Equipment as a Whole

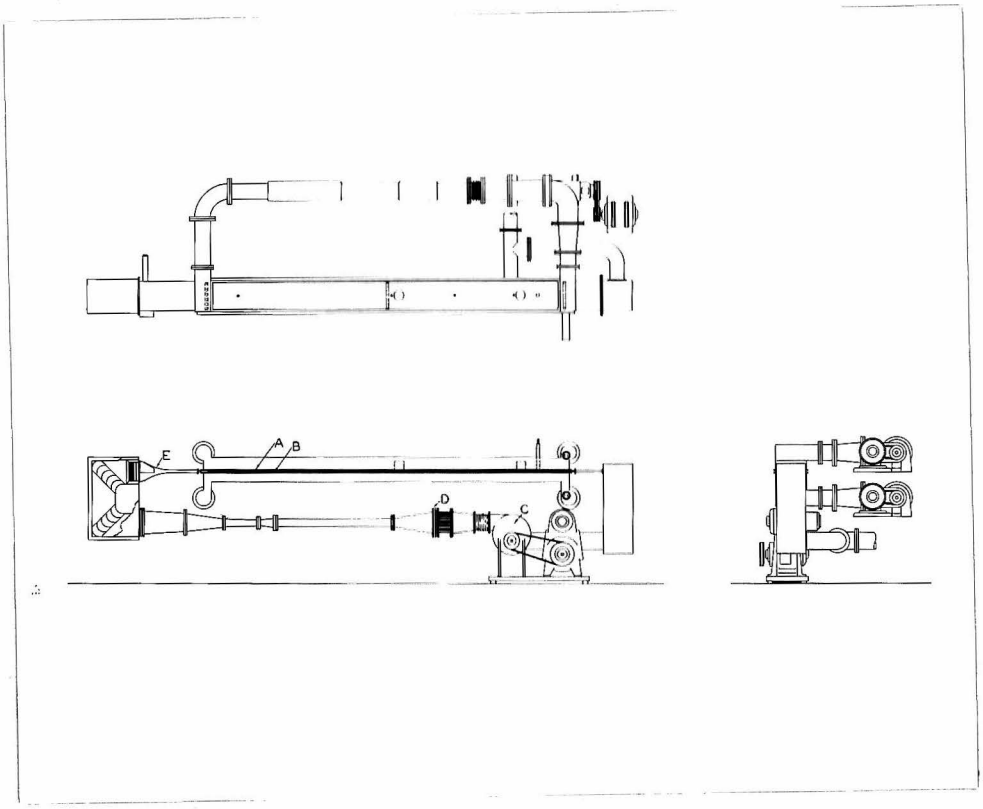

Figure 2. The Essential Parts of the Apparatus

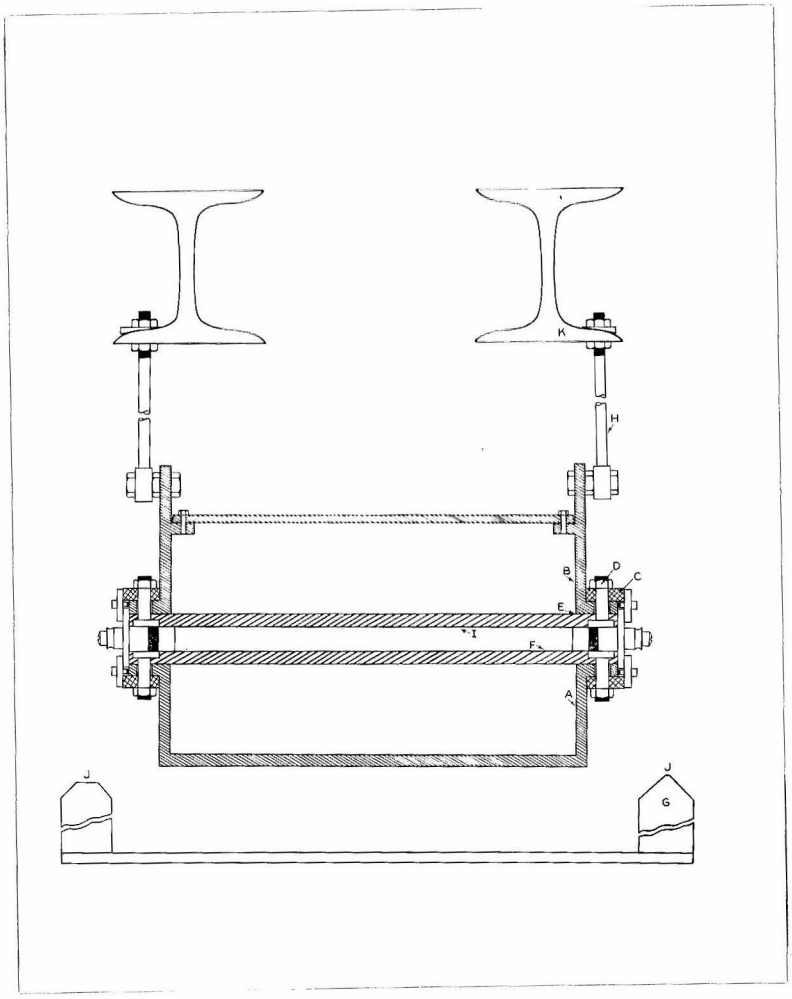

Figure 3. A Cross Section of Oil Baths and Plates

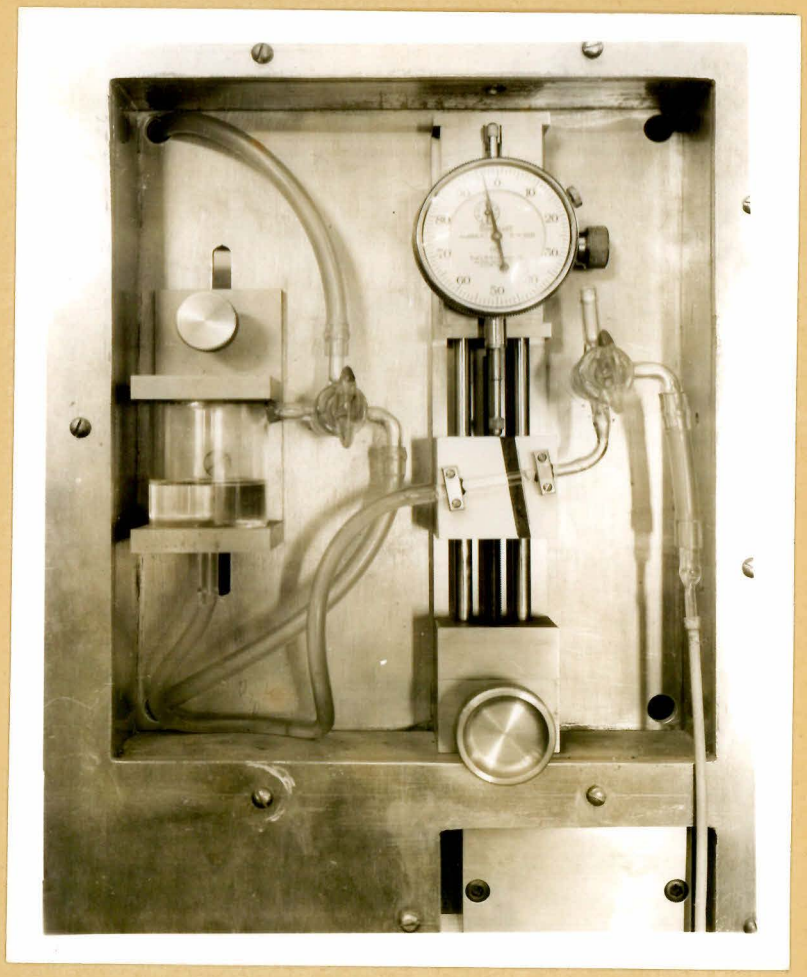

Figure 4. A Micromanometer

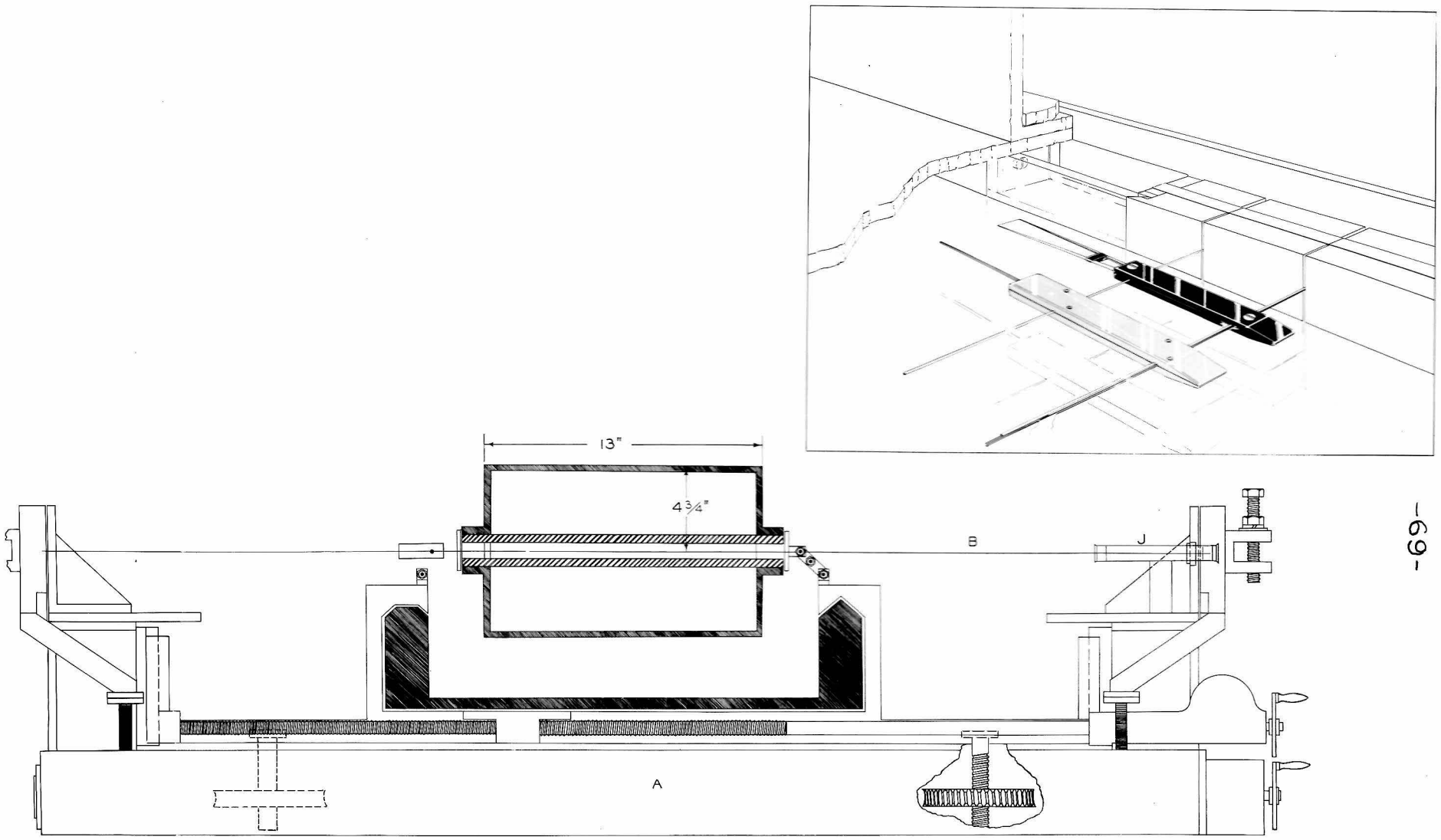

Figure 5. The Thermanemometer and a Cross Section of the Oil Baths and the Traversing Gear

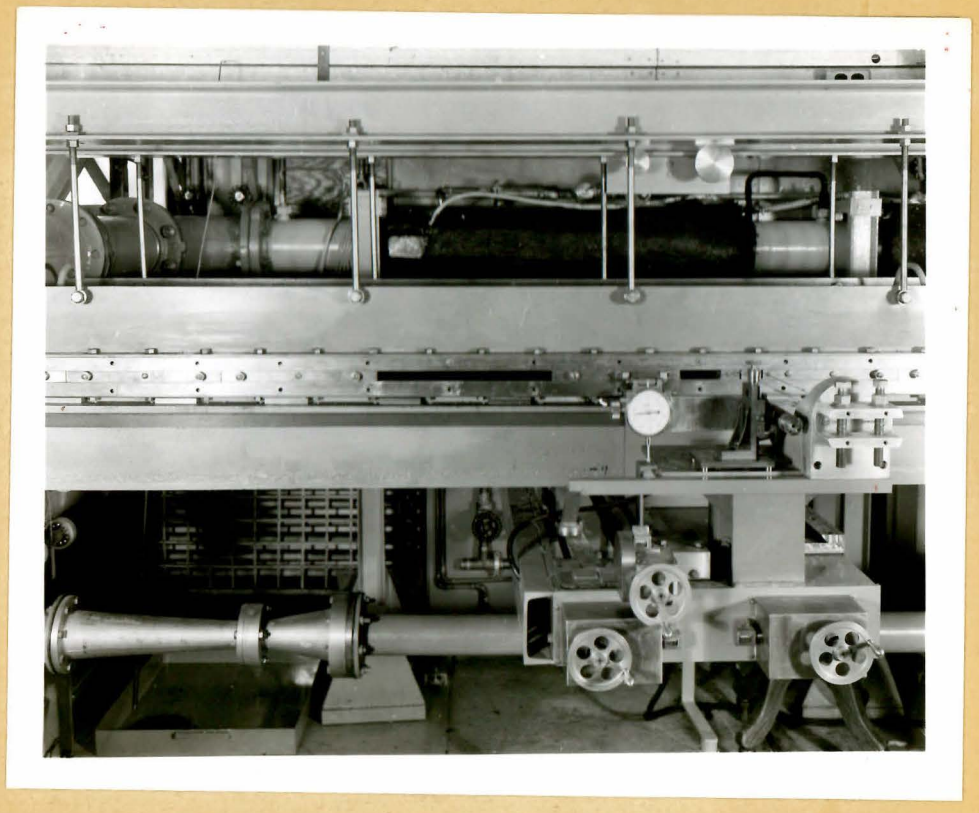

Figure 6. The Working Section of the Equipment

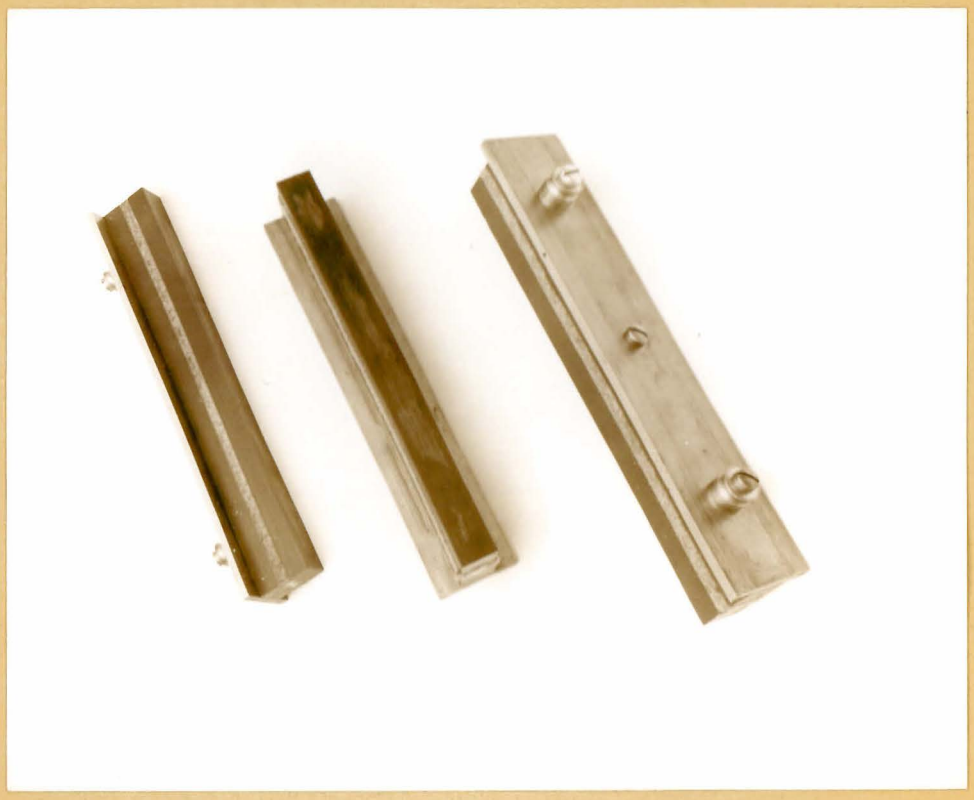

Figure 7. The Sliding Blocks Used as Side Walls

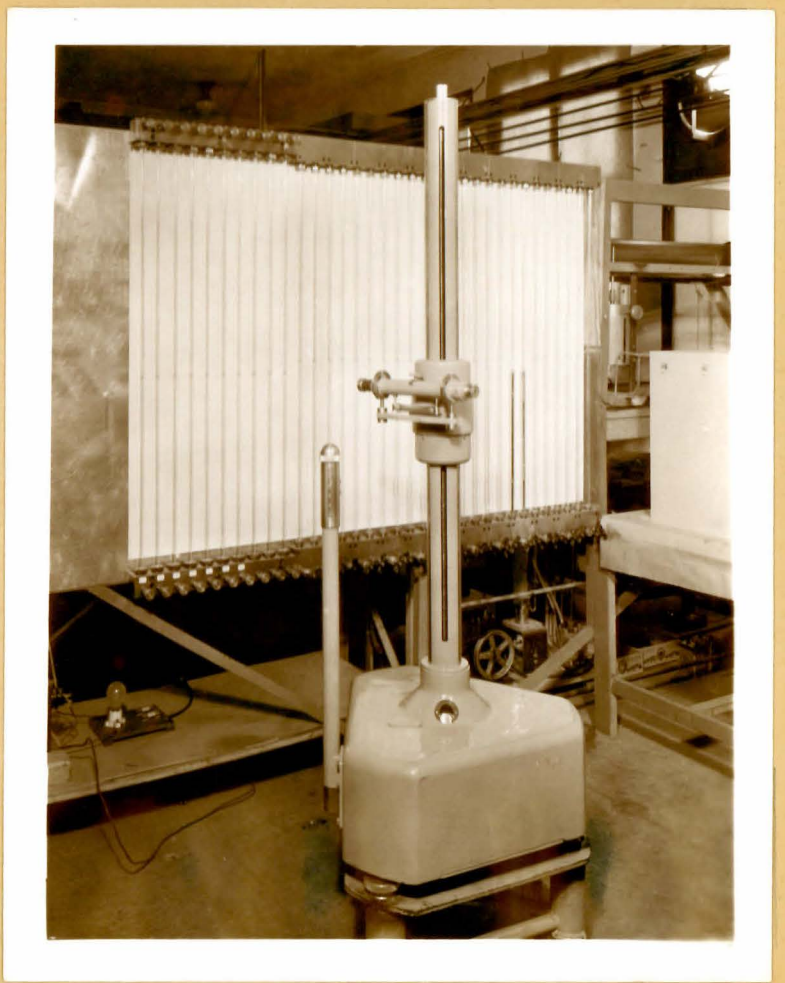

Figure 8. The Manometer Bank and the Cathetometer

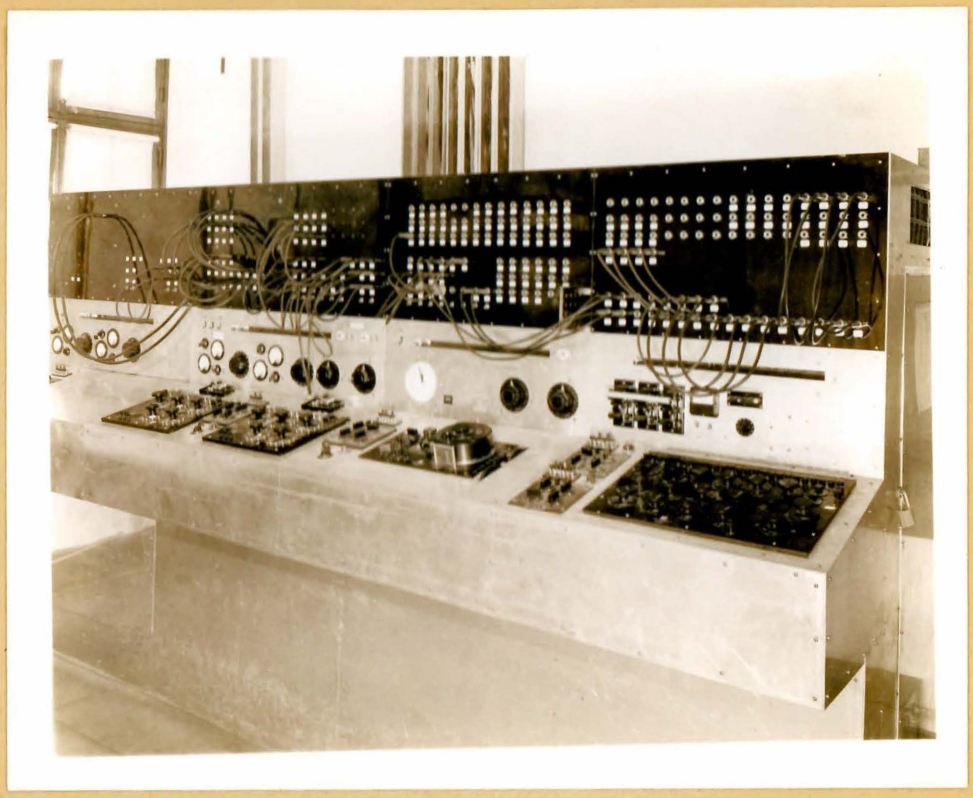

Figure 9. The Temperature Bench

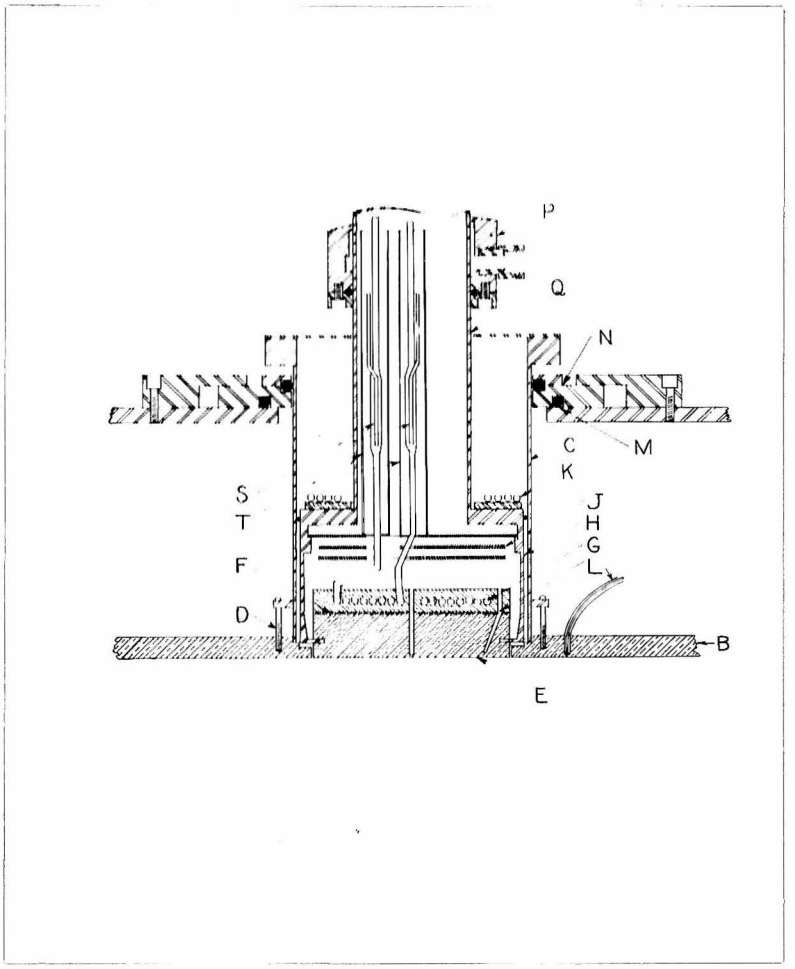

Figure 10. A Cross Section of One of the Calorimeters

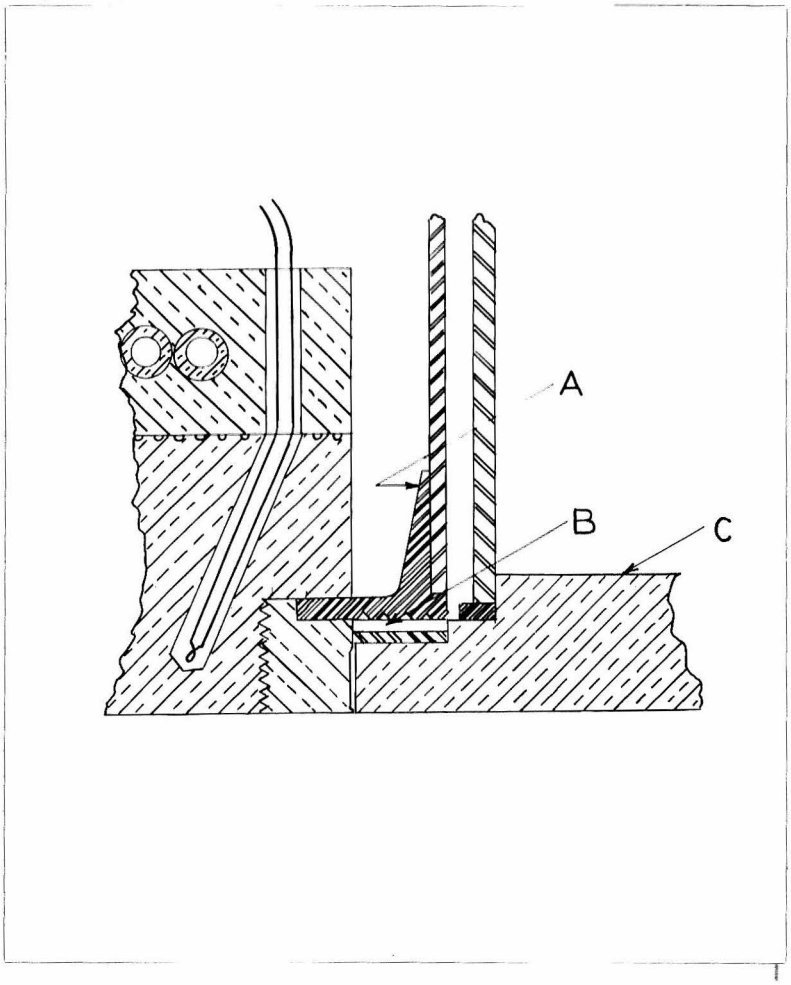

Figure 11. The Region of Contact between the Copper Plate and the Block-Jacket Assembly



Figure 12. The Calorimeter Vacuum Jackets, Sylphon Bellows, Jacket Cooling Coils, and Oil Jacket

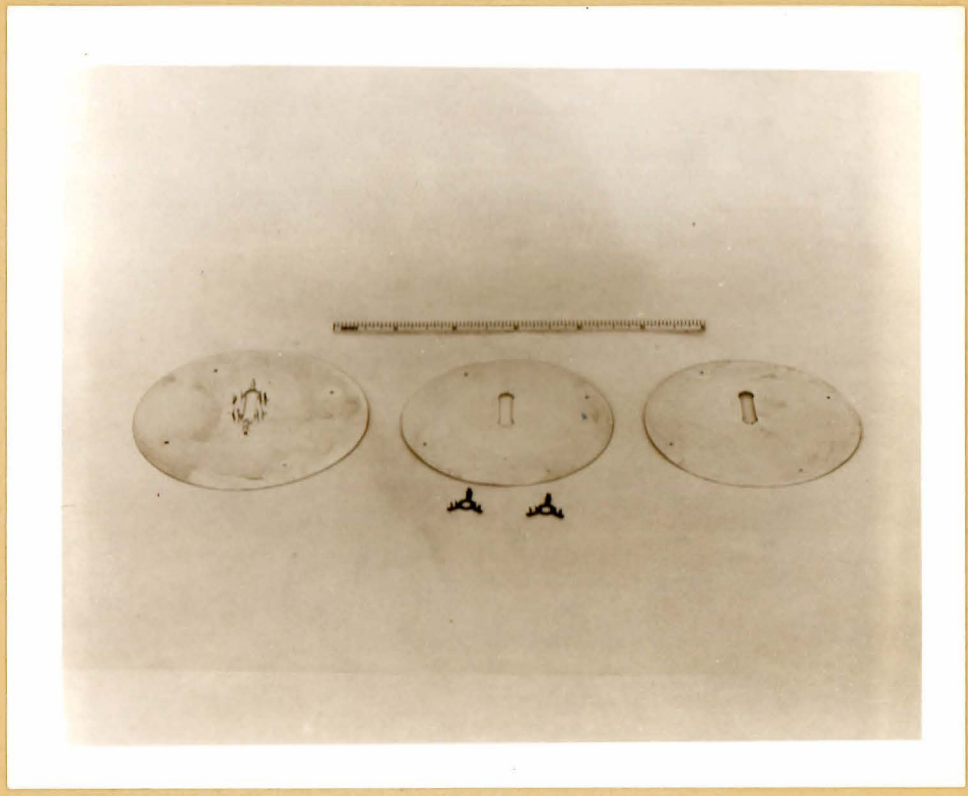

Figure 13. The Calorimeter Radiation Shields



Figure 14. The Assembled Calorimeter Vacuum Jackets, Jacket Cooling Coils, Oil Jacket, and Sylphon Bellows

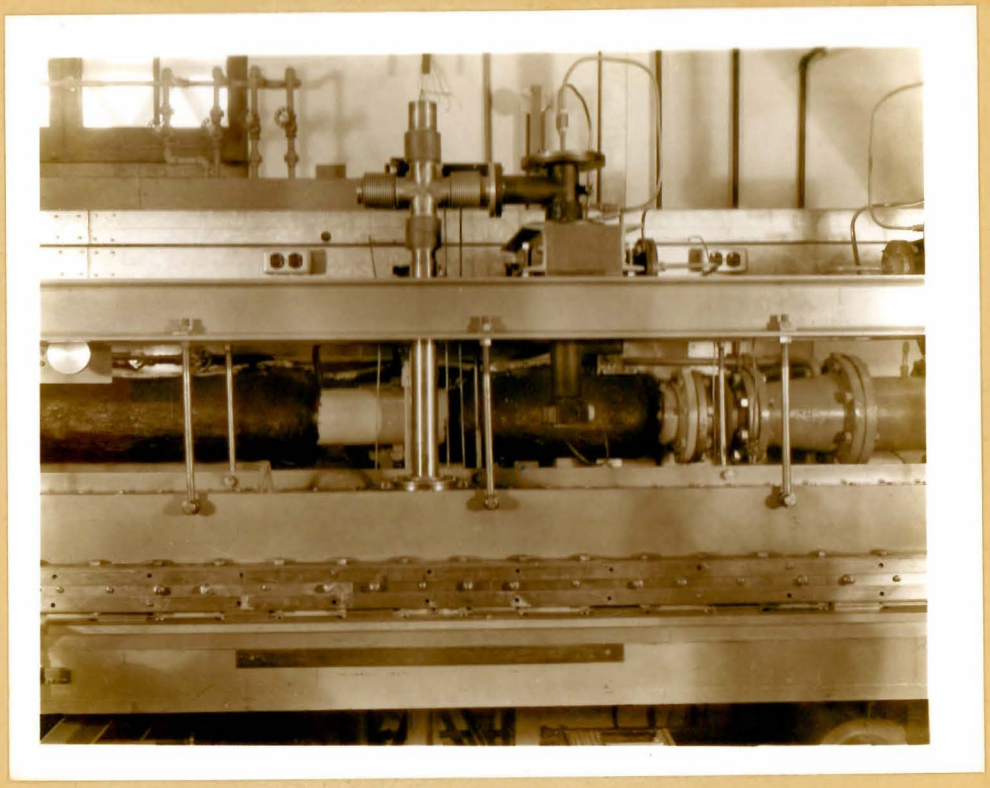

Figure 15. The Assembled Calorimeter Installed in the Upper Plate

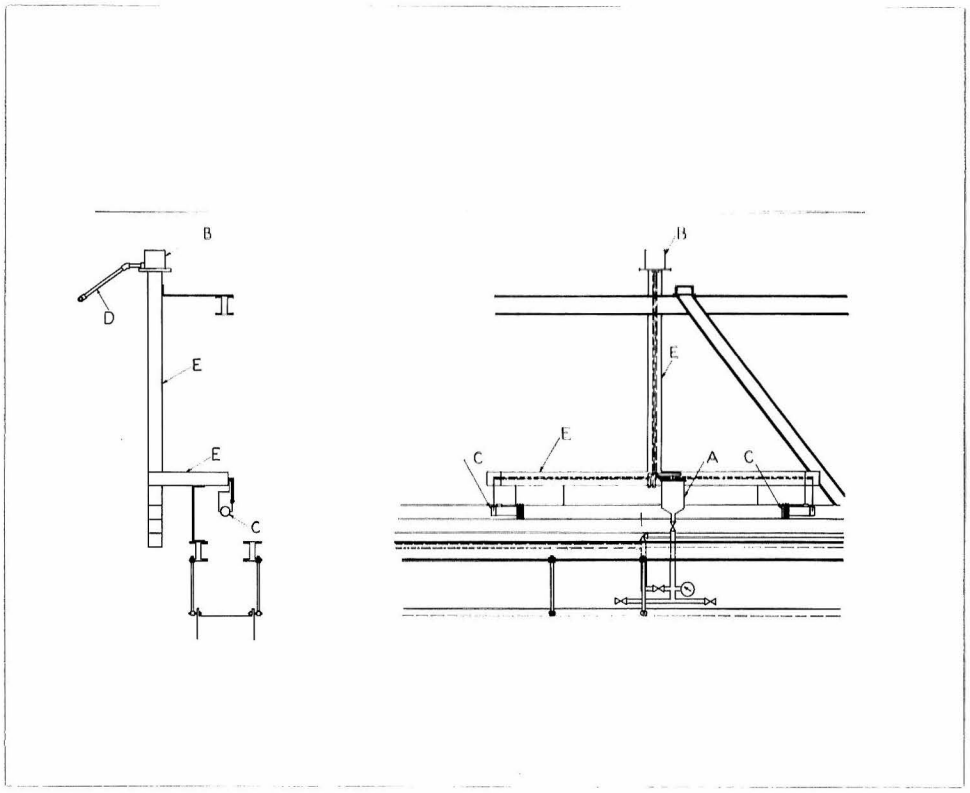

Figure 16. The Calorimeter Cooling System

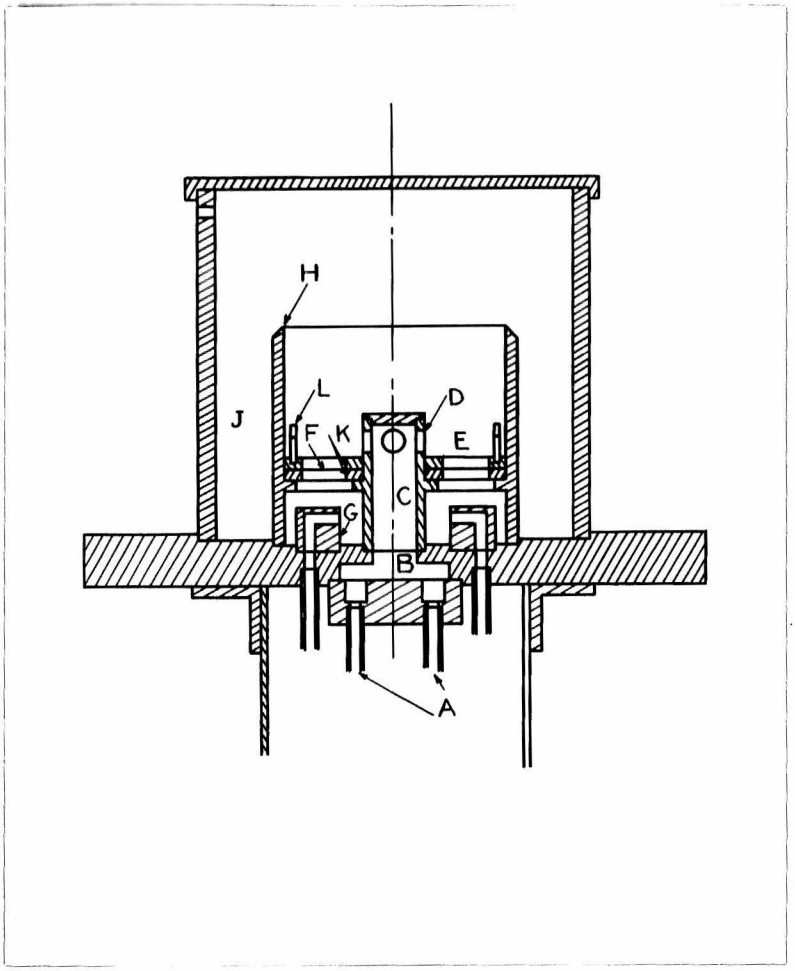

Figure 17. The Constant Head Device

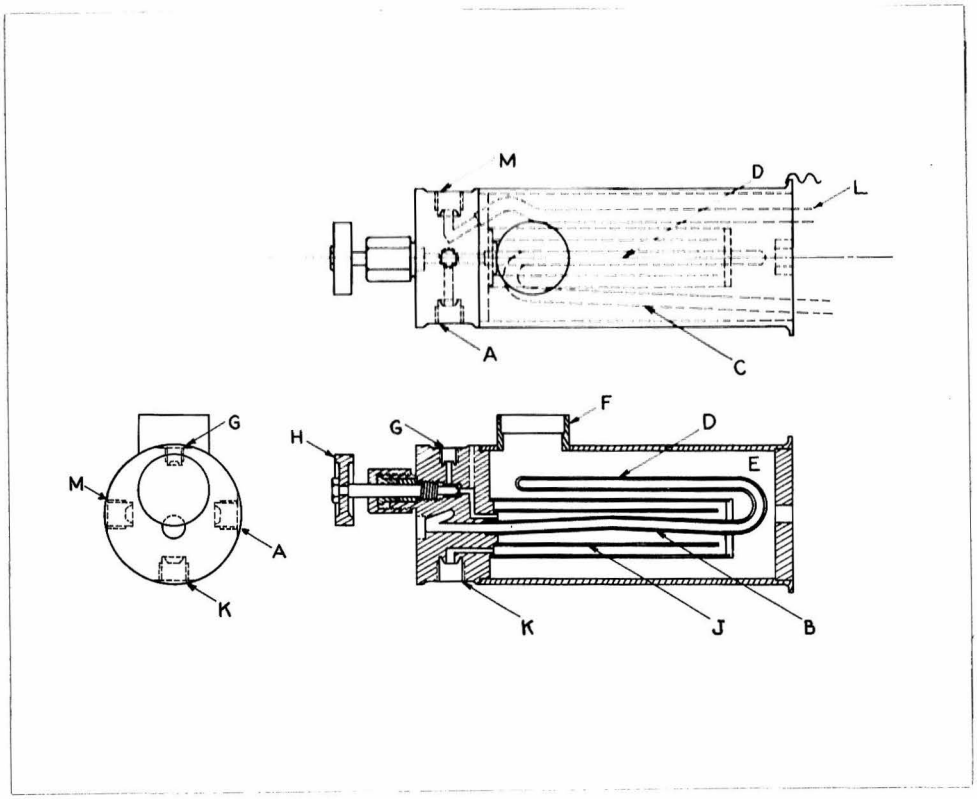

Figure 18. The Freon Cooler

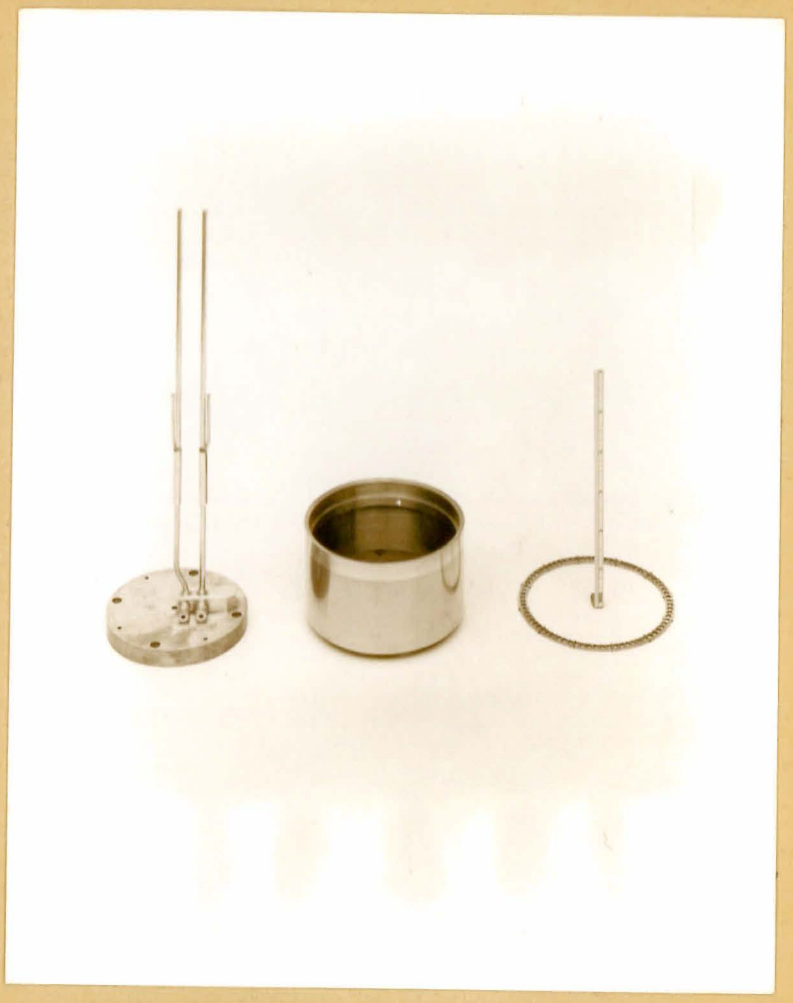

Figure 19. The Calorimeter Cooling Pad and Liquid Lines. The Lower Part of the Vacuum Jacket. The Stainless Steel Grooved Ring

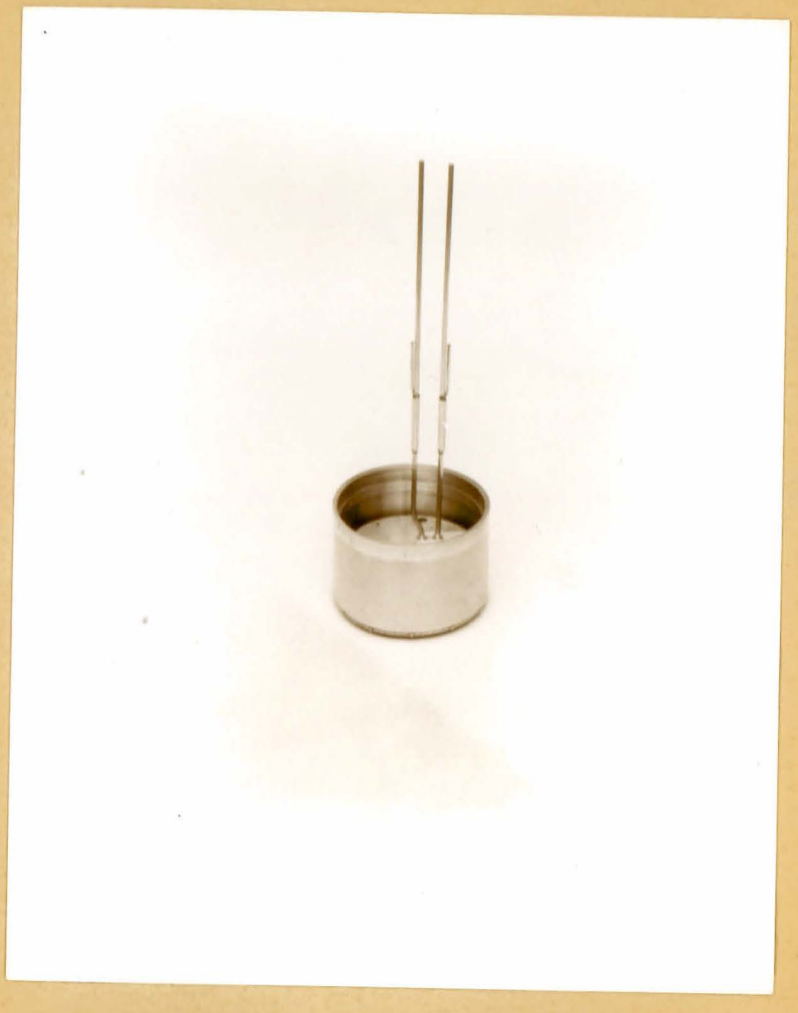

Figure 20. The Assembled Cooling Pad and the Lower Vacuum Jacket

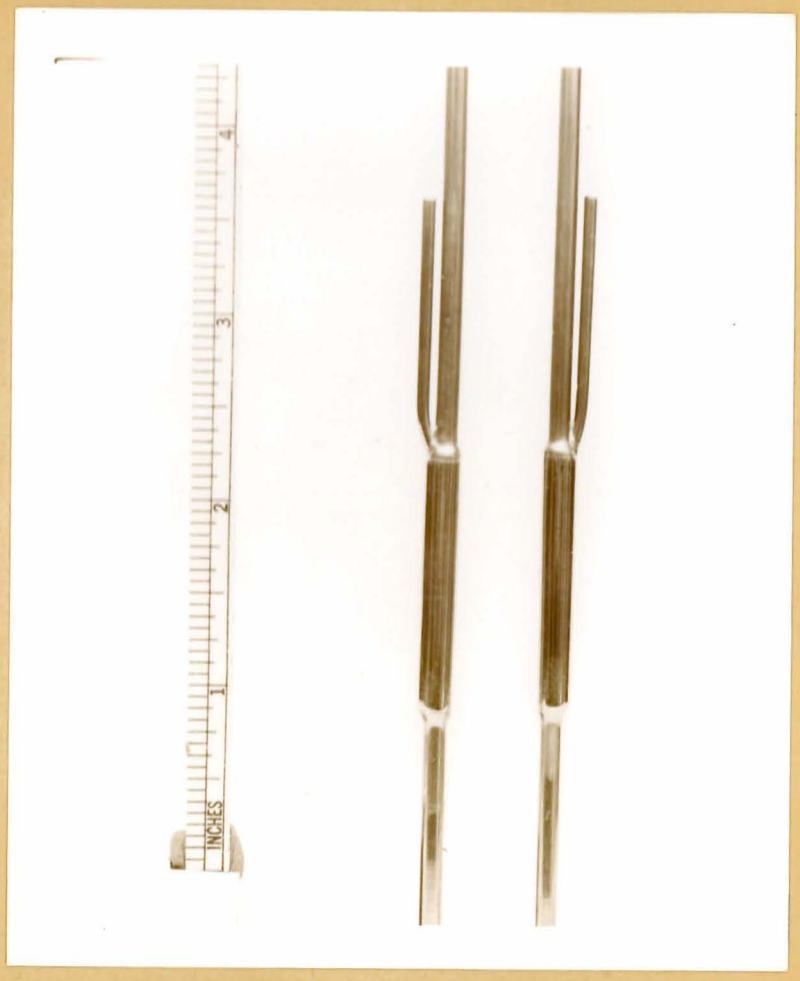

Figure 21. The Cooling Liquid Thermocouple Wells

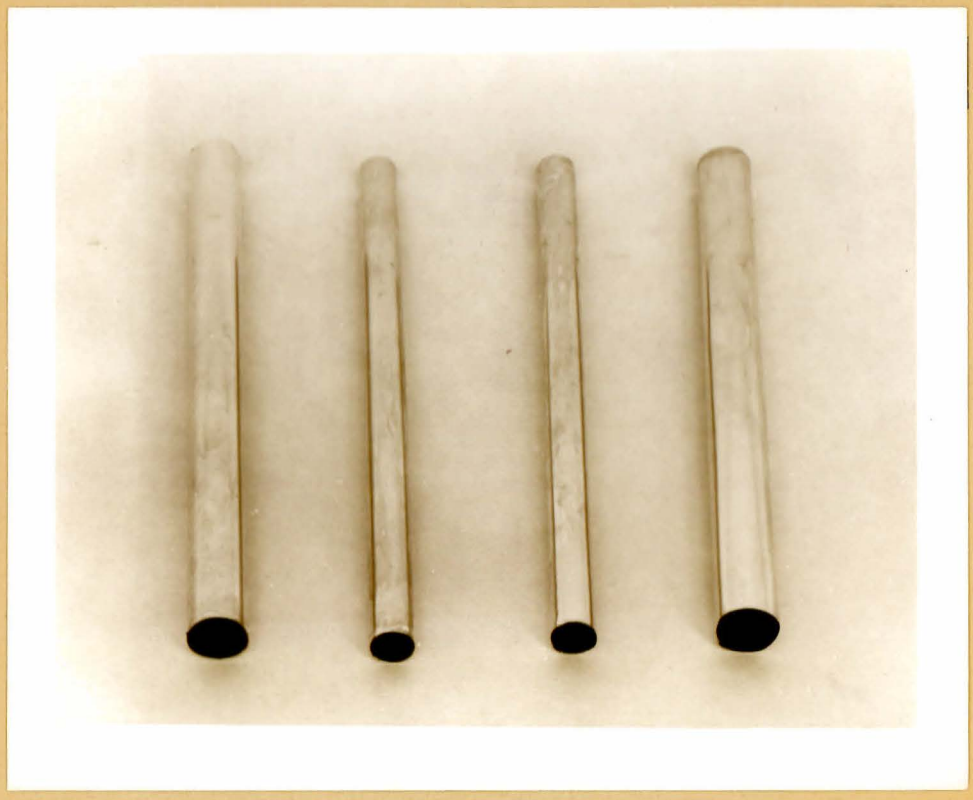

Figure 22. The Cooling Line Radiation Shields

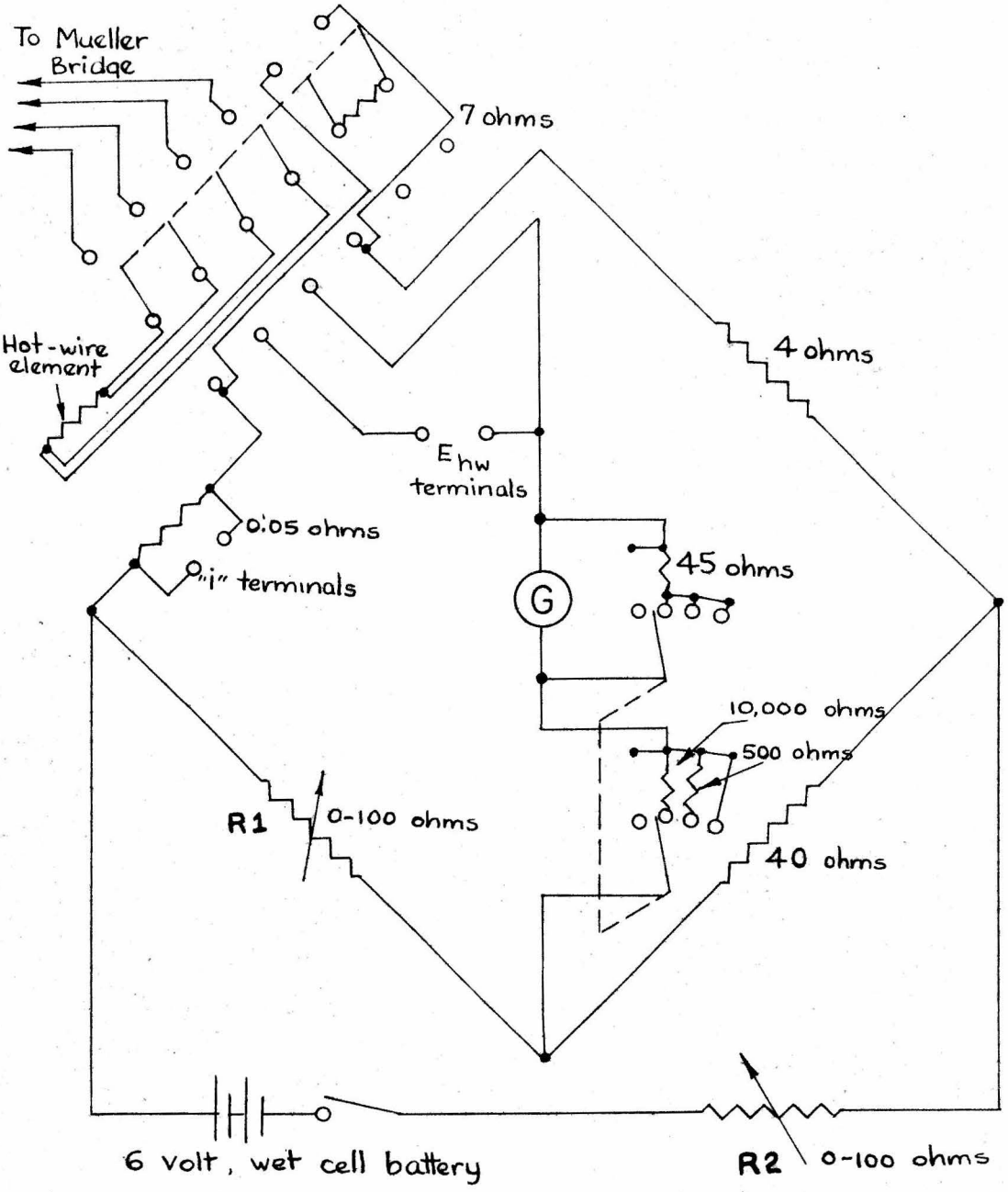

FIGURE 23

THE THERMANEMOMETER CIRCUIT

Figure 24

The Temperature Fields of Tests 60 and 61

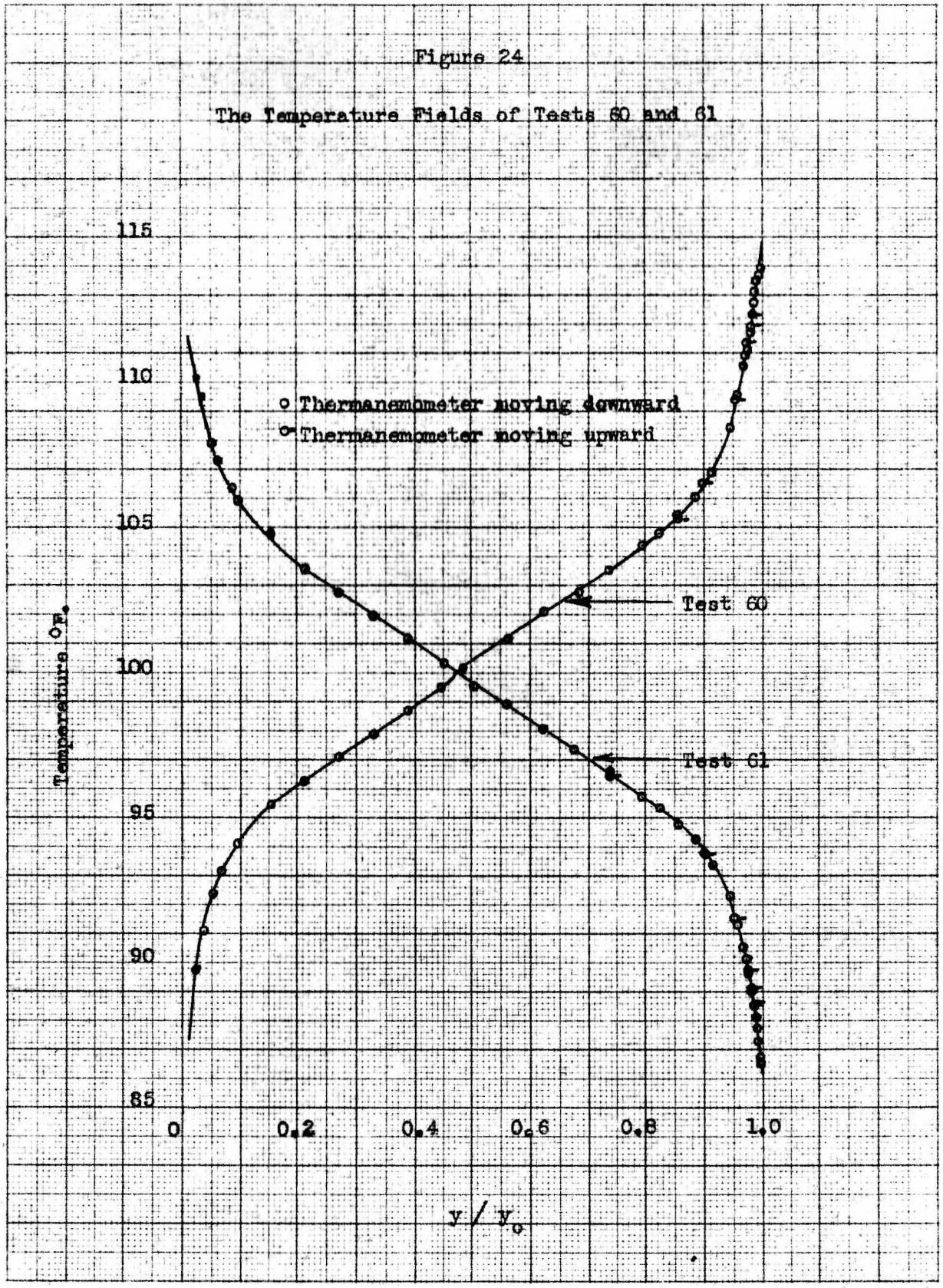

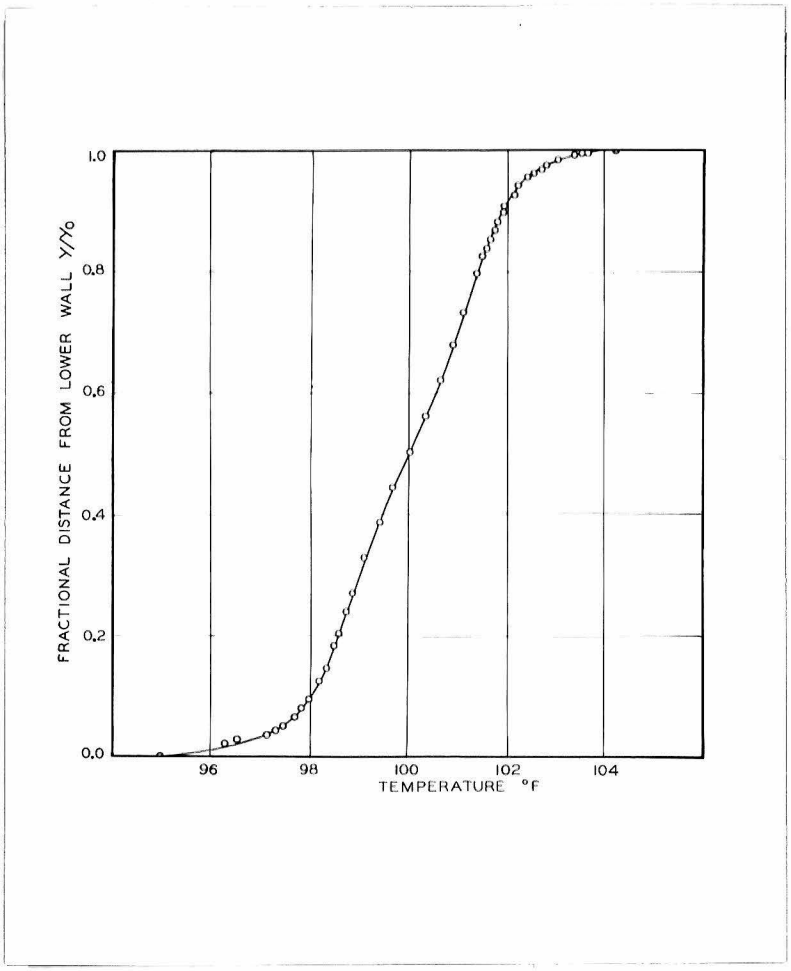

Figure 25. The Temperature Field of Test 40

Figure 26

The Velocity Profile of Test 60

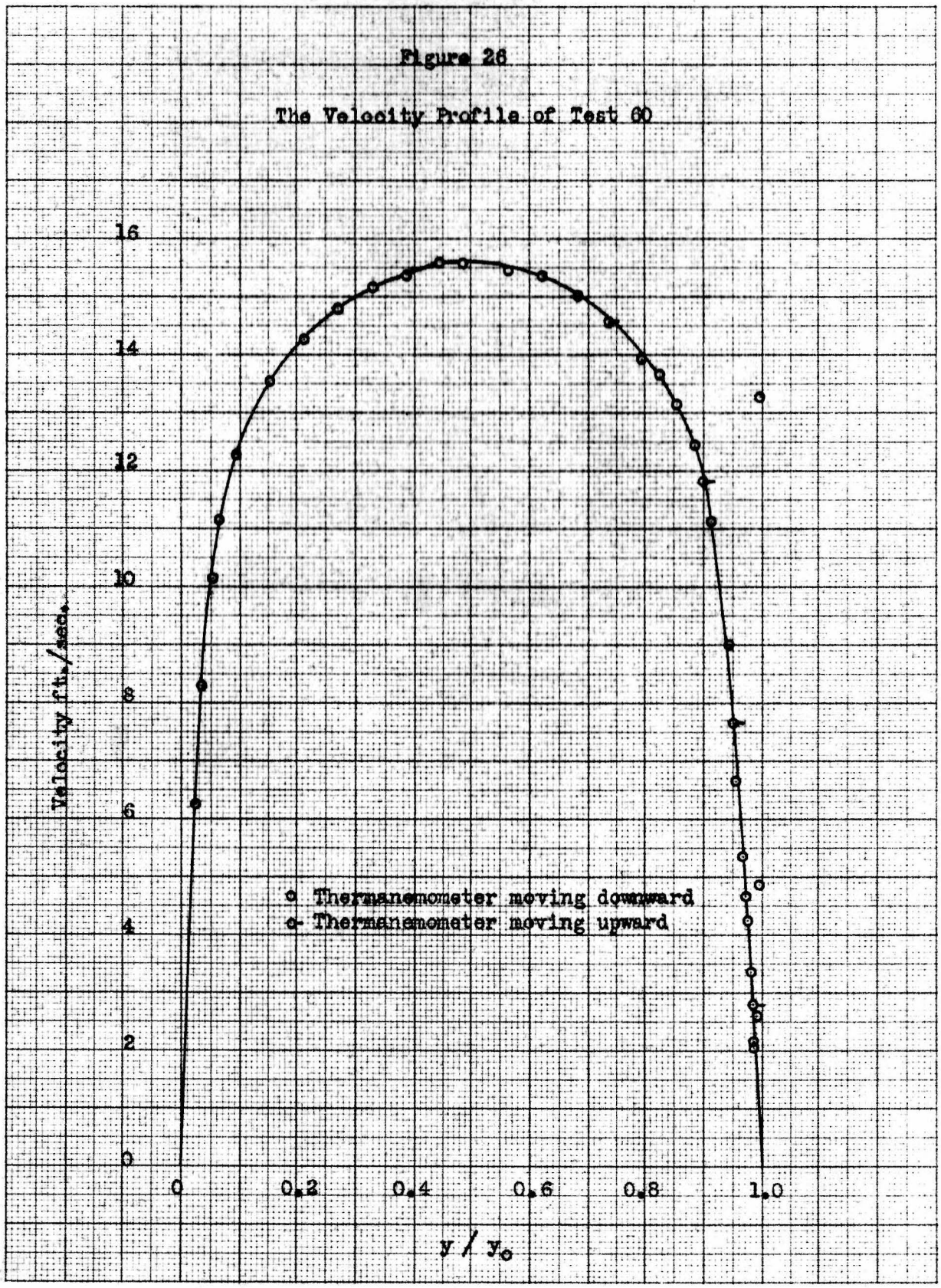

CLEARPRINT PAPER CO. 739 MILLIMETERS BOTH WAYS 160 x 220 DIVISIONS
PRINTED IN U.S.A. ON CLEARPRINT TECHNICAL PAPER NO. 1000H

Figure 27

The Velocity Profile of Test 61

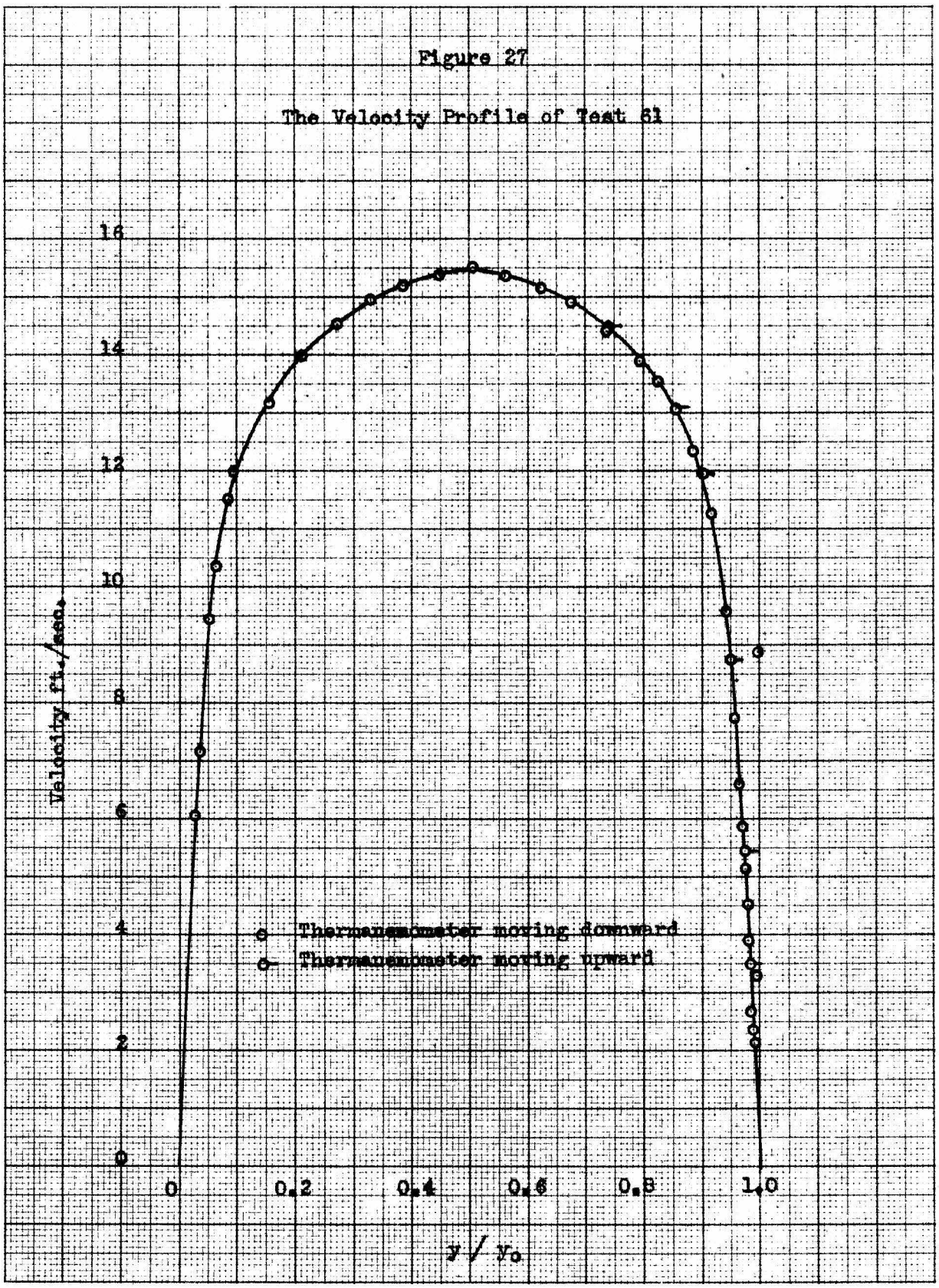

CLEARPRINT PAPER CO. 739 MILLIMETERS BOTH WAYS 180 X 250 DIVISIONS
PRINTED IN U.S.A. ON CLEARPRINT TECHNICAL PAPER NO. 1000H

CLEARPRINT PAPER CO 1539 N. LUNEWAYS BOTH WAYS 180 X 220 DIVISIONS
PRINTED IN U.S.A. ON CLEARPRINT TECHNICAL PAPER NO. 1000H

Figure 28
The Eddy Quantities as Functions of y / y_o for Test 60

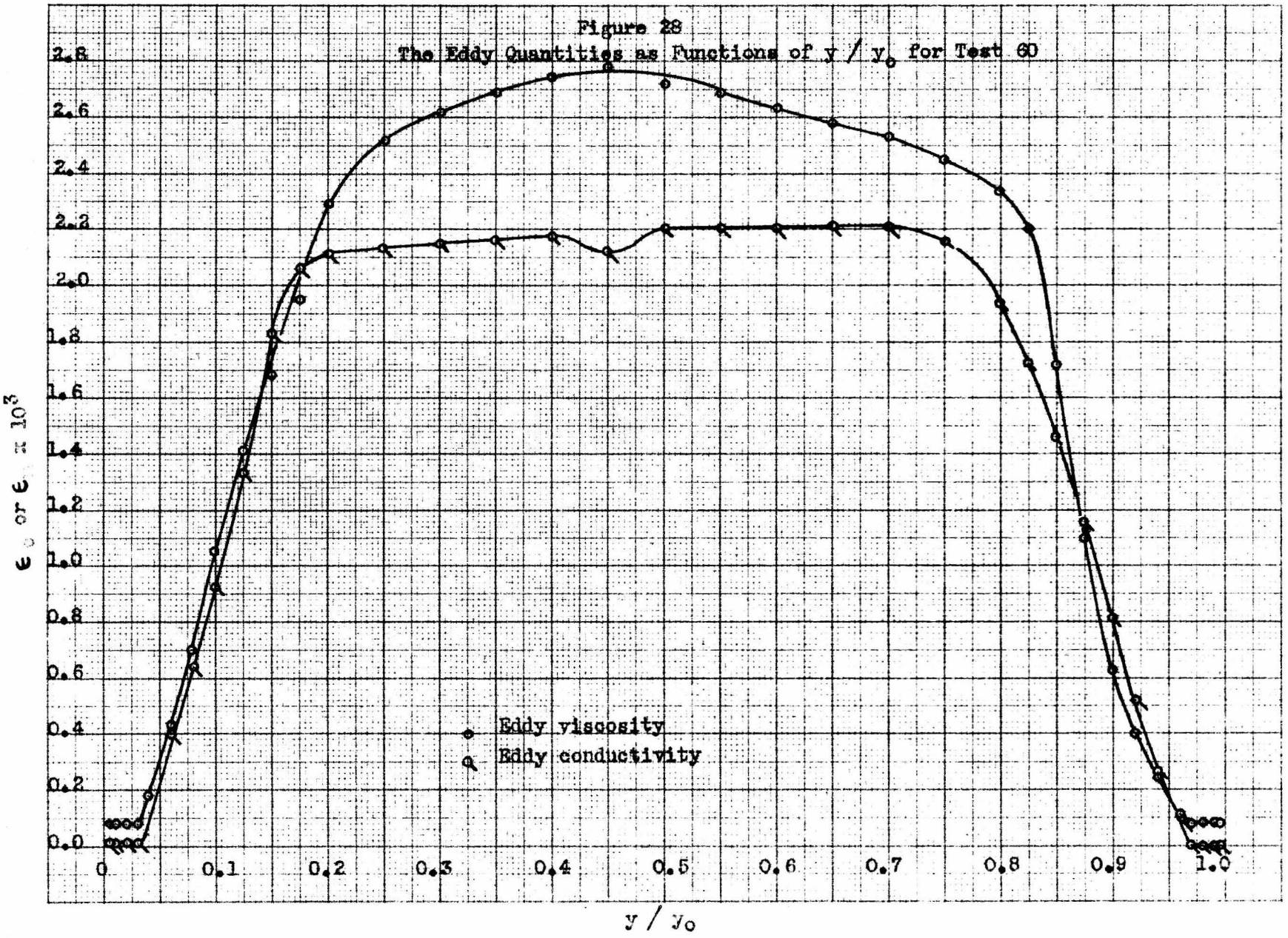

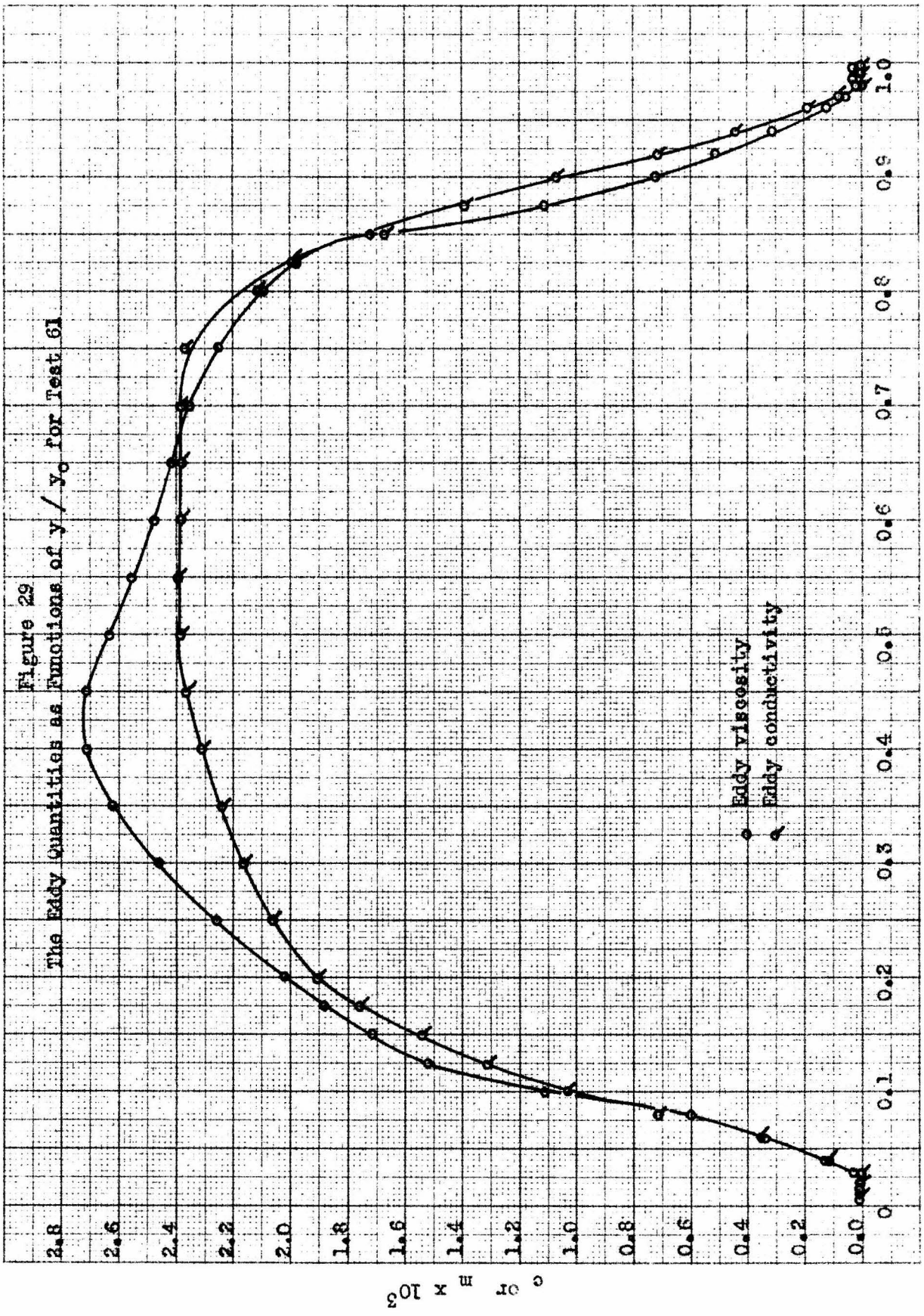
Figure 29
The Eddy Quantities as Functions of y / y_o for Test 61
Eddy viscosity
Eddy conductivity
e or m x 10^3
y / y_o
0.0
0.2
0.4
0.6
0.8
1.0
1.2
1.4
1.6
1.8
2.0
2.2
2.4
2.6
2.8
0
0.1
0.2
0.3
0.4
0.5
0.6
0.7
0.8
0.9
1.0

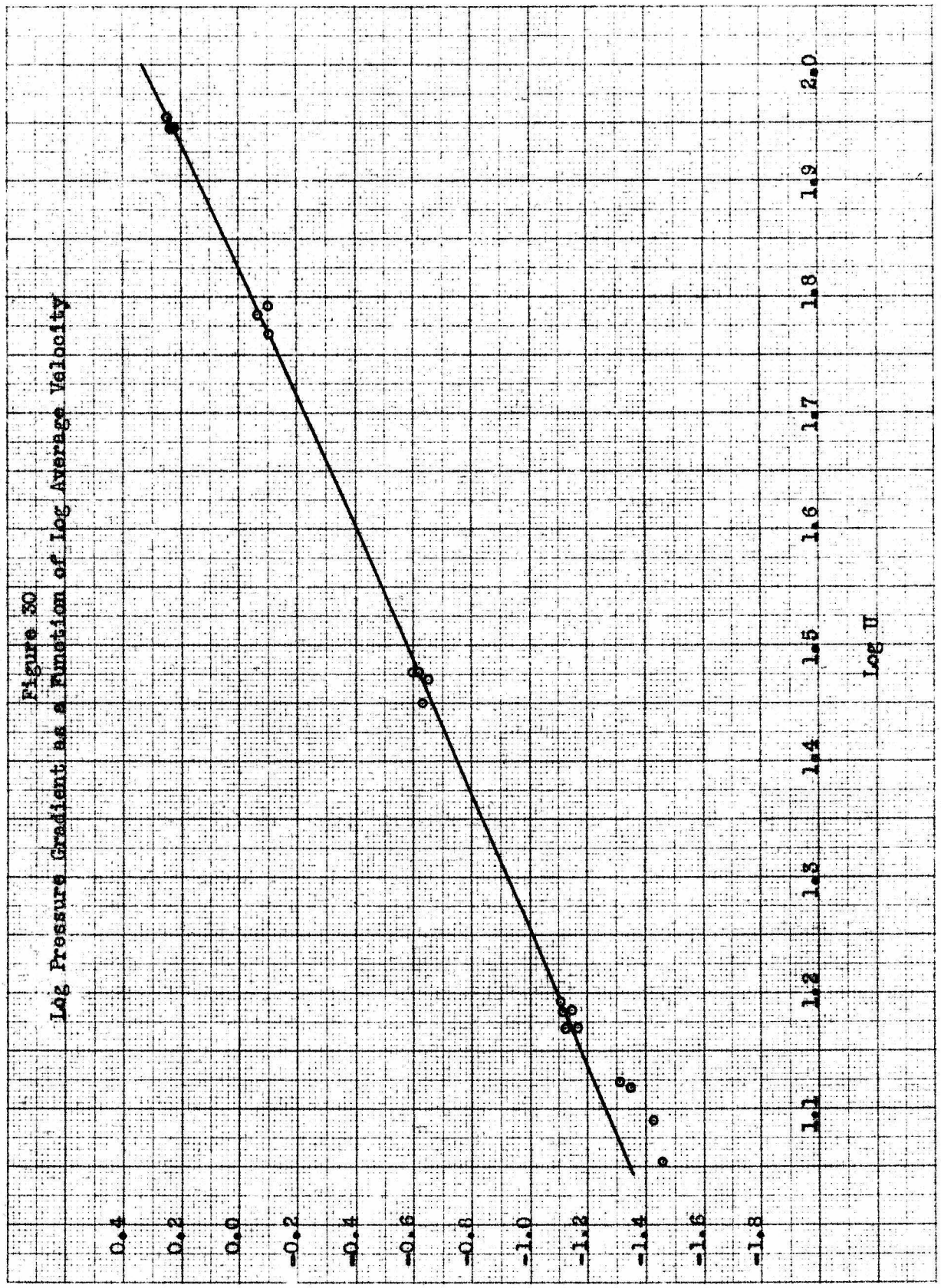

Figure 30
Log Pressure Gradient as a Function of Log Average Velocity

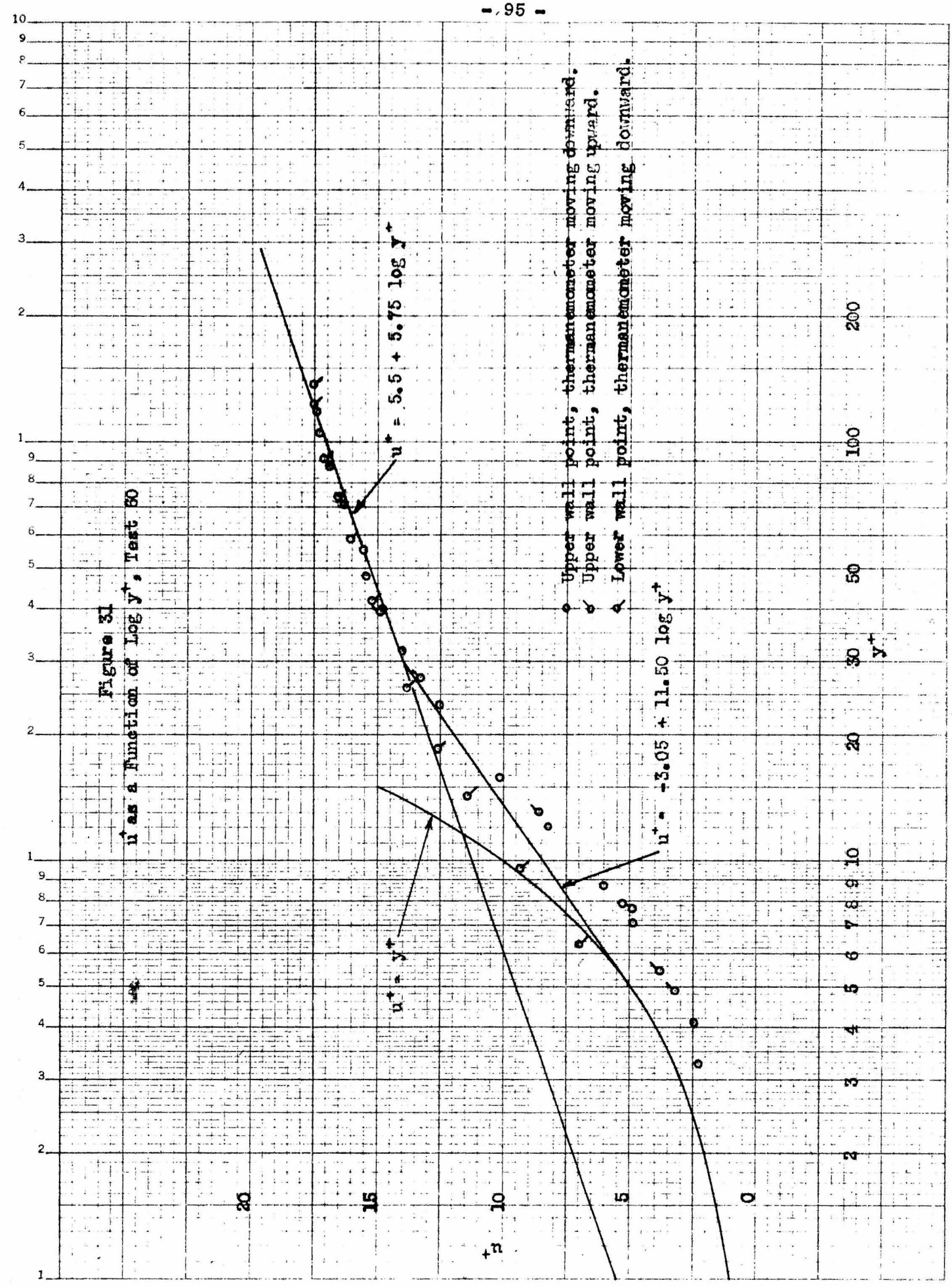

Figure 31
u^+ as a Function of Log y^+, Test 60

KEUFFEL & ESSER CO., N. Y. NO. 359-71
Semi-Logarithmic, 5 Cycles × 10 to the inch, 5th line accented.
MADE IN U. S. A.

KEUFFEL & ESSER CO., N. Y. NO. 389-71
Semi-Logarithmic, 3 Cycles X 10 to the Inch. 5th lines accented.
MADE IN U. S. A.

Figure 32
u^+ as a Function of Log y^+, Test 60
(Revised Definitions of u^* and y^+ Used.)

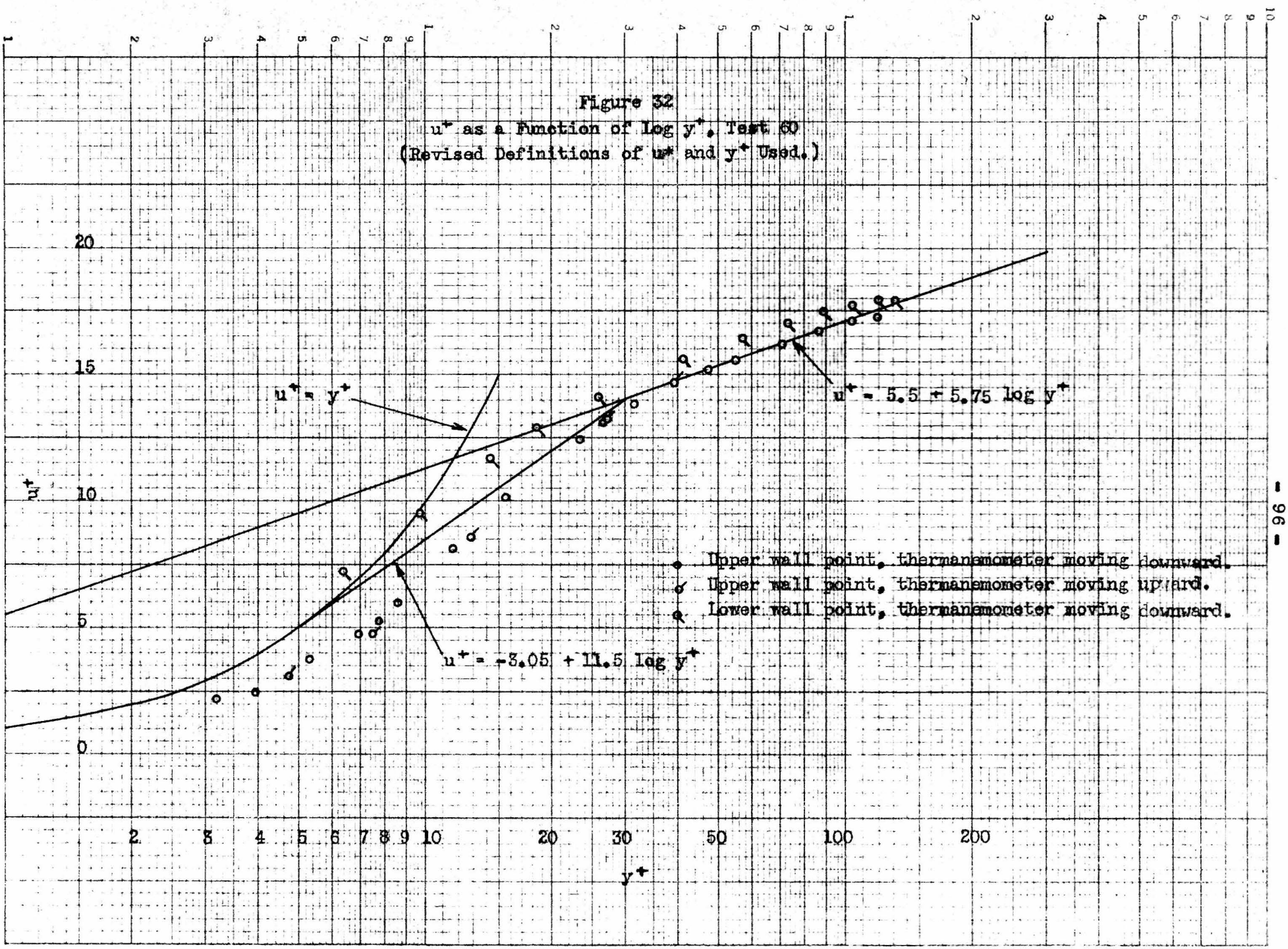

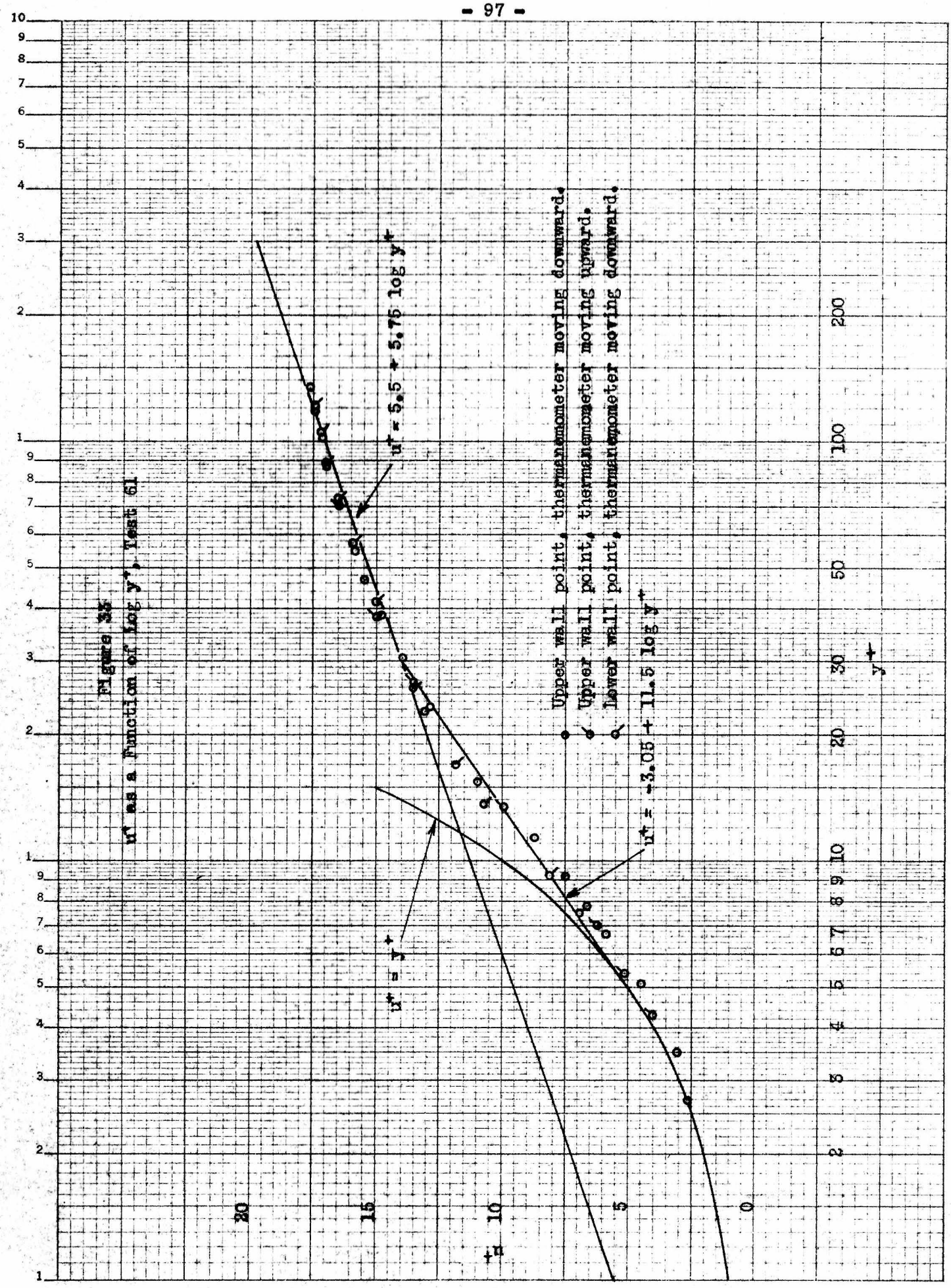

Figure 33
u^+ as a function of $\log y^+$, Test 61

KEUFFEL & ESSER CO., N. Y. NO. 359-71
Semi-Logarithmic, 3 Cycles × 70 to the inch, 5th lines accented.
MADE IN U. S. A.

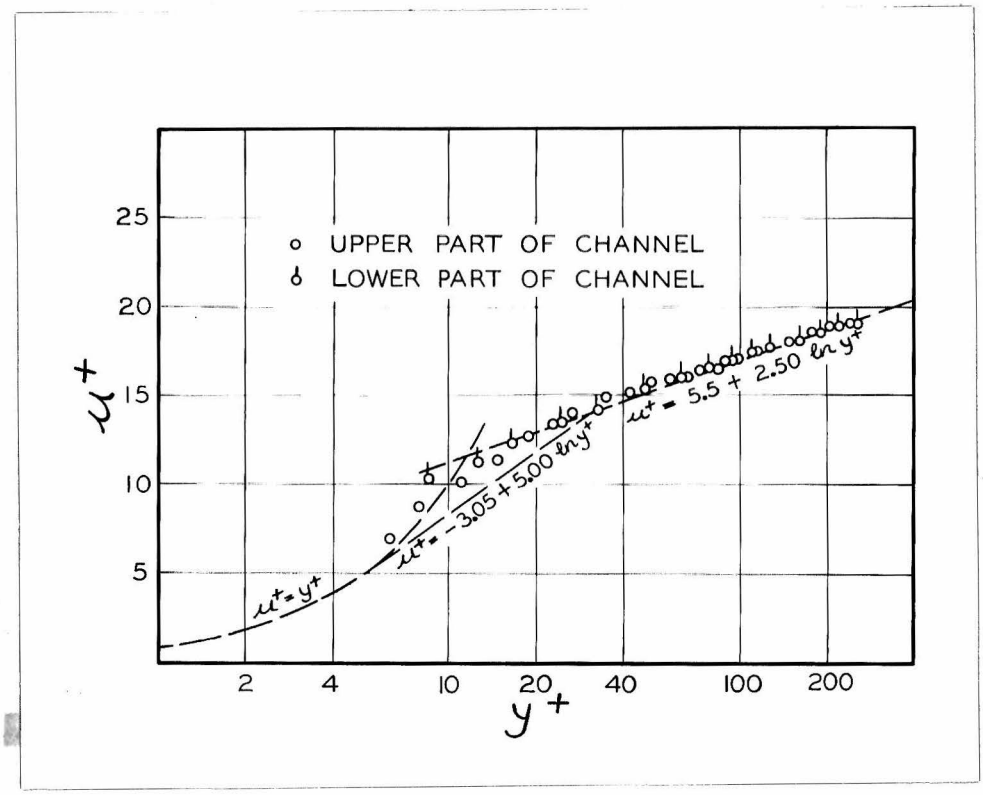

Figure 34. u^+ as a Function of Log y^+, Test 39

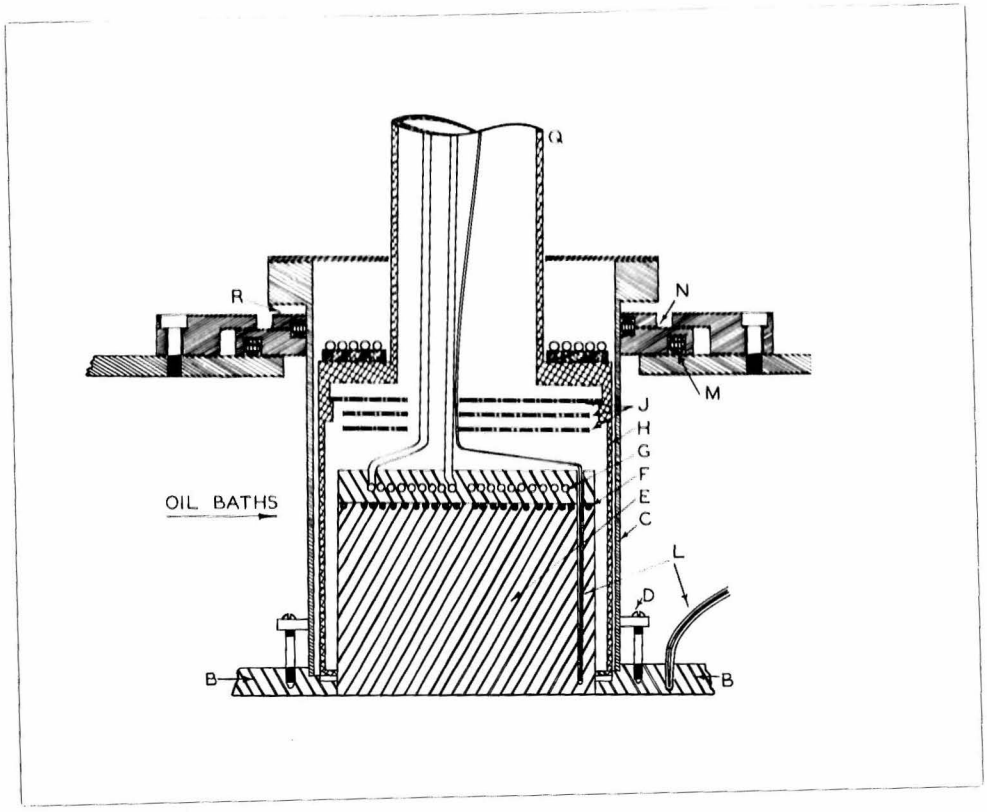

Figure 35. A Cross Section of One of the Calorimeters Before the Block Thickness Was Decreased

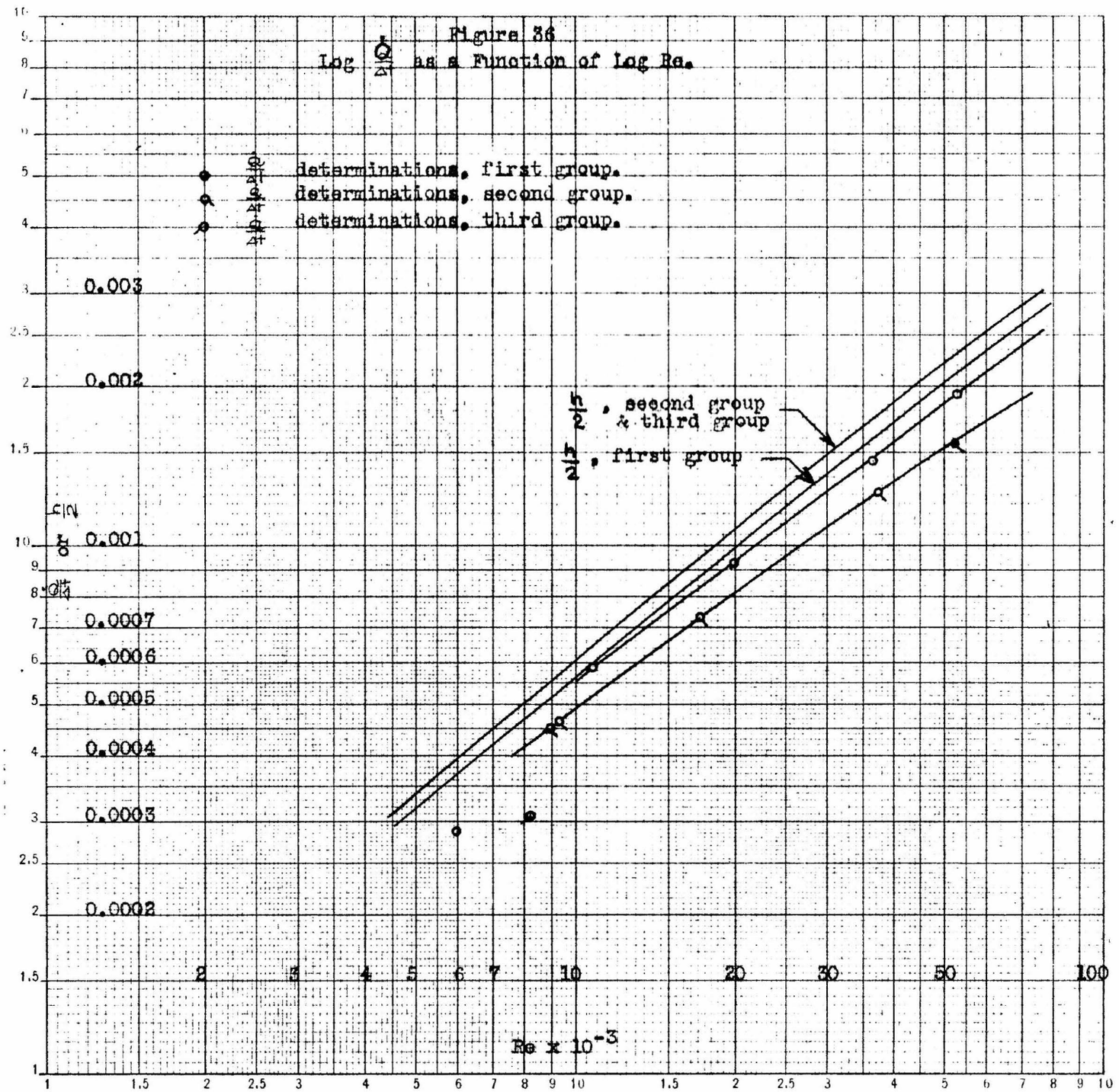
Figure 36
Log $\frac{Q}{\Delta T}$ as a Function of Log Re.
$\frac{Q}{\Delta T}$ determinations, first group.
$\frac{Q}{\Delta T}$ determinations, second group.
$\frac{Q}{\Delta T}$ determinations, third group.
$\frac{h}{2}$, second group & third group
$\frac{h}{2}$, first group
$\frac{h}{2}$
0.003
0.002
0.001
0.0007
0.0006
0.0005
0.0004
0.0003
0.0002
$\frac{Q}{\Delta T}$
Re x 10^{-3}

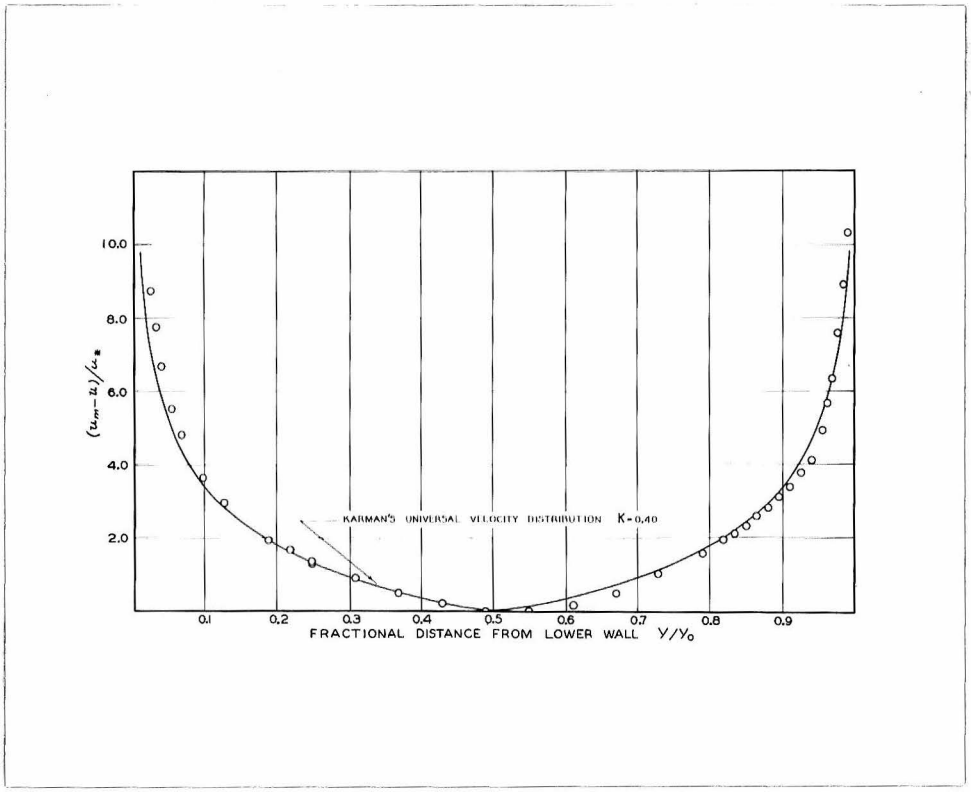

Figure 37. Von Karman's Universal Velocity Distribution

Figure 38

$\left[\frac{\epsilon_m}{(\nu)_{r/r_o=0.5}}\right]\left[\frac{1}{1-\frac{2y^+}{y^+_o}}\right]$ as a Function of y^+

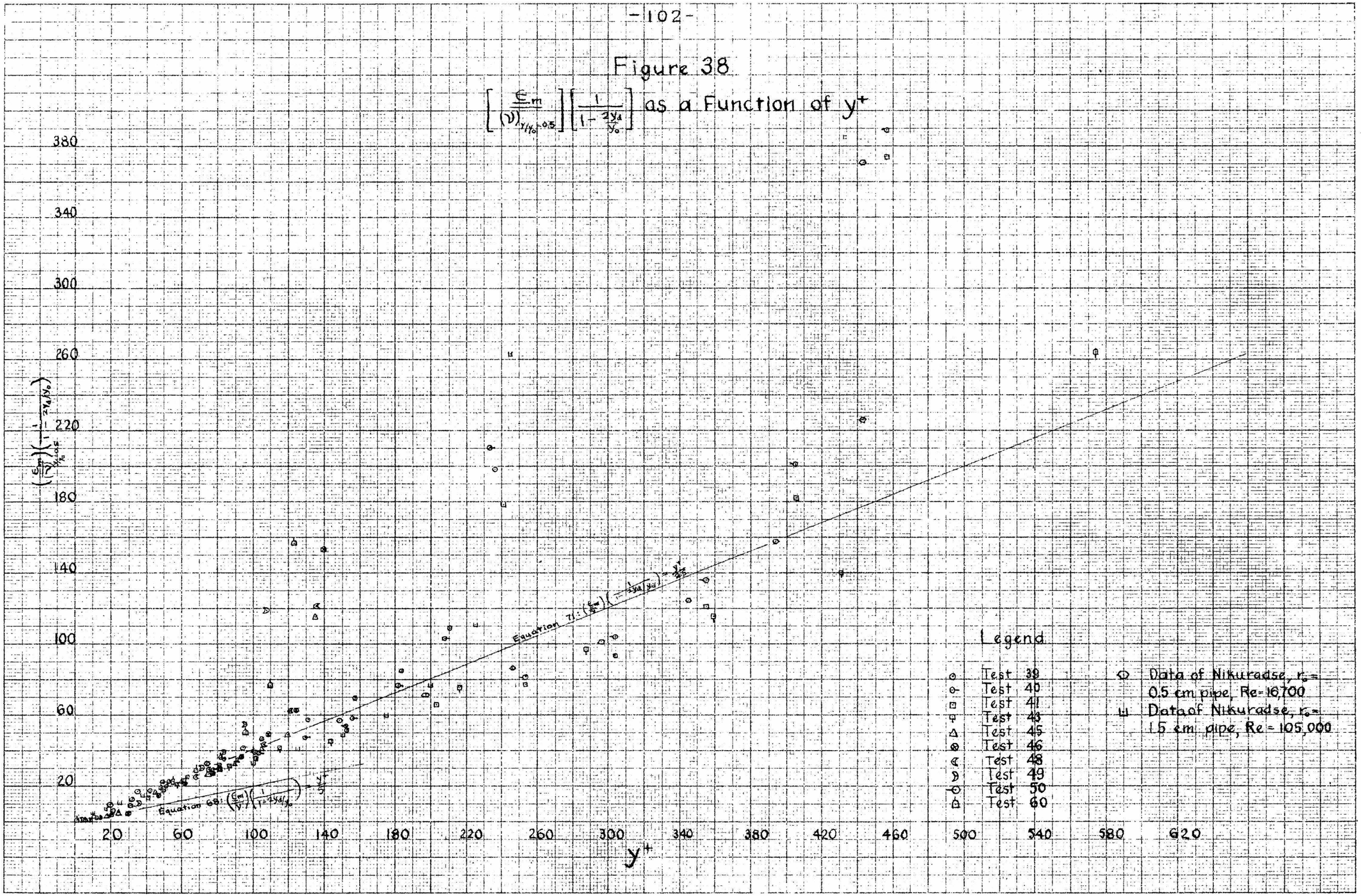

Figure 39

$\left[\frac{\epsilon_m}{(\epsilon)_{y/y_o=0.5}}\right]\left[\frac{1}{1-\frac{2y_d}{y_o}}\right]$ as a Function of y^+

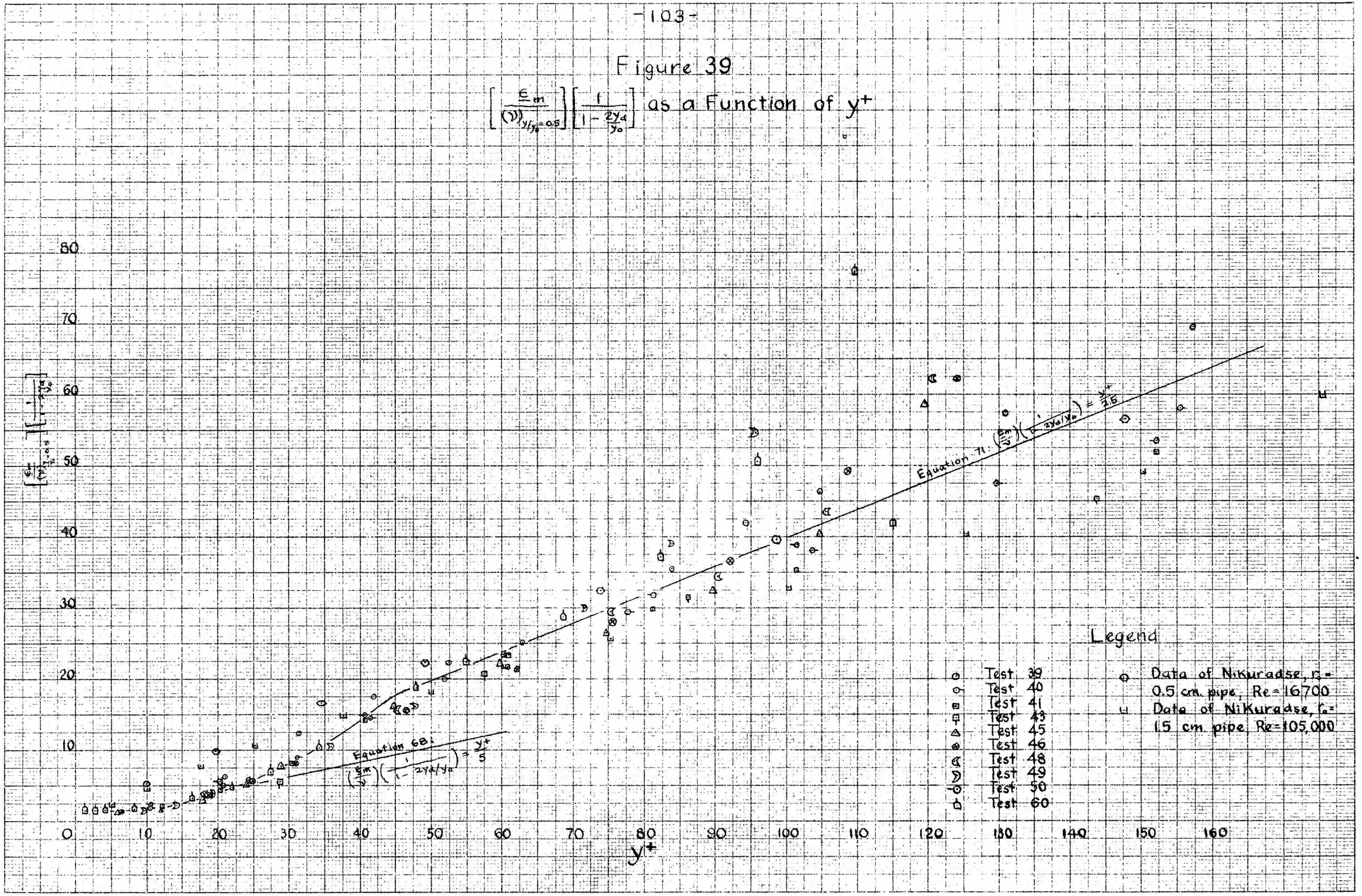

Figure 40

$\left[\frac{\epsilon_E}{(K)_{y/y_o=0.5}}\right]\left[\frac{1}{1-\frac{2y_d}{y_o}}\right]$ as a Function of y^+

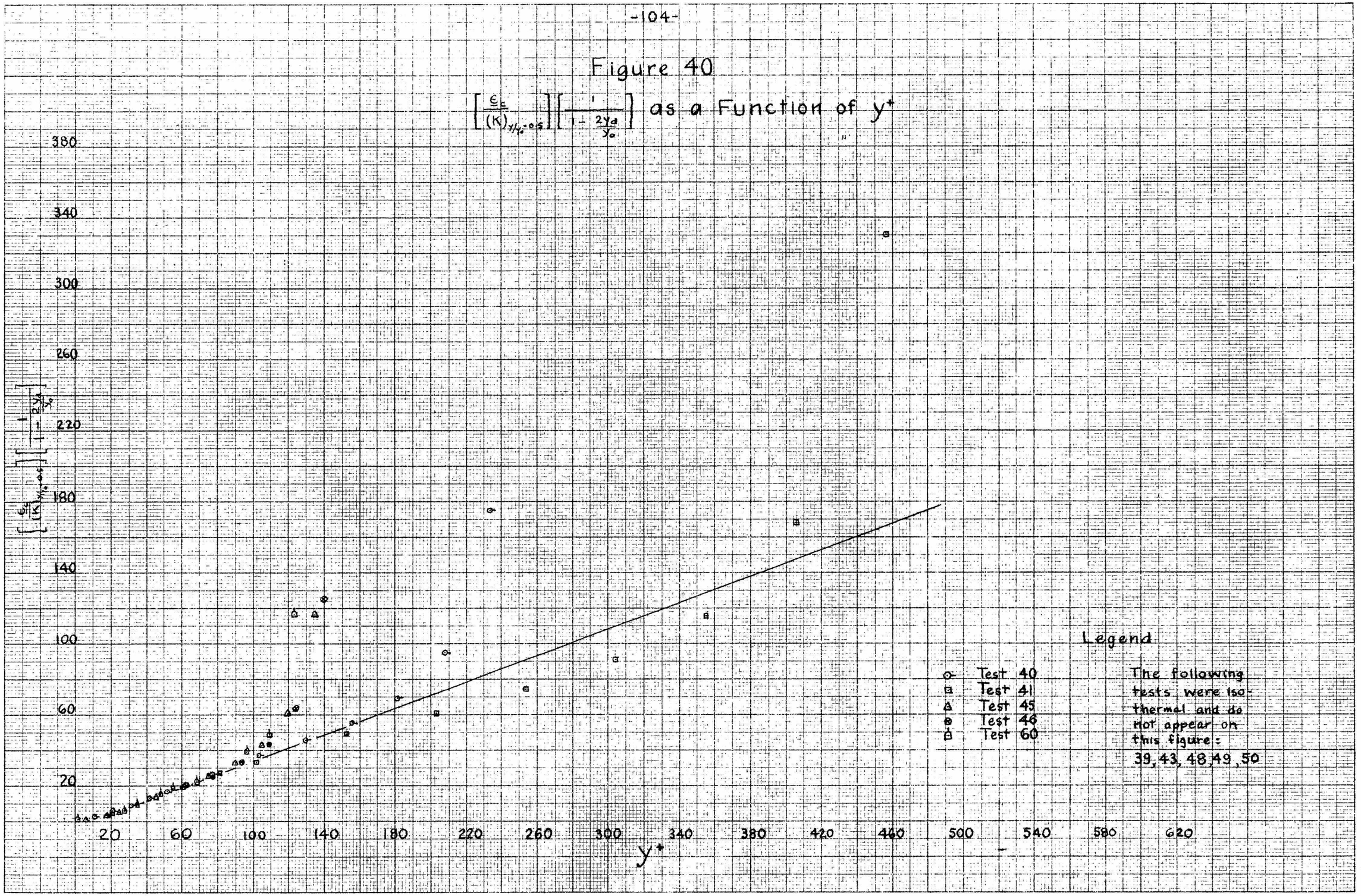

Figure 41

$\left[\frac{\epsilon_m}{(K)_{y/\delta=0.5}}\right]\left[\frac{1}{1-\frac{2y_4}{y_0}}\right]$ as a Function of y^+

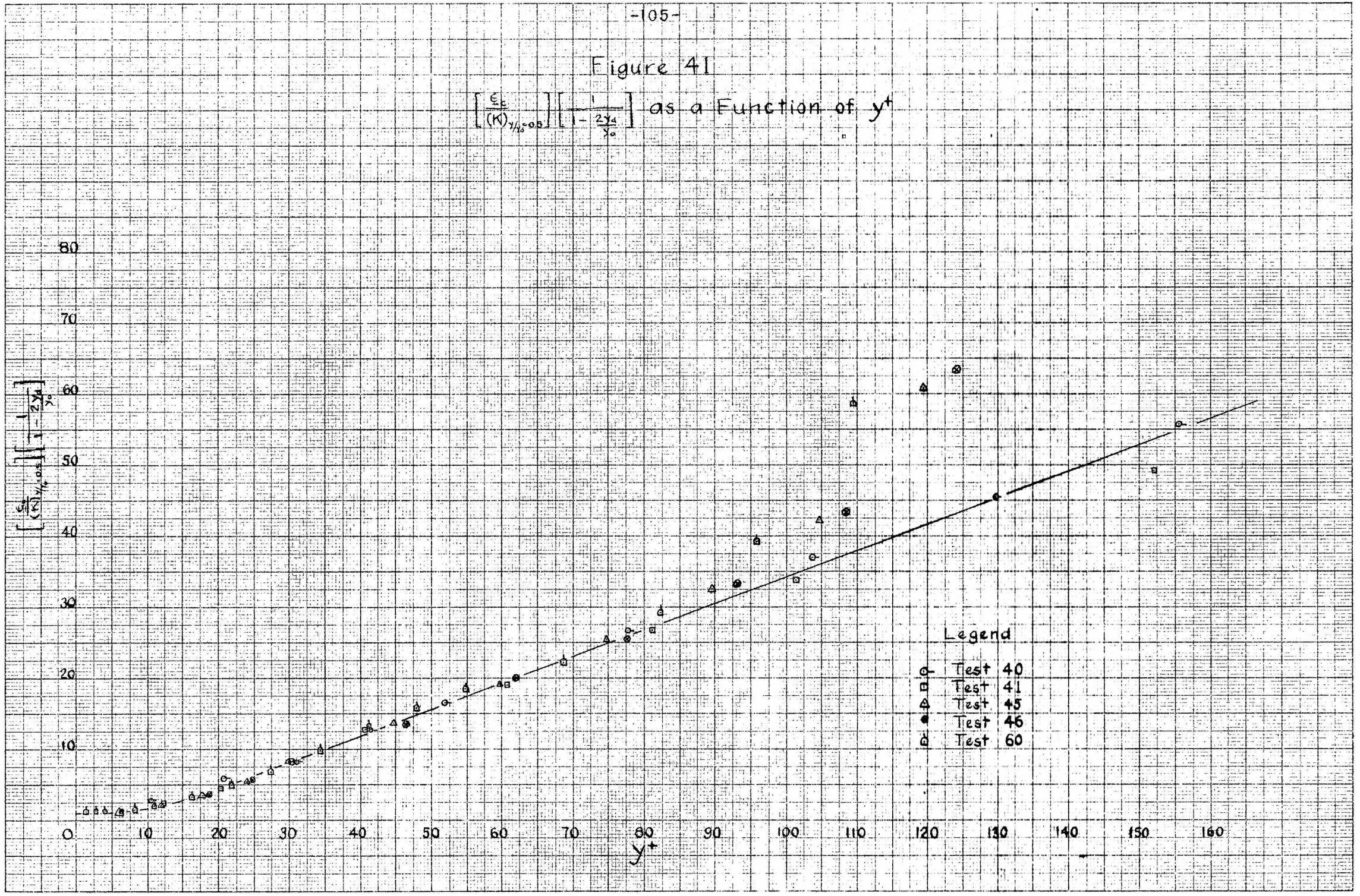

Figure 42

Log $\left[\frac{\epsilon_m}{(\nu)_{y/r_o=0.5}}\right]\left[\frac{1}{1-\frac{2y_a}{y_o}}\right]$ as a Function of Log y^+

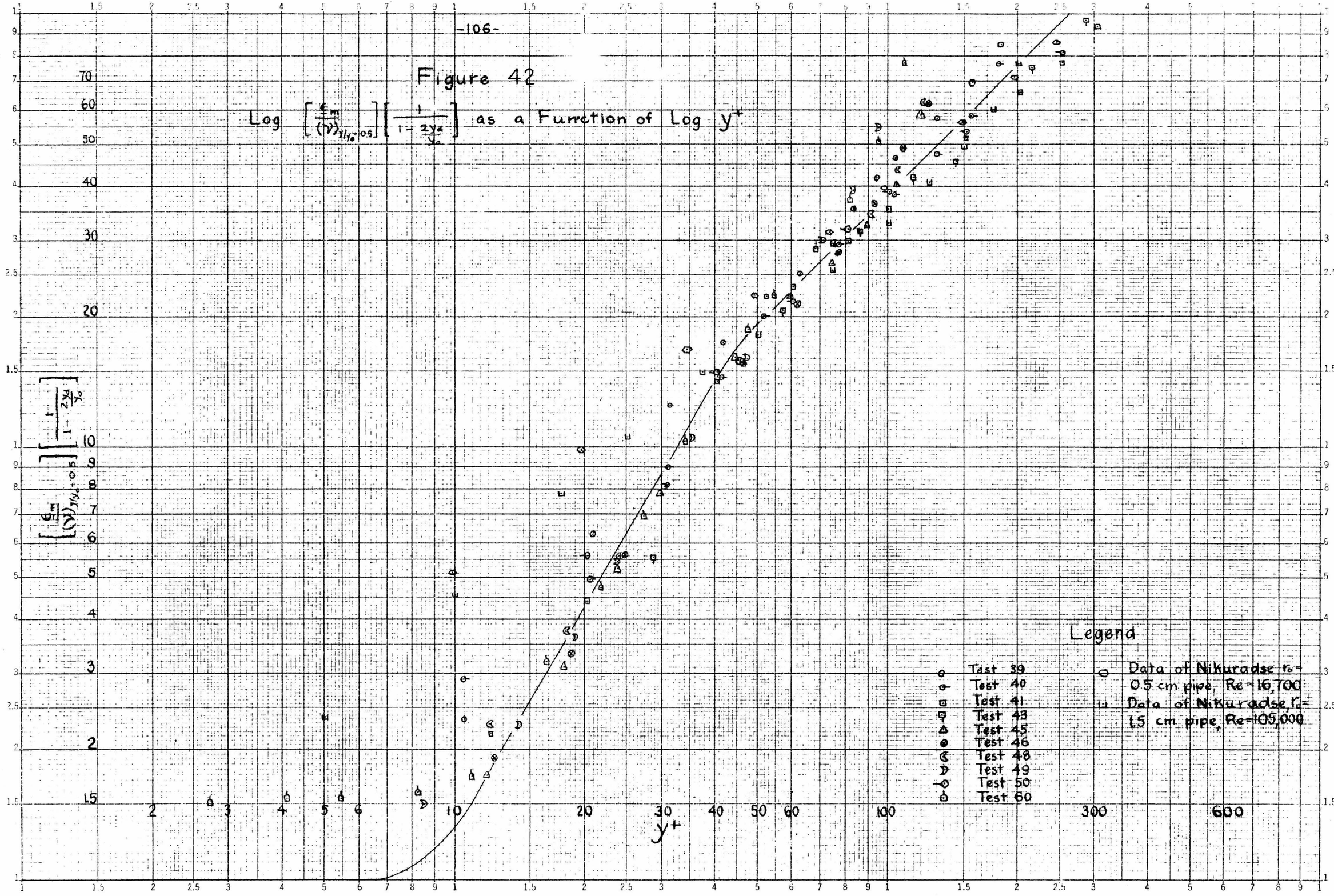

KEUFFEL & ESSER CO., N.Y. NO. 359 112L

Figure 43

Log $\left[\frac{\epsilon_c}{(K)_{y/y_o=.05}}\right]\left[\frac{1}{1-\frac{2y_d}{y_o}}\right]$ as a Function of Log y^+

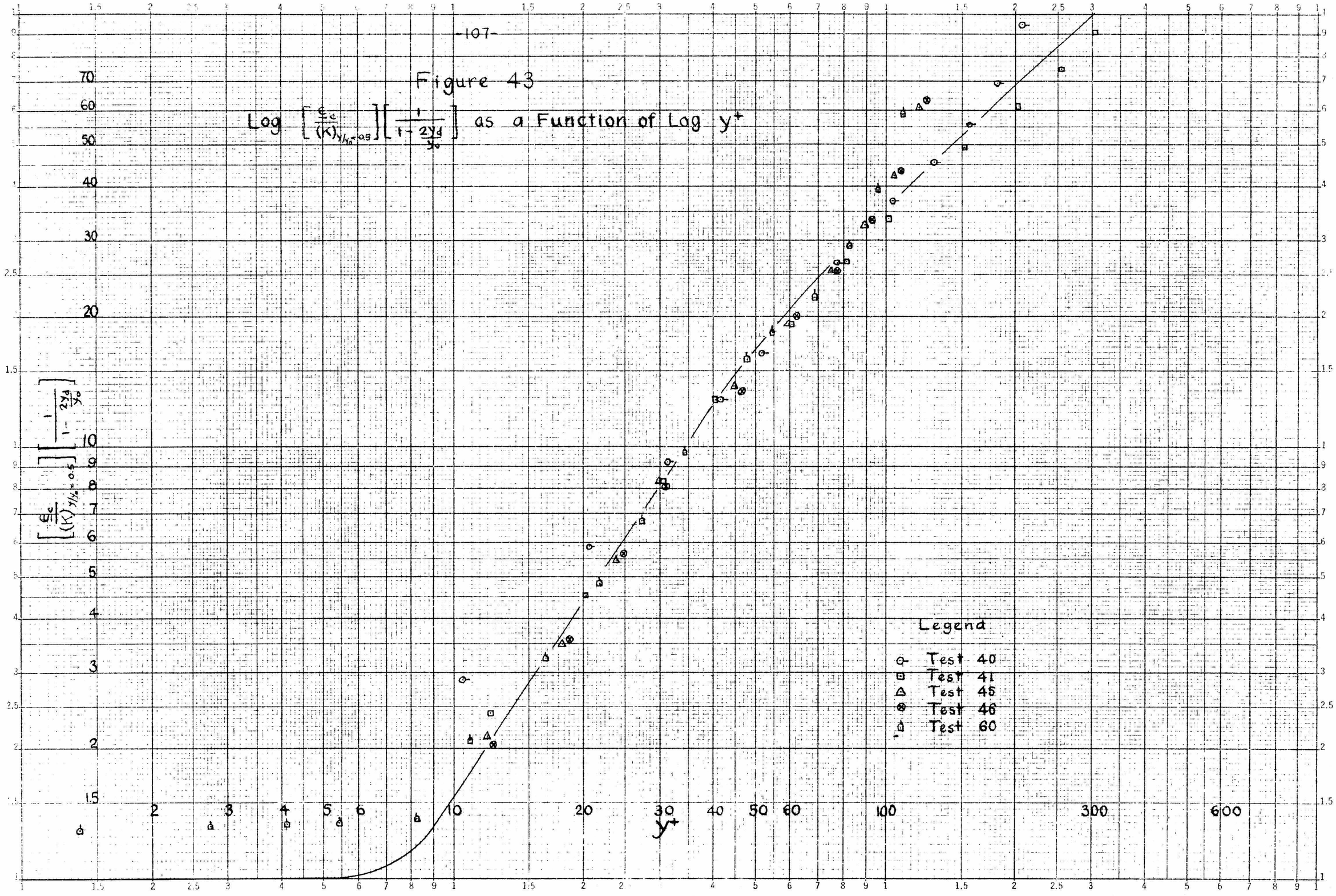

KEUFFEL & ESSER CO. N. Y. NO. 359 112L

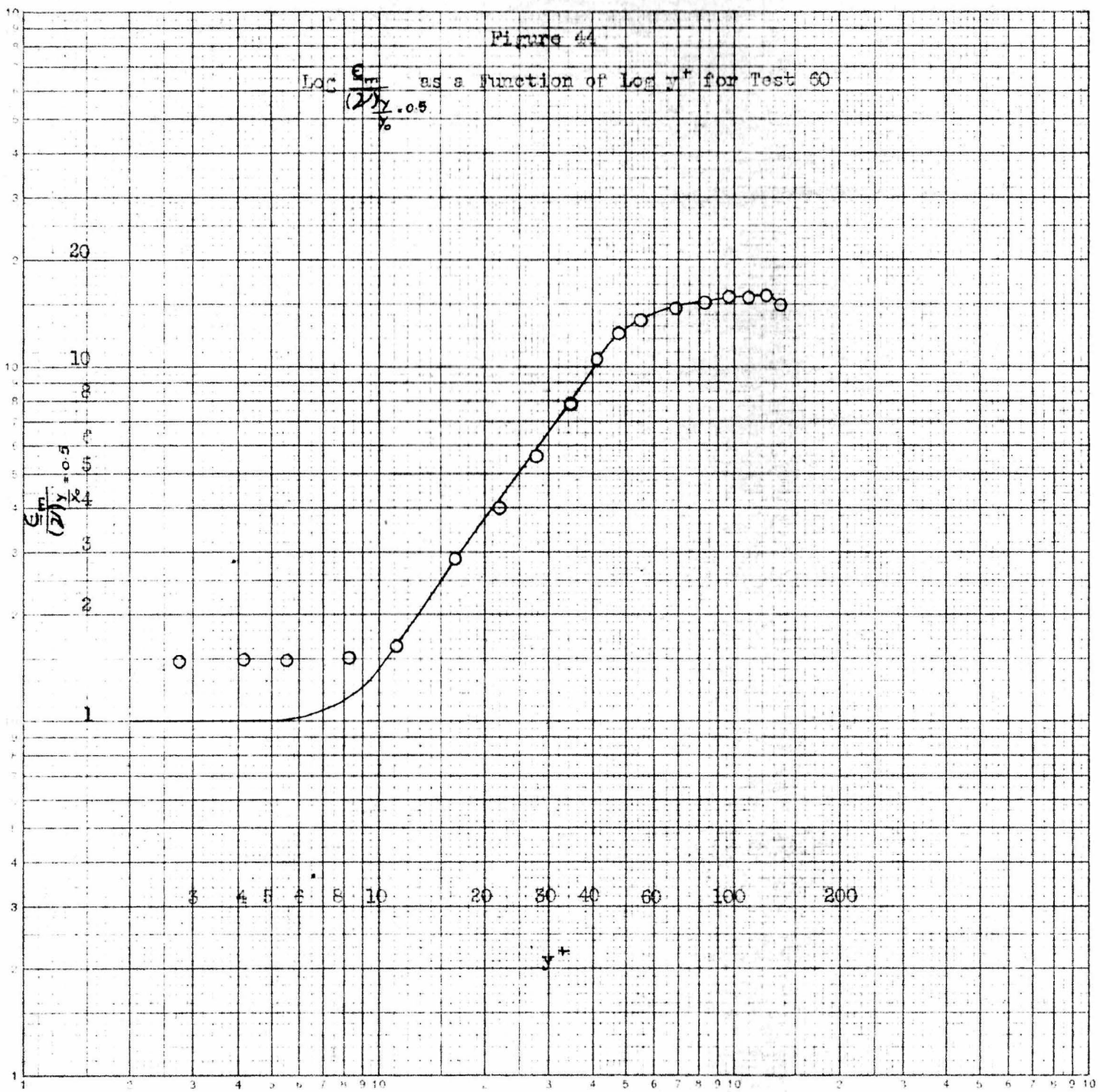
Figure 44
Log $\frac{\varepsilon_m}{(\nu)_{y/r_o=.05}}$ as a function of Log y^+ for Test 60
$\frac{\varepsilon_m}{(\nu)_{y/r_o=.05}}$
20
10
1
3 4 5 6 8 10 20 30 40 60 100 200
y^+

Figure 45

Log $\frac{\varepsilon_c}{(K)_{\frac{y}{y_o}=0.5}}$ as a Function of Log y^+ for Test 60

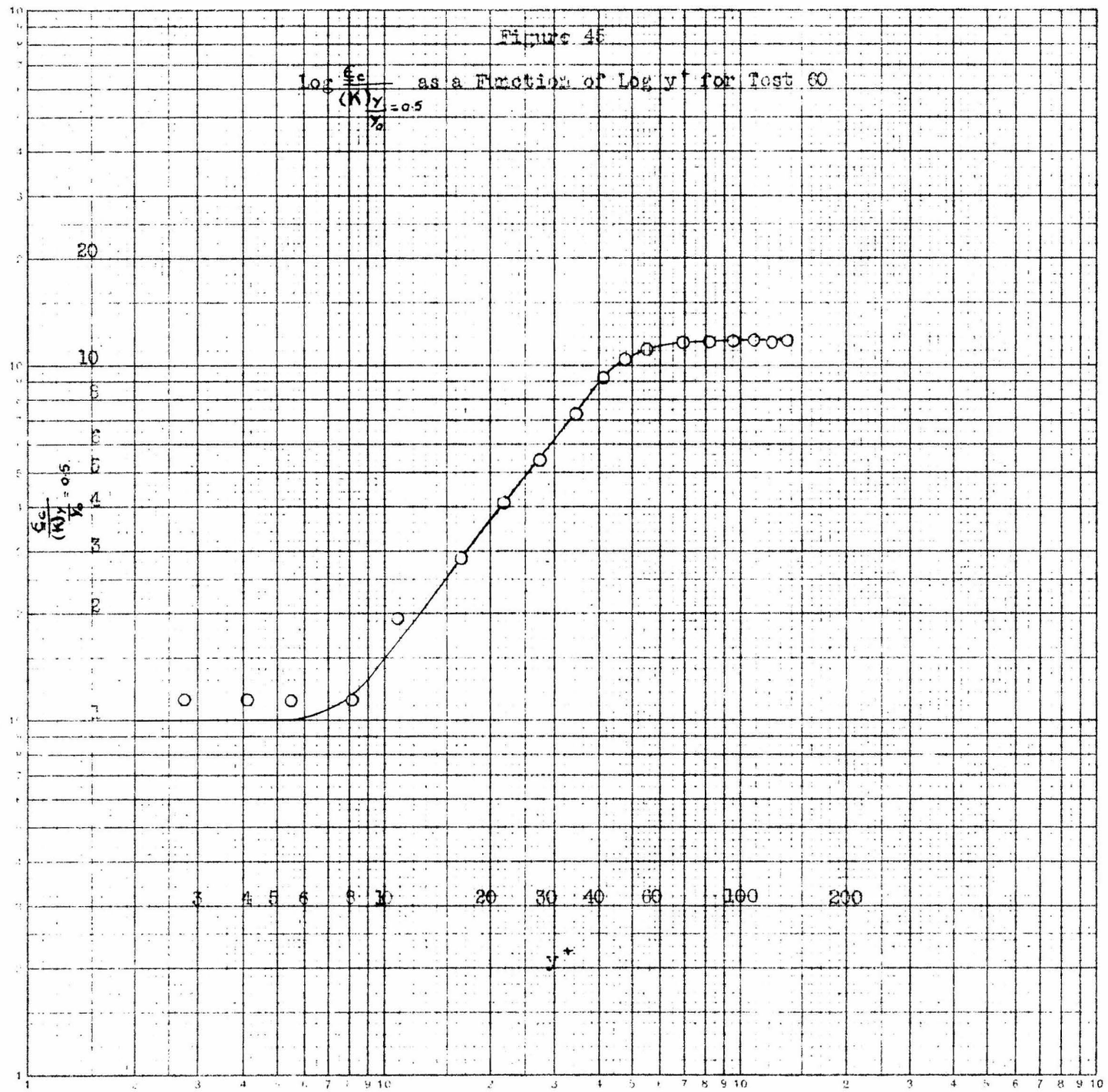

CLEARPRINT PAPER CO. 739 MILLIMETERS 8 1/2" WAYS 180 x 220 DIVISIONS
PRINTED IN U.S.A. ON CLEARPRINT TECHNICAL PAPER NO. 1000H

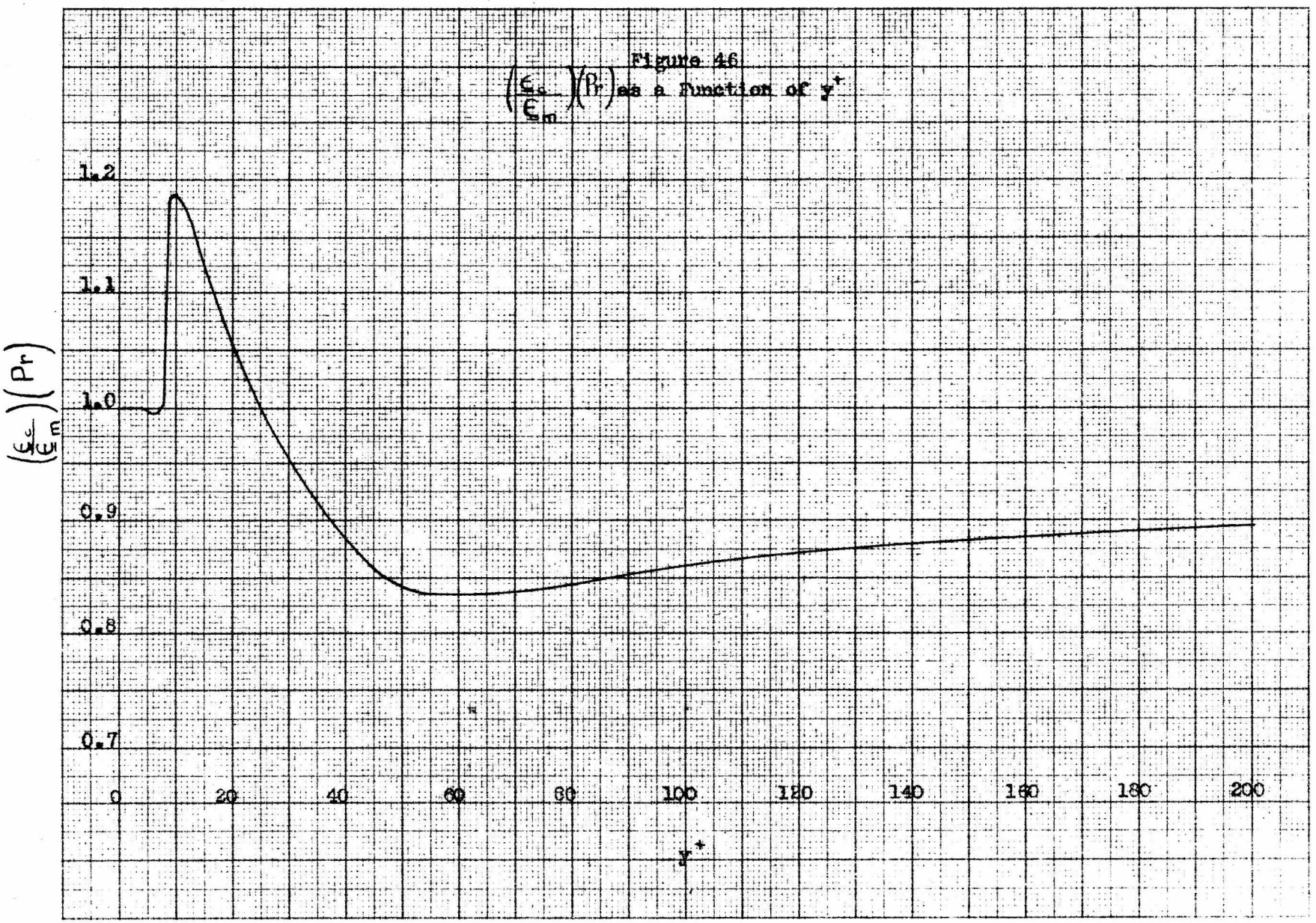

Figure 46
$\left(\frac{\epsilon_c}{\epsilon_m}\right)(Pr)$ as a Function of y^+

CLEARPRINT PAPER CO. 739 MILLIMETERS BOTH WAYS 160 X 220 DIVISIONS
PRINTED IN U.S.A. ON CLEARPRINT TECHNICAL PAPER NO. 1000H

Figure 47

$\left(\frac{\epsilon_c}{\epsilon_m}\right)\left(P_r\right)$ as a Function of y^+, Test 46

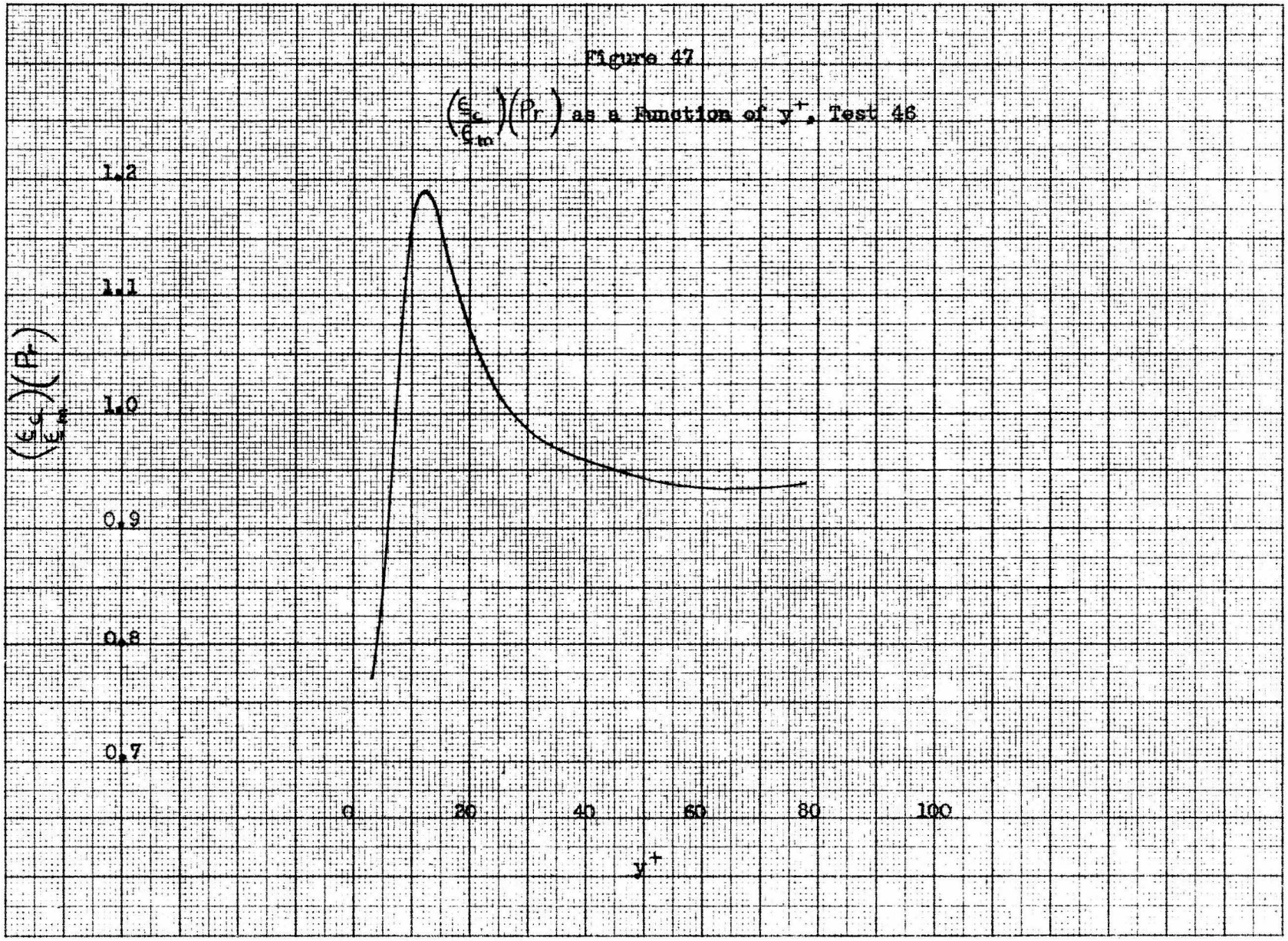

CLEARPRINT PAPER CO 1539 MILLIMETERS BOTH WAYS 180 X 220 DIVISIONS
PRINTED IN U.S.A. ON CLEARPRINT TECHNICAL PAPER NO. 1000H

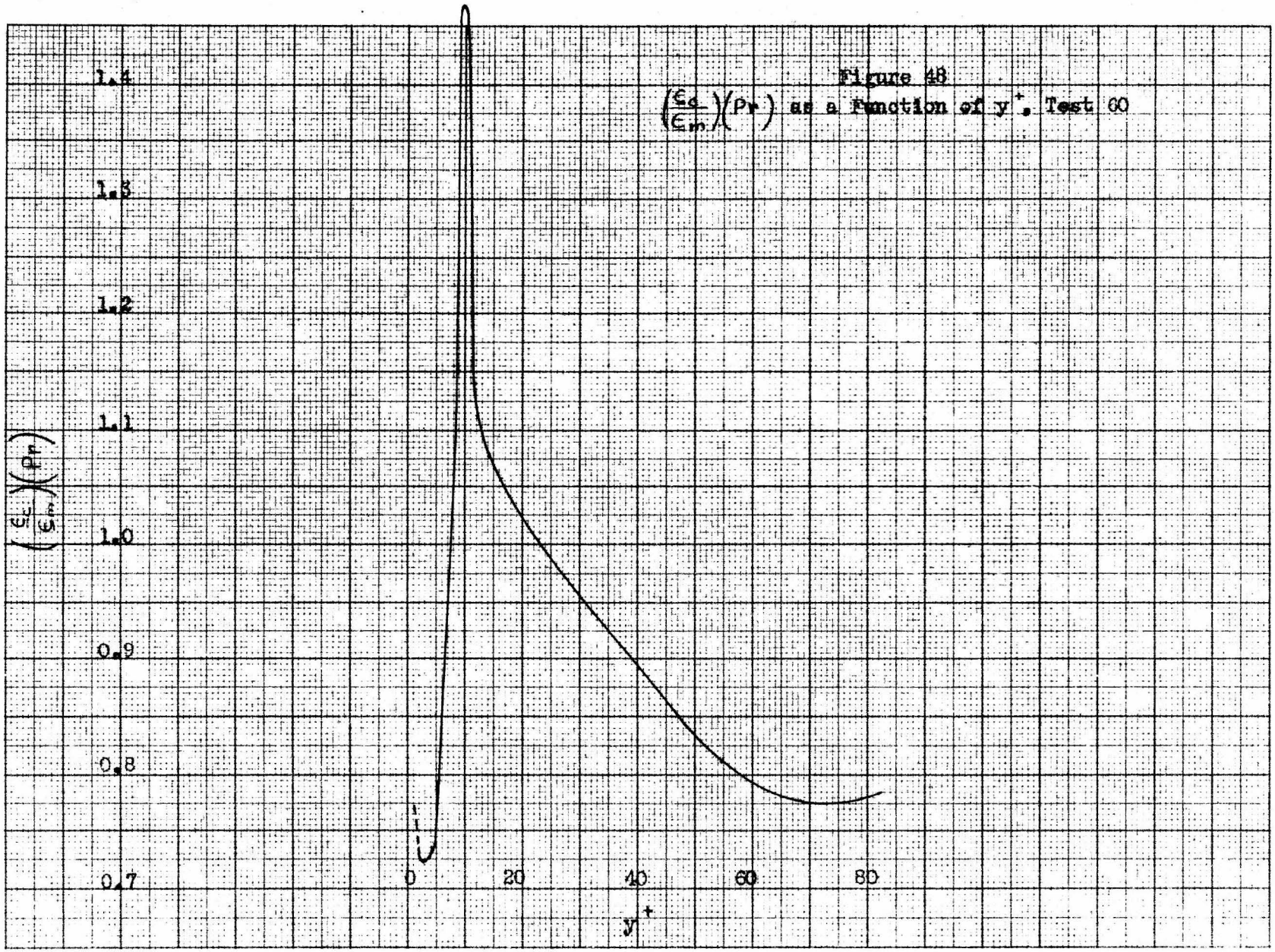

Figure 48
$\left(\frac{\epsilon_c}{\epsilon_m}\right)\left(P_r\right)$ as a Function of y^+, Test 60

Figure 49

Comparison of Total Viscosities of Test 60 and 61

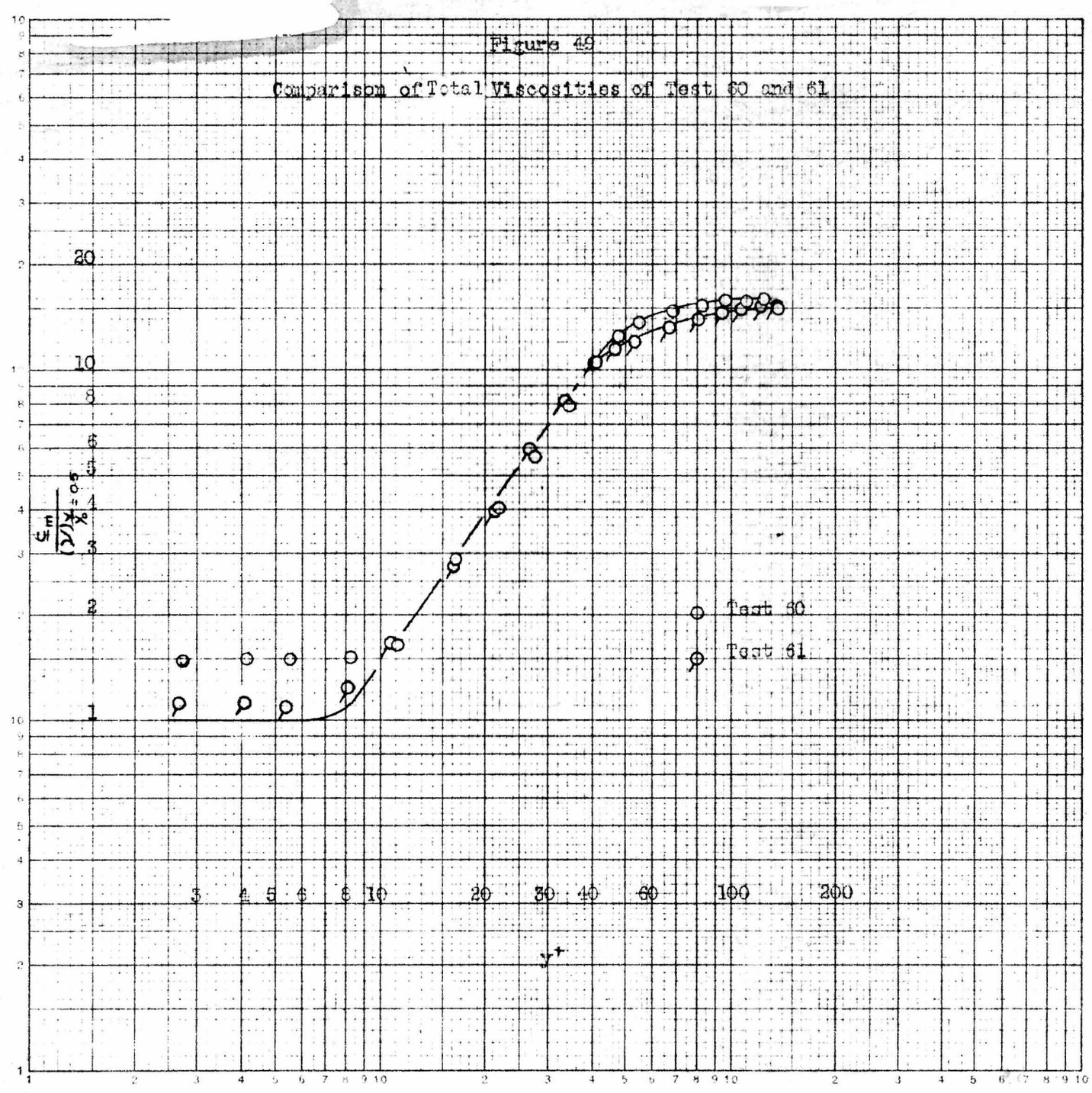

Figure 50

Comparison of Total Conductivities of Tests C0 and C1

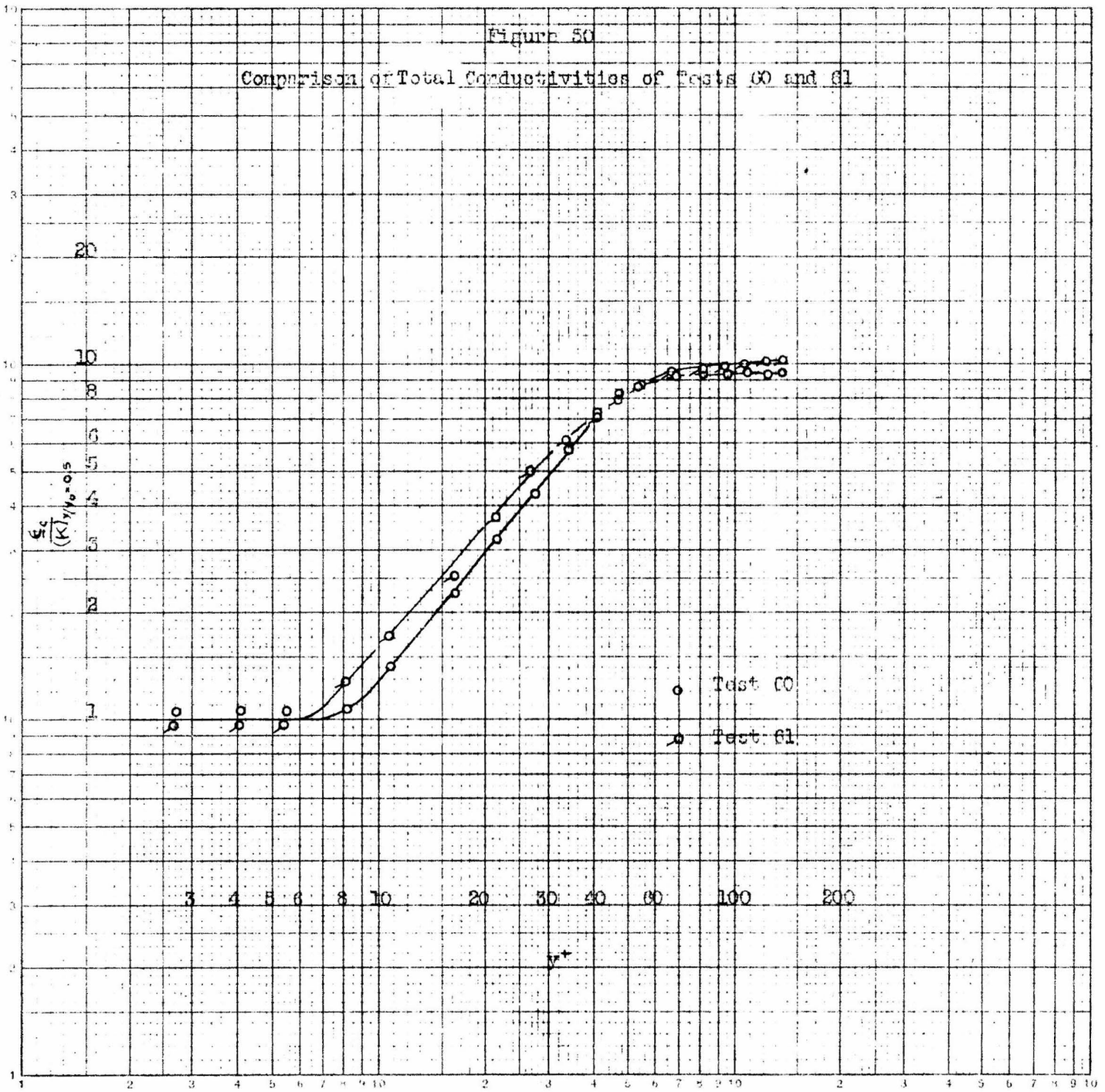

List of Tables

I	Point Values of Temperature and Velocity for Test 60.
II	Point Values of Temperature and Velocity for Test 61.
III	Miscellaneous Data of Tests 60 and 61.
IV	Eddy Properties of Tests 60 and 61.
V	Properties of Dry Air at 14.696 lb./in.^{2}
VI	Pressure Gradient Data.
VII	Summary of Calorimetric Data.
VIII	Total Viscosity and Total Conductivity for Various Tests.

Table I. Point Values of Temperature and Velocity for Test 60.

y / y_o	t^b °F.	u ft./sec.	y / y_o	t^b °F.	u ft./sec.
0.997	113.90	13.28	0.971	110.05	4.67
0.994	113.70	4.88	0.968	110.56	5.33
0.991	113.47	2.60	0.956	109.56	7.30
0.988	113.09	2.01	0.952[a]	109.40	7.63
0.985	112.71	2.13	0.942	108.41	9.00
0.982[a]	112.31	2.80	0.913	106.92	11.12
0.980	111.74	3.36	0.901[a]	106.54	11.77
0.980[a]	111.89	3.57	0.900[a]	106.54	11.81
0.974	111.13	4.25	0.884	106.02	12.42
0.972[a]	111.38	4.24	0.856[a]	105.34	13.16

[a] Thermanemometer moving upward. For points undesignated thermanemometer was moving downward.

[b] Corrected for heating effect of bridge current. Impact correction was less than experimental uncertainty.

[c] Pitot tube measurement. For points undesignated velocity is a hot wire measurement.

Table I. (Cont'd.) Point Values of Temperature and Velocity for Tes

y / y_o	t^b °F.	u ft./sec.	y / y_o	t^b °F.	u ft./sec.
0.854	105.39	13.15	0.447	99.48	15.59
0.825	104.79	13.65	0.389	98.66	15.38
0.796	104.38	13.91	0.330	97.93	15.16
0.739[a]	103.53	14.55	0.271	97.09	14.79
0.738	103.51	14.51	0.212	96.26	14.28
0.681	102.77	15.00	0.153	95.45	13.54
0.622	102.07	15.36	0.095	94.11	12.29
0.565	101.15	15.46	0.067	93.18	11.16
0.488	100.18	15.58	0.052	92.38	10.15
0.488		15.29[c]	0.035	91.06	8.30
			0.023	89.77	6.25

[a] Thermanemometer moving upward. For points undesignated thermanemometer was moving downward.

[b] Corrected for heating effect of bridge current. Impact correction was less than experimental uncertainty.

[c] Pitot tube measurement. For points undesignated velocity is a hot wire measurement.

Table II. Point Values of Temperature and Velocity for Test 71.

y / y_o	t^b °F.	u ft./sec.	y / y_o	t^b °F.	u ft./sec.
0.998	86.54	8.80	0.971	90.14	9.86
0.996	86.77	5.20	0.966	90.52	6.59
0.993	87.27	2.11	0.958	91.20	7.72
0.990	87.73	2.34	0.950[a]	91.51	8.73
0.987	88.07	2.08	0.943	92.20	9.57
0.984[a]	88.53	3.49	0.914	93.37	11.20
0.981	89.00	3.30	0.901[a]	93.79	11.98
0.980[a]	89.11	4.51	0.886	94.18	12.33
0.975	89.62	5.13	0.858[a]	94.72	13.00
0.974[a]	89.72	5.42	0.856	94.76	13.04

[a] Thermanemometer moving upward. For points undesignated thermanemometer was moving downward.

[b] Corrected for heating effect of bridge current. Impact correction was less than experimental uncertainty.

[c] Pitot tube measurement. For points undesignated velocity is a hot wire measurement.

Table II. (Cont'd.) Point Values of Temperature and Velocity for Test 61

y / y_o	t^b °F.	u ft./sec.	y / y_o	t^b °F.	u ft./sec.
0.826	95.29	13.53	0.388	101.16	13.19
0.797	95.72	13.89	0.330	101.96	14.95
0.740[a]	96.48	14.48	0.272	102.77	14.62
0.739	96.57	14.41	0.213	103.57	13.98
0.674	97.38	14.91	0.155	104.77	13.18
0.622	98.04	15.14	0.096	105.96	11.09
0.561	98.90	15.34	0.085	106.34	11.51
0.505	99.53	15.61	0.063	107.27	10.35
0.505		14.93[c]	0.051	107.93	9.42
0.450	100.33	15.37	0.034	109.48	7.14
			0.028	110.14	6.06

[a] Thermanemometer moving upward. For points undesignated thermanemometer was moving downward.

[b] Corrected for heating effect of bridge current. Impact correction was less than experimental uncertainty.

[c] Pitot tube measurement. For points undesignated velocity is a hot wire measurement.

Table III. Miscellaneous Data of Tests 60 and 61

Variable	Symbol	Units	Test 60	Test 61
Distance between[a] Plates	y_o	ft.	0.0572	0.0571
Distance of Traversing Point from Inlet[b]		ft.	12.5	12.5
Incoming Air Temperature		^oF	100.0	100.0
Upper Plate Temperature		^oF	115.3	84.9
Lower Plate Temperature		^oF	85.0	115.0
Average Velocity	U	ft./sec.	13.3	13.2
Pressure[c]	P	lb./in.^{2}	14.375	14.305
Pressure Gradient[d]	dP/dx	lb./ft.^{3}	-0.0592	-0.0579
Thermal Flux Density	$\dot{Q}$	B.T.U./ft.^{2}sec.	0.0096	0.0100
Weight Fraction Water			0.0115	0.0145
Reynolds Number	Re		8200	8040
Friction Velocity	u*	ft./sec.	0.869	0.881

[a] As measured at traversing point.

[b] Both traverses were made on lateral middle line of apparatus.

[c] Absolute pressure at the traversing point.

[d] See "Pressure Gradients" under "Analysis of Results."

Table IV. Eddy Properties of Tests 60 and 61

A Test 60

y/y_o	$\epsilon_m \times 10^3$ ft.^{2}/sec.	$\epsilon_m \times 10^3$ ft.^{2}/sec.	$\epsilon_c \times 10^3$ ft.^{2}/sec.	$\epsilon_c \times 10^3$ ft.^{2}/sec.
0.005	0.26	0.08	0.26	0.01
0.010	0.25	0.08	0.26	0.01
0.015	0.25	0.08	0.26	0.01
0.020	0.26	0.08	0.26	0.01
0.030	0.26	0.08	0.26	0.01
0.040	0.36	0.18	0.44	0.18
0.060	0.61	0.43	0.66	0.40
0.080	0.89	0.70	0.90	0.64
0.100	1.24	1.05	1.18	0.92
0.125	1.59	1.41	1.59	1.33
0.150	1.87	1.68	2.09	1.83
0.175	2.13	1.95	2.32	2.06
0.200	2.48	2.29	2.37	2.11
0.250	2.71	2.52	2.39	2.13
0.300	2.81	2.62	2.41	2.15
0.350	2.87	2.69	2.42	2.16
0.400	2.92	2.74	2.44	2.17
0.450	2.97	2.78	2.39	2.12

Table IV. (Cont'd.) Eddy Properties of Tests 60 and 61

A Test 60

y/y_o	$\epsilon_m \times 10^3$ ft.^{2}/sec.	$\epsilon_m \times 10^3$ ft.^{2}/sec.	$\epsilon_o \times 10^3$ ft.^{2}/sec.	$\epsilon_o \times 10^3$ ft.^{2}/sec.
0.500	2.91	2.72	2.46	2.20
0.550	2.87	2.69	2.46	2.20
0.600	2.82	2.63	2.47	2.20
0.650	2.77	2.58	2.47	2.21
0.700	2.72	2.53	2.47	2.21
0.750	2.64	2.45	2.43	2.16
0.800	2.53	2.34	2.20	1.94
0.825	2.39	2.20	1.98	1.72
0.850	1.91	1.72	1.72	1.46
0.875	1.29	1.10	1.43	1.16
0.900	0.82	0.63	1.08	0.81
0.920	0.59	0.40	0.79	0.52
0.940	0.43	0.24	0.53	0.26
0.960	0.30	0.11	0.37	0.10
0.970	0.28	0.08	0.27	0.00
0.980	0.28	0.08	0.27	0.00
0.985	0.28	0.08	0.27	0.00
0.990	0.27	0.08	0.27	0.00
0.995	0.27	0.08	0.27	0.00

Table IV. (Cont'd.) Eddy Properties of Tests 60 and 61

B Test 61

y/y_o	$\epsilon_m \times 10^3$ ft.^{2}/sec.	$\epsilon_m \times 10^3$ ft.^{2}/sec.	$\epsilon_o \times 10^3$ ft.^{2}/sec.	$\epsilon_c \times 10^3$ ft.^{2}/sec.
0.005	0.21	0.01	0.26	-0.01
0.010	0.21	0.01	0.26	-0.01
0.015	0.20	0.01	0.26	-0.01
0.020	0.20	0.01	0.26	-0.01
0.030	0.22	0.03	0.28	0.00
0.040	0.32	0.13	0.39	0.12
0.060	0.53	0.34	0.62	0.35
0.080	0.79	0.60	0.98	0.71
0.100	1.30	1.11	1.30	1.03
0.125	1.71	1.52	1.57	1.31
0.150	1.91	1.72	1.81	1.54
0.175	2.06	1.88	2.02	1.76
0.200	2.20	2.02	2.16	1.90
0.250	2.45	2.26	2.33	2.06
0.300	2.65	2.46	2.42	2.16
0.350	2.80	2.62	2.51	2.24
0.400	2.89	2.71	2.58	2.31
0.450	2.90	2.71	2.64	2.37

Table IV. (Cont'd.) Eddy Properties of Tests 60 and 61

B Test 61

y/y_o	$\epsilon_m \times 10^3$ ft.^{2}/sec.	$\epsilon_m \times 10^3$ ft.^{2}/sec.	$\epsilon_c \times 10^3$ ft.^{2}/sec.	$\epsilon_c \times 10^3$ ft.^{2}/sec.
0.500	2.81	2.63	2.65	2.38
0.550	2.74	2.55	2.65	2.39
0.600	2.66	2.47	2.65	2.38
0.650	2.60	2.41	2.64	2.38
0.700	2.54	2.35	2.64	2.38
0.750	2.44	2.25	2.63	2.37
0.800	2.28	2.09	2.37	2.11
0.825	2.16	1.98	2.15	1.89
0.850	1.90	1.72	1.92	1.67
0.875	1.30	1.11	1.65	1.39
0.900	0.91	0.72	1.33	1.07
0.920	0.69	0.51	0.96	0.71
0.940	0.49	0.31	0.70	0.44
0.960	0.31	0.12	0.45	0.19
0.970	0.23	0.05	0.34	0.08
0.980	0.20	0.02	0.25	0.00
0.985	0.21	0.03	0.25	0.00
0.990	0.21	0.03	0.25	0.00
0.995	0.21	0.03	0.25	0.00

Table V. Properties of Dry Air at 14.696 lb./in.^{2}

Property	Symbol	Units	70°F	100°F	130°F
Absolute Viscosity x 10^7	η	lb.sec./ft.^{2}	3.82	3.98	4.14
Specific Heat	C_p	B.T.U./lb.°F	0.2403	0.2406	0.2409
Thermal Conductivity x 10^7	k	B.T.U./sec.°F.ft.	4.14	4.34	4.54

Table VI. Pressure Gradient Data

Test No.	Traverse[a] Location	Average Velocity ft./sec.	$-dP/dx$ lb./ft.^{3}
37	8.1	29.9	0.240
37	8.1	29.6	0.222
39	12.5	30.0	0.251
40	12.5	28.1	0.252
41	12.5	61.0	0.857
43	12.5	88.7	1.696
43	8.1	90.2	1.752
44	12.5	88.4	1.684
44	8.1	88.4	1.729
45	12.5	14.8	0.075
45	8.1	15.6	0.078
46	12.5	15.3	0.076
48	12.5	14.8	0.063
48	8.1	15.3	0.072
49	12.5	11.3	0.035
49	8.1	12.3	0.038
50	12.5	58.7	0.789
50	8.1	62.0	0.794
60	12.5	13.3	0.049
61	12.5	13.2	0.046

[a] Distance of traversing point from the end of the converging section, ft.

Table VII. Summary of Calorimetric Data

Group No.	Test No.	Reynolds Number	Temp. Difference between the Plates Δt °F	$\dot{Q}/\Delta t$ [a] x 10^3	$\dot{Q}/\Delta t$ [b] x 10^3	$h/2$ [c] x 10^3	% by Which Column 6 Exceeds Column 5	% by Which Column 7 Exceeds Column 5
1	30	10850	60	0.588		0.597		1.5
1	31	19900	60	0.925		0.970		4.9
1	32	36400	60	1.44		1.548		7.5
1	33	52000	60	1.93		2.115		9.6
1	34	5980	60	0.288	0.198 [d]	0.365	-31.2	26.7

[a] From calorimetric measurements, B.T.U./sec. ft.^{2} °F.

[b] From slope of temperature curve at the wall, B.T.U./sec. ft.^{2} °F.

[c] From Relation 4C, p. 168 of Heat Transmission by McAdams (18), B.T.U./sec. ft.^{2} °F.

[d] From slope of temperature curve at the upper wall.

Table VII. (Cont'd.) Summary of Calorimetric Data

Group No.	Test No.	Reynolds Number	Temp. Difference between the Plates Δt °F	$\dot{Q}/\Delta t$ [a] x 10^3	$\dot{Q}/\Delta t$ [b] x 10^3	$h/2$ [c] x 10^3	% by Which Column 6 Exceeds Column 5	% by Which Column 7 Exceeds Column 5
2	40	17100	10	0.732		0.927		26.6
2	41	37300	10	1.26		1.740		38.1
2	44	52500	10	1.56		2.300		47.4
2	45	8980	10	0.450	0.559[d]	0.551	24.2	22.4
2	45	8980	10	0.450	0.415[e]	0.551	-7.8	22.4
2	46	9370	30	0.464		0.568		22.4
3	60	8200	30	0.308	0.320[d]	0.514	3.9	66.9

[a] From calorimetric measurements, B.T.U./sec. ft.^{2} °F.

[b] From slope of temperature curve at the wall, B.T.U./sec. ft.^{2} °F.

[c] From Relation 4C, p. 163 of Heat Transmission by McAdams (18), B.T.U./sec. ft.^{2} °F.

[d] From slope of temperature curve at the upper wall.

[e] From slope of temperature curve at the lower wall.

Table VIII. Total Viscosity and Total Conductivity for Various Tests

A Test 39

y_d/y_o	y^+	$\frac{\epsilon}{m} \times 10^3$ ft.^{2}/sec.
0.02	10.5	0.42
0.04	21.0	1.09
0.06	31.4	2.05
0.08	41.9	2.76
0.10	52.4	3.35
0.12	62.9	3.53
0.16	83.8	4.54
0.18	94.3	5.04
0.20	104.8	5.23
0.25	131.0	5.41
0.30	157.2	5.23
0.35	183.4	4.79
0.40	209.6	4.09
0.45	235.7	3.73
0.50	261.9	3.61

Incoming air temperature	100°F
Upper plate temperature	100°F
Lower plate temperature	100°F
Average velocity	30.0 ft./sec.
Reynolds number	17700
Friction velocity	1.78 ft./sec.
$(\nu)_{y/y_o = 0.5}$	0.000188 ft.^{2}/sec.

Table VIII. (Cont'd.) Total Viscosity and Total Conductivity for Various Tests

B Test 40

y_d/y_o	y^+	$\frac{\epsilon}{\nu}_m \times 10^3$ ft.^{2}/sec.	$\frac{\epsilon}{\nu}_b \times 10^3$ ft.^{2}/sec.
0.02	10.4	0.52	0.74
0.04	20.7	0.86	1.46
0.06	31.1	1.48	2.18
0.08	41.5	2.28	2.89
0.10	51.8	3.00	3.56
0.15	77.7	3.86	5.03
0.20	103.6	4.30	5.97
0.25	129.6	4.46	6.12
0.30	155.5	4.36	5.99
0.35	181.4	4.32	5.61
0.40	207.3	3.84	5.10
0.45	233.2	3.94	4.70
0.494	256.0	3.89	4.56

Incoming air temperature	100°F
Upper plate temperature	104.2°F
Lower plate temperature	95.0°F
Average velocity	28.1 ft./sec.
Reynolds number	17100
Friction velocity	1.70 ft./sec.
$(\nu)_{y/y_o = 0.5}$	0.000188 ft.^{2}/sec.
$(K)_{y/y_o = 0.5}$	0.000269 ft.^{2}/sec.

Table VIII. (Cont'd.) Total Viscosity and Total Conductivity for Various Tests

C Test 41

y_d/y_o	y^+	$\epsilon_m \times 10^3$ ft.^{2}/sec.	$\epsilon_c \times 10^3$ ft.^{2}/sec.
0.012	12.2	0.40	0.62
0.02	20.3	0.79	1.14
0.03	30.4	1.42	2.05
0.04	40.6	2.43	3.10
0.06	60.8	3.83	4.41
0.08	81.1	4.65	5.93
0.10	101.4	5.25	7.11
0.15	152.1	6.76	9.04
0.20	202.8	7.35	9.63
0.25	253.5	7.19	9.78
0.30	304.2	6.95	9.51
0.35	354.9	6.75	9.14
0.40	405.6	6.77	8.85
0.45	456.3	6.96	8.69
0.498	505.0	7.07	8.63

Incoming air temperature	100.0°F
Upper plate temperature	105.1°F
Lower plate temperature	94.6°F
Average velocity	61.0 ft./sec.
Reynolds number	37300
Friction velocity	3.32 ft./sec.
$(\nu)_{\frac{y}{y_o}=0.5}$	0.000186 ft.^{2}/sec.
$(K)_{\frac{y}{y_o}=0.5}$	0.000263 ft.^{2}/sec.

Table VIII. (Cont'd.) Total Viscosity and Total Conductivity for Various Tests

D Test 43

y_d/y_o	y^+	$\frac{\epsilon}{\nu}_m \times 10^3$ ft.^{2}/sec.
0.02	28.7	1.02
0.04	57.5	3.61
0.06	86.2	5.29
0.08	115.0	6.69
0.10	143.7	7.65
0.15	215.5	10.02
0.20	287.4	11.07
0.25	359.2	10.99
0.30	431.0	10.64
0.35	502.9	10.27
0.40	574.7	10.03
0.45	646.6	9.90
0.497	722.7	9.80

Incoming air temperature	100.0°F
Upper plate temperature	99.9°F
Lower plate temperature	100.0°F
Average velocity	88.7 ft./sec.
Reynolds number	55200
Friction velocity	4.79 ft./sec.
$(\nu)_{y/y_o = 0.5}$	0.000190 ft.^{2}/sec.

Table VIII. (Cont'd.) Total Viscosity and Total Conductivity for Various Tests

E Test 45

y_d/y_o	y^+	$\epsilon_m \times 10^3$ ft.^{2}/sec.	$\epsilon_c \times 10^3$ ft.^{2}/sec.
0.02	6.0	0.24	0.29
0.04	12.0	0.30	0.53
0.06	17.9	0.52	0.83
0.08	23.9	0.83	1.24
0.10	29.9	1.19	1.80
0.15	44.8	2.13	2.61
0.20	59.8	2.53	3.11
0.25	74.7	2.51	3.43
0.30	89.6	2.46	3.52
0.35	104.6	2.28	3.43
0.40	114.5	2.22	3.26
0.45	134.4	2.18	3.15
0.50	149.4	2.21	3.10

Incoming air temperature	100.0°F
Upper plate temperature	105.0°F
Lower plate temperature	94.7°F
Average velocity	14.8 ft./sec.
Reynolds number	8980
Friction velocity	0.984 ft./sec.
$(\nu)_{y/y_o = 0.5}$	0.000189 ft.^{2}/sec.
$(K)_{y/y_o = 0.5}$	0.000270 ft.^{2}/sec.

Table VIII. (Cont'd.) Total Viscosity and Total Conductivity for Various Tests

F Test 46

y_d/y_o	y^+	$\frac{\epsilon}{m} \times 10^3$ ft.^{2}/sec.	$\frac{\epsilon}{t} \times 10^3$ ft.^{2}/sec.
0.02	6.2	0.24	0.32
0.04	12.4	0.33	0.51
0.06	18.6	0.65	0.84
0.08	24.8	0.89	1.27
0.10	31.0	1.23	1.74
0.15	46.5	2.05	2.52
0.20	62.1	2.41	3.23
0.25	77.6	2.64	3.43
0.30	93.1	2.75	3.60
0.35	108.6	2.77	3.49
0.40	124.1	2.90	3.41
0.45	139.6	2.88	3.35
0.50	155.2	2.88	3.23

Incoming air temperature	100.0°F
Upper plate temperature	115.8°F
Lower plate temperature	84.6°F
Average velocity	15.3 ft./sec.
Reynolds number	9370
Friction velocity	1.01 ft./sec.
$(\nu)_{y/y_o = 0.5}$	0.000188 ft.^{2}/sec.
$(K)_{y/y_o = 0.5}$	0.000269 ft.^{2}/sec.

Table VIII. (Cont'd.) Total Viscosity and Total Conductivity for Various Tests

G Test 48

y_d/y_o	y^+	$\frac{\epsilon}{\nu}_m \times 10^3$ ft.^{2}/sec.
0.02	6.0	0.23
0.04	12.0	0.40
0.06	18.1	0.62
0.08	24.1	0.88
0.10	30.1	1.22
0.15	45.2	2.08
0.20	60.3	2.63
0.25	75.3	2.75
0.30	90.4	2.68
0.35	105.5	2.45
0.40	120.5	2.33
0.45	135.6	2.27
0.487	146.8	2.09

Incoming air temperature	100°F
Upper plate temperature	100°F
Lower plate temperature	100°F
Average velocity	14.8 ft./sec.
Reynolds number	9110
Friction velocity	0.981 ft./sec
$(\nu)_{y/y_o = 0.5}$	0.000137 ft.^{2}/sec.

Table VIII. (Cont'd.) Total Viscosity and Total Conductivity for Various Tests

H Test 49

y_d/y_o	y^+	$\epsilon_m \times 10^3$ ft.^{2}/sec.
0.02	4.8	0.25
0.04	9.6	0.26
0.06	14.3	0.33
0.08	19.1	0.57
0.10	23.9	0.81
0.15	35.9	1.30
0.20	47.8	1.80
0.25	59.8	2.08
0.30	71.7	2.24
0.35	83.7	2.20
0.40	95.6	2.05
0.45	107.6	2.22
0.495	118.3	2.21

Incoming air temperature	100.0°F
Upper plate temperature	100.0°F
Lower plate temperature	100.0°F
Average velocity	11.3 ft./sec.
Reynolds number	6960
Friction velocity	0.777 ft./sec.
$(\nu)_{y/y_o = 0.5}$	0.000187 ft.^{2}/sec.

Table VIII. (Cont'd.) Total Viscosity and Total Conductivity for Various Tests

I Test 50

y_d/y_o	y^+	$\frac{\epsilon}{\nu}_m \times 10^3$ ft.^{2}/sec.
0.02	20.3	1.00
0.04	40.6	2.56
0.06	60.8	3.58
0.08	81.1	5.00
0.10	101.4	5.83
0.15	152.1	7.00
0.20	202.7	7.43
0.25	253.4	7.62
0.30	304.1	7.78
0.35	354.8	7.64
0.40	405.5	7.48
0.45	456.2	7.28
0.50	506.8	7.21

Incoming air temperature	100.0°F
Upper plate temperature	100.0°F
Lower plate temperature	100.0°F
Average velocity	58.7 ft./sec.
Reynolds number	36400
Friction velocity	3.27 ft./sec.
$(\nu)_{y/y_o = 0.5}$	0.000187 ft.^{2}/sec.

Table VIII. (Cont'd.) Total Viscosity and Total Conductivity for Various Tests

J Test 60

y_d/y_o	y^+	$\epsilon_m \times 10^3$ ft.^{2}/sec.	$\epsilon_c \times 10^3$ ft.^{2}/sec.
0.005	1.4	0.27	0.34
0.010	2.7	0.27	0.34
0.015	4.1	0.28	0.34
0.020	5.5	0.28	0.34
0.030	8.2	0.28	0.34
0.040	11.0	0.30	0.51
0.060	16.4	0.52	0.75
0.080	21.9	0.74	1.06
0.100	27.4	1.03	1.42
0.125	34.2	1.44	1.90
0.150	41.1	1.89	2.40
0.175	47.9	2.26	2.70
0.200	54.8	2.50	2.87
0.250	68.5	2.67	3.03
0.300	82.2	2.76	3.07
0.350	95.8	2.82	3.08
0.400	109.5	2.87	3.08
0.450	123.2	2.92	3.05
0.500	136.9	2.72	3.10

Incoming air temperature	100.0°F
Upper plate temperature	115.3°F
Lower plate temperature	85.0°F
Average velocity	13.3 ft./sec.
Reynolds number	8200
Friction velocity	0.389 ft./sec.
$(\nu)_{y/y_o = 0.5}$	0.000186 ft.^{2}/sec.
$(K)_{y/y_o = 0.5}$	0.000262 ft.^{2}/sec.

Table VIII. (Cont'd.) Total Viscosity and Total Conductivity for Various Tests

K Test 61

y_d/y_o	y^+	$\epsilon_m \times 10^3$ ft.^{2}/sec.	$\epsilon_h \times 10^3$ ft.^{2}/sec.
0.005	1.4	0.21	0.25
0.010	2.7	0.21	0.25
0.015	4.0	0.21	0.25
0.020	5.4	0.20	0.25
0.030	8.1	0.23	0.34
0.040	10.8	0.31	0.45
0.060	16.2	0.51	0.66
0.080	21.6	0.74	0.97
0.100	26.9	1.10	1.31
0.125	33.7	1.50	1.61
0.150	40.4	1.90	1.87
0.175	47.1	2.11	2.09
0.200	53.9	2.24	2.26
0.250	67.3	2.44	2.48
0.300	80.8	2.59	2.53
0.350	94.3	2.70	2.57
0.400	107.7	2.78	2.61
0.450	121.2	2.82	2.64
0.500	134.7	2.81	2.65

Incoming air temperature	100.0°F
Upper plate temperature	84.9°F
Lower plate temperature	115.0°F
Average velocity	13.2 ft./sec.
Reynolds number	8040
Friction velocity	0.881 ft./sec.
$(\nu)_{y/y_o = 0.5}$	0.000187 ft.^{2}/sec.
$(K)_{y/y_o = 0.5}$	0.000263 ft.^{2}/sec.

Part II

Evaporation of Water Drops in a Turbulent Air Stream

Introduction

The evaporation of water drops in a turbulent air stream was investigated as part of the comprehensive program of experimental studies of transfer processes now under way in the Chemical Engineering Department of the California Institute of Technology. More specifically the research was initiated with the hope of obtaining data which would be of assistance to air conditioning engineers in designing humidifying or dehumidifying equipment.

Of the many previous investigators of water evaporation, some, such as Gilliland and Sherwood (1), were concerned with the evaporation of water from a wetted wall. Others, such as Frössling (2) and Houghton (3), considered the evaporation of drops but not under the conditions to be found in air conditioning equipment. The present work was undertaken with a view to duplicating more closely the situation obtaining in such apparatus.

The experimental work consisted of a study of the evaporation of water drops sprayed by an atomizing nozzle into a stream of air in turbulent flow. The approximate range of drop diameters was from 0.5 to 150 microns. The bulk velocity of the air was approximately 9 ft./sec. which corresponded to a Reynolds number of approximately 25,000. Before the air reached the nozzle it had been conditioned to a temperature of 100°F and to a humidity of 0.015 weight fraction water. At six distances downstream from the nozzle measurements were made of velocity,

composition, and apparent temperature as functions of position at right angles to the direction of flow. At two distances from the nozzle suspensions of the drops in oil were obtained at various locations across the stream. These suspensions were examined by means of a microscope and the drops were measured and counted. From the data obtained it was possible to calculate and compare the eddy diffusivity of water vapor and the eddy conductivity for the nonuniform situation under consideration. The relationship between the eddy diffusivity and eddy conductivity is of interest since it may be possible to extend the analogy between momentum and thermal transfer, considered in Part I of this thesis, to include the transfer of material. Thus corresponding to Equations 1 and 10 of Part I we would have the relationship:

$$\dot{m} = (\epsilon_d + D)\frac{dC}{dx} \qquad (1)$$

where ϵ_d and D are the eddy and molecular diffusivities respectively.

Apparatus

The general arrangement of the apparatus is shown in Figure 1. In principle the equipment consisted of facilities for conditioning the air and for passing it by the nozzle. The drops were sprayed into the stream in the direction of air flow. Equipment for making measurements of temperature, velocity, and composition, and for collecting drop samples, was located downstream from the nozzle.

The path of the air through the apparatus may be followed in Figure 1. Air was fed by a blower into a chamber containing a steam

heater, an electric heater, and a humidifying device. Here the air was conditioned to a humidity of 0.015 weight fraction water and to a temperature somewhat above 100°F. From the conditioning chamber the air was passed into a vertical section of approximately 6-inch inside diameter brass pipe. This vertical section carried the air to the ceiling of the laboratory where it entered a plenum chamber fitted with turning vanes. From the chamber the air flowed downward through a second section of brass tube of outside diameter slightly less than 6 inches. This tube extended for some 14 diameters downward from the plenum chamber. The atomizing nozzle was supported at the end of the tube by the lines carrying the air and water which produced the spray. The air passed by the nozzle at 100°F and entered a length of transparent lucite tubing. The lucite section had an inside diameter of exactly 6 inches and could be moved in telescopic fashion over the section of brass tube above it. After leaving the transparent section the air flowed through brass pipes which discharged it at a point outside the laboratory.

A pitot tube and thermocouple (Figure 2) were mounted on a traversing screw at the lower end of the lucite section. Since the lucite tube could be telescoped over the brass tube above it, determinations of temperature and velocity could be made at various distances from the nozzle. The traversing screw allowed the position of the thermocouple and pitot tube to be varied relative to the axis of the flow.

The pitot tube served as a sampling tube as well as a velocity measuring device. In determining the composition of the stream, kerosene was allowed to run from a cylinder of measured volume of which the upper end was connected through two calcium chloride tubes to the pitot tube. The weight of water associated with a definite volume of air was obtained by weighing the calcium chloride tubes before and after draining the kerosene from the calibrated cylinder.

The thermocouple was made from a 0.001-inch diameter platinum wire and a 0.001-inch diameter 90% platinum, 10% iridium wire. Short sections of these were fused together end to end with no increase in diameter and the combination was soldered to small copper posts on the probe of Figure 2. The copper posts were insulated from the metal of the probe by bakelite inserts. Leads of the same compositions as the thermocouple wires were obtained. Each was soldered to the proper copper post and was passed along the probe through glass spaghetti insulation to an ice bath. The leads were joined to copper wires here and the latter connected to the potential terminals of a White potentiometer.

The humidifying device of the conditioning chamber consisted of a calibrated needle valve, bleeding steam into the conditioning chamber at a point just upstream from the heaters. The humidity of the air passing into the blower inlet was measured by means of a continuous reading wet and dry bulb psychrometer consisting of an electric fan blowing air on a wet and a dry bulb thermometer. The calibrated valve was adjusted frequently to bring the total humidity of the air to the

required 0.015 weight fraction water. A constant pressure was maintained on the steam side of the needle valve by connecting it through a 1/2-inch line to the bottom of a water column approximately six feet in depth and open to the atmosphere at the top.

The nozzle was a Sprayco air atomizing head, model number 125, with air tip F 2070.

A drop sampling probe could be mounted in place of the pitot tube and thermocouple assembly. It consisted of a bar of lucite as shown in Figure 3. The small well in the end of the probe was used to hold oil in which water drops became suspended when the well was exposed in the heterogeneous part of the air and water stream.

Experimental Methods

The air velocity was controlled by adjusting a gate valve at the blower inlet so that a constant pressure drop was maintained across a sharp-edged orifice in the first vertical section of brass tube. The pressure drop was measured by means of a micromanometer of the same general type as that shown in Figure 4 of Part I of this thesis. It is estimated that the Reynolds number was constant at 25,000 within ± 5% during all of the tests. In five of the six traverses at varying distances from the nozzle the Reynolds number was within 3% of the quoted value.

The needle valve used for supplying steam to the air in the conditioning chamber was provided with a graduated dial. The dial was calibrated with the flows of air and water to the nozzle cutoff. The

valve was set to a dial reading and the difference between room humidity and the humidity of the air at the entrance to the test section was determined by reading the wet and the dry bulb thermometers and by withdrawing a sample through the pitot tube and calcium chloride tubes. The procedure was repeated for several settings of the valve and a calibration curve was obtained which showed the weight fraction of water added as a function of valve dial reading. The calibration was checked frequently during the experiments and a slight drift in calibration was noted. It is estimated that the inlet weight fraction water was maintained at 0.015 $\pm 10\%$ in all the tests. During 80% of the operating time control was probably to within 7% of the desired inlet composition.

The inlet air temperature was controlled by manual adjustment of a variac transformer supplying energy to the electric heater. The steam heater was left at a constant setting since it had a larger lag than did its electrically operated counterpart. The input to the electric heater was varied so that a constant temperature was maintained at the exit of the plenum chamber as indicated by a thermocouple located there. The constant temperature to be maintained at this point was determined in the following way. The flows of air and water to the nozzle were turned off. The lucite tube was raised until the probe thermocouple reached the entrance of the test section. The temperature of the air was adjusted by means of the electric heater until this thermocouple indicated 100°F. The desired reading of the thermocouple at the exit of the plenum chamber was then obtained. Frequent checks

of the setting were made. It is estimated that the air temperature at the entrance to the test section was controlled at 100°F ±0.3°F during all the tests.

Distilled water was fed to the nozzle from a tank located near the blower. The top of the tank was connected by a valve to the laboratory air line. The pressure on the water surface in the tank could therefore be varied and the rate of flow of water to the nozzle controlled. The valve between the tank and the air line was kept closed except while adjustments of the pressure in the tank were being made. In order to allow the use of a pressure which could be read conveniently on a gauge, a coil of small diameter copper tubing was installed as part of the line between the tank and the nozzle. The water tank was provided with a sight glass which was connected by valves to the tank at its top and bottom. The line to the nozzle was connected on the sight glass side of the lower valve, and the sight glass was provided with a calibrated scale. The rate of supply of water to the nozzle could be determined by finding the rate of fall of the water in the glass when the lower valve was closed. A stop watch was used to determine the rate and the rate was reset just before each determination of the composition. The rate of flow of water to the nozzle was maintained at 0.000228 lb./sec. ±3%.

The rate of air flow to the nozzle was maintained constant by manual adjustment of a throttle valve between the laboratory air system and the air line to the nozzle. A constant pressure difference was

maintained across an orifice in this air line. The pressure difference was measured by means of a water-in-glass manometer. The rate of air flow to the nozzle was maintained at 0.00178 lb./sec. ± 4%.

As mentioned previously the sampling system consisted of the pitot tube, two weighed calcium chloride tubes, and a calibrated glass cylinder filled with kerosene. The parts were connected in series with the line between the second calcium chloride tube and the glass cylinder, entering the latter at the top of the vessel. Compositions were obtained by allowing the kerosene to drain from the cylinder and draw material from the channel through the weighed calcium chloride tubes. The latter were then reweighed. The gain in weight equalled the amount of water present in a volume of the flowing air equal to the volume of the glass cylinder. Compositions were obtained by a simple calculation.

When samples were taken in the heterogeneous region of the flowing stream, the rate of draining was adjusted so that the velocity of the material entering the end of the pitot tube approximated the velocity of the stream at the point where the samples were being taken. In certain regions close to the nozzle the resistance to flow of air through the calcium chloride tubes was sufficiently high as to make the proper adjustment impossible. However, where it could be made, it insured that the sample would be as representative as possible of the actual conditions at the point being studied. A velocity which was too high at the pitot tube mouth would result in too many drops being collected. Too low a velocity would result in some drops being deflected around the

tube and too few drops would be collected. When a sample was about to be taken, air was sucked through the pitot tube and a spare calcium chloride drying tube in series with it until the instant at which the kerosene began to drain from the calibrated vessel. By an arrangement of stopcocks the sample stream was then started through the weighed calcium chloride tubes. By this means it was insured that approximately the same amount of liquid remained in the pitot tube before and after sampling.

The weight fractions of water were measured with an approximate uncertainty of ± 5%.

Velocity measurements were made with the pitot tube connected to one side of the micromanometer mentioned previously. A piezometer ring at the base of the lucite section was connected to the opposite side of the micromanometer so that impact pressures and therefore velocities could be obtained. The static pressure was measured by closing the valve leading from the micromanometer to the pitot tube and opening a valve leading to the atmosphere on the same side of the micromanometer. Velocity measurements showed an uncertainty of approximately ±0.2 ft./sec. Their absolute accuracy was probably only slightly less.

Temperature measurements in the test section were made with the thermocouple mounted on the probe as previously described. The thermocouple at the exit from the plenum chamber was a standard copper constantan couple. All thermocouple readings were made with a White double potentiometer.

In preliminary work, readings were taken on the center line of the test section at various distances from the nozzle with a temporary thermocouple made from 30-gauge copper and constantan wire. A platinum resistance thermometer made from 0.001-inch diameter platinum wire was used to measure the temperature at the same locations. Finally, a third set of readings was made with the fine platinum and 90% platinum-10% iridium thermocouple previously described. The flows of air and water were the standard ones described. The results of the measurements were almost the same when the 0.001-inch wires were used. However the 30-gauge wires gave very different results at certain locations. The readings of the 0.001-inch thermocouple and the 30-gauge thermocouple are compared in Table I and Figure 4. Evidently in the very wet portions of the tube the fine wire read slightly less than the coarse one did. However, where water drops were fewer the fine wire gave much higher results than did the coarse one, and evidently the fine wire suffered on the average a much smaller wet bulb effect. It was therefore chosen as the temperature measuring device for the subsequent work. However, it was evidently subject to a certain error of unknown magnitude as a result of what has been termed the wet bulb effect. In other words the wire was cooled below the true gas phase temperature by the evaporation of water from its surface. For this reason the temperatures recorded in Table II have been labeled <u>apparent temperatures</u>. Measurements of the apparent temperature were made with an uncertainty of approximately $\pm 0.3^{\circ}F$.

The drop samples were taken with the help of the probe described previously and illustrated in Figure 3. The small well at the

end of the probe was half filled with water-saturated machine oil. The samples were taken by mounting the probe temporarily on the traversing screw in the position normally occupied by the thermocouple and pitot tube probe. The position of the lucite section was adjusted and the traversing screw turned until the well was in the desired position in the heterogeneous part of the stream. The oil in the well was then exposed by sliding back the covering bar, shown in Figure 3, for an interval of time which was measured by means of a stopwatch. The probe was then removed from the traversing screw and a drop of oil was added to that already in the well, in order to prevent the evaporation of any water drops remaining on the surface of the oil. However, most of the drops were found to pass through the oil surface. They then fell gradually downward through that liquid. The technique of collecting the drops in oil was a modification of a method by Ermilova (4).

The well and its contents were examined under a 100-power microscope fitted with a micrometer eyepiece. The sizes of the drops were measured by comparing them with the divisions of the eyepiece scale. The drops were counted also. The diameter of the well was 0.0628 inch so that when it was examined under the microscope it just filled the field of vision.

Experimental Results

Primary Data

Measurements of apparent temperature, velocity, and composition were made at 6 distances from the nozzle under the standard flow conditions

described in the preceding section. The distances were 8, 12, 16, 24, 32, and 60 inches. At each distance measurements were taken at one half inch intervals across a diameter of the tube. Since the velocity and composition measurements both depended on the use of the pitot tube, the positions at which those measurements were made were exactly the same. Furthermore, they were made at approximately the same time. Radial symmetry was assumed, so that measurements were made on only one diameter at each distance from the nozzle. Actually some asymmetry was apparent in the experimental measurements.

The apparent temperatures are listed in Table II. Smoothed values are shown in graphical form in Figure 5. Temperature contours for the tube are presented in Figure 6. The cooling of the air by the evaporation of water in the vicinity of the nozzle is very evident. At a distance of 24 inches from the nozzle turbulent diffusion of thermal energy has very nearly restored a uniform temperature profile in the stream. The temperature profiles are completely uniform at 32 and 60 inches from the nozzle.

Compositions are listed in Table III and smooth values are shown graphically in Figure 7. Very large weight fractions of water are of course obtained immediately below the nozzle. Evaporation and turbulent diffusion have produced a uniform composition profile in the stream before it has reached a distance of 32 inches from the nozzle.

The experimental measurements of velocity are listed in Table IV. They are shown smoothed in graphical form in Figure 8. Immediately under

the nozzle the velocity is high as a result of the introduction of the high velocity flow of air used to atomize the liquid water. At a distance of 32 inches from the nozzle transfer of momentum has reestablished a normal turbulent velocity profile.

Drop diameter distributions were obtained at distances of 12 and 24 inches from the nozzle. As with temperatures, velocities, and compositions, data were obtained at points one half inch apart along a diameter of the tube. No samples were taken at distances greater than 1 1/2 inches from the center of the tube because the time for collection of some 30 drops became comparatively long in such regions of the stream. In Table V the number of drops of each diameter in the various samples are listed. Table VI shows the rate of collecting drops at each sample point. Figure 9 gives the same information in graphical form. When each distribution was plotted on logarithmic probability paper, reasonably straight lines were obtained. The distributions for the most part, therefore, followed patterns which were skewed somewhat from the normal pattern (5), (10). Figure 10 is a representative logarithmic probability plot showing one of these size distributions.

Derived Data

Average apparent temperatures were calculated at the distances from the nozzle where measurements had been made. These averages were obtained by graphical integration. Consider a plan view of the tube with a ring-like element of width dr as shown.

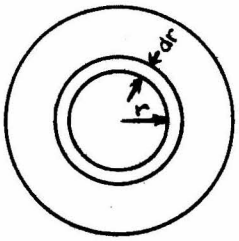

Take the enthalpy of the gas phase to be zero at 100°F. Assume constant specific heat of the gas phase between 60°F and 100°F and neglect the effect of water vapor on C_p. Water vapor never exceeded 8% of the gas phase by weight. Then the total enthalpy which passes through the cross section shown per second is given by:

$$2\pi C_p \int_0^{r_o} u \sigma r (t-100)\, dr \qquad (2)$$

and also by:

$$2\pi C_p (t_{ave.}-100) \int_0^{r_o} u \sigma r\, dr \qquad (3)$$

Suppose that all the gas phase passing through the cross section of the tube under consideration were collected for one second, placed in an adiabatic container, and mixed. Furthermore, suppose that heats of mixing were zero. Then $t_{ave.}$ would be the temperature assumed by the mixture. This average temperature is the one which must be used to determine the net cooling which has occurred in the gas phase at any distance from the nozzle as a result of water drop evaporation. Assuming a perfect gas,

$$\sigma = \frac{P}{bT} \qquad (4)$$

and since the pressure remained approximately constant during each traverse, Equations 2, 3, and 4 may be combined as follows:

$$2\pi C_p \frac{P}{b}\int_0^{r_o}\frac{urt}{T}\,dr = 2\pi C_p \frac{P}{b} t_{ave.}\int_0^{r_o}\frac{urdr}{T} \qquad (5)$$

Canceling the constant coefficients from Equation 5 and solving for $t_{avo.}$ gives the result:

$$t_{ave.} = \frac{\int_0^{r_o}\frac{urt}{T}\,dr}{\int_0^{r_o}\frac{ur}{T}\,dr} \qquad (6)$$

In obtaining the average temperatures from the above equation each integration was performed twice, once using the experimental points on one side of the tube axis, and once using the points on the other side. The results were then averaged. This procedure was necessary because of the presence of a degree of asymmetry in the experimental data.

The weight rate of gas phase flow at each distance from the nozzle was calculated by means of a graphical integration expressed by the equation:

$$\dot{m}_g = 241.54\int_0^{r_o}\frac{ur}{T}\,dr \qquad (7)$$

The asymmetry in the experimental data was taken into account by evaluating the integral for the points on each side of the center line and averaging. Equation 7 was derived by considering once more the element of area in the diagram above. Then:

$$\dot{m}_g = \int_0^{r_o} 2\pi r u \rho\, dr \qquad (8)$$

If Equation 4 is written for 32°F and the same pressure, there is obtained:

$$\sigma_{32} = \frac{P}{b\ 491.7} \tag{9}$$

Dividing Equation 4 by Equation 8 and rearranging the result produces:

$$\sigma = \sigma_{32}\ \frac{491.7}{T} \tag{10}$$

The quantity σ_{32} was calculated from the perfect gas law. Neglecting the water from the nozzle, which was only 0.2% of the total flow, the average molecular weight of the gas phase was 28.71. An average barometric pressure of 743 millimeters was assumed. Then:

$$\sigma_{32} = \left(\frac{28.71}{359}\right)\left(\frac{743}{760}\right) \tag{11}$$

Combining Equations 8, 10, and 11 produced Equation 7.

An equation similar to Equation 7 was used to calculate the weight rate of flow of water at the various distances from the nozzle at which experimental data were obtained. This equation was derived similarly to Equation 7 and in its final form was the following:

$$\dot{m}_w = 241.54 \int_0^{r_o} \frac{u X r}{T}\ dr \tag{12}$$

The integration was performed graphically and the asymmetry of the data was taken into account as previously described. Equation 12 gives the sum of the weight rates of gaseous and liquid water flow. The use of Equation 12 assumes that the water drops travel at the same velocity as the gas phase and that the unevaporated drops have no effect on the density of the air stream. The latter part of the assumption is

certainly satisfactory since the maximum weight fraction of both evaporated and unevaporated water is 0.020.

Enthalpies per pound of the flowing gas phase were calculated from the apparent temperatures and corresponding weight rates of flow at the various distances from the nozzle. The enthalpy was taken to be zero at 100°F. The contribution to the enthalpy of the water vapor resulting from the evaporation of nozzle water was neglected. Only a minute error was involved since the nozzle water was only some 0.2% of the total flow. Both the air and the water vapor of the gas phase were treated as perfect gases. In other words the assumption was made that:

$$H = f(T) \tag{13}$$

The assumption was an excellent one for the air and quite satisfactory for the water vapor, since the latter amounted to less than 2% of the total weight rate of flow where the water concentration was a maximum. The tables of Keenan and Keyes (6) and of Keenan and Kaye (7) were used as the sources of the enthalpy data. The weight rates of flow used were those calculated by means of Equation 7. The use of these weight rates was somewhat inconsistent with the earlier assumption whereby the enthalpy of the evaporated water was neglected. However, the error involved was negligible since the water flow to the nozzle was such a small fraction of the total weight rate.

The plots of the drop size distributions were analyzed in the following manner. The geometric mean, D_g, and the standard geometric deviation, σ_g, were determined for each plot. These quantities may be

defined (8) by the equations given below:

M_g = diameter corresponding to an abscissa of 50% on the plot (14)

$$\sigma_g = \frac{\text{diameter at 84.13\%}}{\text{diameter at 50\%}} = \frac{\text{diameter at 50\%}}{\text{diameter at 15.87\%}} \tag{15}$$

The average volume diameter may be defined by the equation:

$$D_v = \sqrt[3]{\frac{\Sigma (n \delta^3)}{\Sigma n}} \tag{16}$$

and the average surface diameter by the equation:

$$\Delta = \sqrt{\frac{\Sigma (n \delta^2)}{\Sigma n}} \tag{17}$$

These last two quantities were calculated for each sample point by using the equations listed below (References 8, 9, and 10):

$$\log_{10} D_v^3 = \log_{10} M_g^3 + 10.3617 \log_{10}^2 \sigma_g \tag{18}$$

$$\log_{10} \Delta^2 = \log_{10} M_g^2 + 4.6052 \log_{10}^2 \sigma_g \tag{19}$$

The average weight of a drop was calculated from the quantity D_v, and the average surface area from the quantity Δ. The ratio of the average surface area to the average weight gave the specific surface of liquid water at the sample point. The specific surface and the average volume and average surface diameters are listed in Table VII. The average volume diameters are shown as a function of radial distance in Figure 11.

Numerical integrations were made to obtain the total weight rate of flow of liquid water at distances of 12 and 24 inches from the nozzle. The rate at which the drops were collected at each sample point was determined. The average weight of a drop was known and also the area of the well at the end of the probe. The rate at which liquid water passed through a unit area at the sample point was therefore easily obtainable. The rate at each sample point was multiplied by the appropriate area. The sums of these products for one distance from the nozzle gave the total rate of liquid water flow at that distance. The part of the tube outside of the sampled region was included in the integration, since the sum of the products was plotted versus distance from the center and the curve was extrapolated to the wall.

The calculated values of the average apparent temperatures, the corresponding enthalpies, the total weight rate of gas phase flow, and the total weight rate of water flow are listed in Table VIII for six distances from the nozzle. The total weight rate of liquid water flow is listed for two distances from the nozzle. These last two figures are probably somewhat in error for reasons which will be indicated later.

Eddy conductivities were calculated from the temperature data for the nonuniform flow situation below the nozzle. For reasons to be indicated in the next section it was believed that, although evaporation was still going on, 98% of the liquid introduced by the nozzle had been vaporized 8 inches below it. Therefore it was possible to calculate the eddy conductivites from the temperature profiles, neglecting the effect of further evaporation on the temperature.

The equation used to calculate eddy conductivities was derived

by making an energy balance on an annular element in the flowing stream:

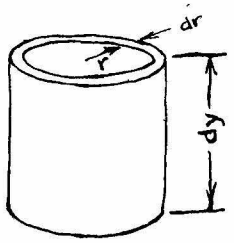

The following equation may be written to express the thermodynamic quantity work for the open system consisting of the annular element (11):

$$-\underline{w} = -P d\underline{V} + P'V'dm + \underline{j} \tag{20}$$

Since

$$d\underline{V} = 0 \tag{21}$$

and

$$P'V' = PV \tag{22}$$

Equation 20 becomes

$$-\underline{w} = PV dm \tag{23}$$

or

$$\frac{-\underline{w}}{d\theta} = PV \frac{dm}{d\theta} \tag{24}$$

Then the rate of accumulation of energy in the element as the result of work done on the element by the surroundings and by the element on the surroundings is given by the equation

$$-\frac{\partial}{\partial r}\left[\frac{-W}{d\theta}\right]dr = -\frac{\partial}{\partial r}\left[PV\frac{dm}{d\theta}\right]dr \qquad (25)$$

where material transfer in the r direction only is considered. If $\dot{m}_r$ is the rate of flow in lb/sec. ft.^{2} in the radial direction, Equation 25 may be written for flow across the boundaries of the element in that direction as,

$$-\frac{\partial}{\partial r}\left[\frac{-W}{d\theta}\right]dr = -\frac{\partial}{\partial r}\left[PV\dot{m}_r\, 2\pi r\, dy\right]dr \qquad (26)$$

For flow in the y direction Equation 26 becomes,

$$-\frac{\partial}{\partial y}\left[\frac{-W}{d\theta}\right]dy = -\frac{\partial}{\partial y}\left[PV\dot{m}_y\, 2\pi r\, dr\right]dy \qquad (27)$$

If energy transferred as the result of a temperature gradient is not considered for the moment, the rate of accumulation of all other forms of energy in the element as a result of flow in the radial direction is given by:

$$-\frac{\partial}{\partial r}\left[\dot{m}_r\left(E+PV+\frac{u_r^2}{2g}+h\right)2\pi r\, dy\right]dr \qquad (28)$$

where the term $(PV)(\dot{m}_r)(2\pi r\, dy)$ is the work term expressed by Equation 26. If the very small energy terms involving kinetic energy and elevation are neglected, and if E + PV is replaced by H, Equation 28 reduces to

$$-\frac{\partial}{\partial r}\left[\dot{m}_r H\, 2\pi r\, dy\right]dr \qquad (29)$$

A corresponding equation applies for flow in the axial direction. Thus,

$$-\frac{\partial}{\partial y}\left[\dot{m}_y H 2\pi r dr\right] dy \tag{30}$$

Now r and y are independent variables and

$$\dot{m}_r = u_r \sigma \tag{31}$$

and

$$\dot{m}_y = u_y \sigma \tag{32}$$

Hence Equations 28, 29, and 30 reduce to

$$-2\pi \frac{\partial}{\partial r}\left[u_r \sigma r H\right] dy dr \tag{33}$$

and

$$-2\pi \frac{\partial}{\partial y}\left[u_y \sigma r H\right] dy dr \tag{34}$$

The rate of accumulation in the element of energy other than that transferred by temperature gradients is then given by the sum of Equations 33 and 34:

$$-2\pi \frac{\partial}{\partial r}\left[u_r \sigma r H\right] dy dr - 2\pi \frac{\partial}{\partial y}\left[u_y \sigma r H\right] dy dr$$

$$= -2\pi\left[u_r \sigma r \frac{\partial H}{\partial r} + H \frac{\partial (u_r \sigma r)}{\partial r}\right] dy dr \tag{35}$$

$$-2\pi\left[u_y \sigma r \frac{\partial H}{\partial y} + H \frac{\partial (u_y \sigma r)}{\partial y}\right] dy dr$$

However the equation of continuity (12) written for the situation under consideration is:

$$\frac{1}{r}\left[\frac{\partial(r\sigma u_r)}{\partial r} + \frac{\partial(r\sigma u_y)}{\partial y}\right] = 0 \qquad (36)$$

Equation 36 allows the reduction of Equation 35 to the following:

$$-2\pi\left[u_r \sigma r \frac{\partial H}{\partial r} + u_y \sigma r \frac{\partial H}{\partial y}\right] dy\, dr \qquad (37)$$

Now, assuming a perfect gas,

$$dH = C_p\, dt \qquad (38)$$

Equation 37 becomes

$$-2\pi\left[u_r \sigma r C_p \frac{\partial t}{\partial r} + u_y \sigma r C_p \frac{\partial t}{\partial y}\right] dy\, dr \qquad (39)$$

The rate of accumulation of energy in the element as a result of temperature gradients is given by the equation:

$$2\pi\left\{\frac{\partial}{\partial r}\left[C_p \sigma(\epsilon_c + K) r \frac{\partial t}{\partial r}\right] + \frac{\partial}{\partial y}\left[C_p \sigma(\epsilon_c + K) r \frac{\partial t}{\partial y}\right]\right\} dy\, dr \qquad (40)$$

which results from the application of Equation 14 of Part I of this thesis. The total rate of accumulation of energy in the element is zero since a steady state exists. Thus Equations 39 and 40 sum to zero and after the cancellation of common factors the relation given below results:

$$\frac{\partial}{\partial r}\left[C_p \sigma (\epsilon_c + K) r \frac{\partial t}{\partial r}\right] + \frac{\partial}{\partial y}\left[C_p \sigma (\epsilon_c + K) r \frac{\partial t}{\partial y}\right]$$

$$= u_r \sigma r C_p \frac{\partial t}{\partial r} + u_y \sigma r C_p \frac{\partial t}{\partial y} \qquad (41)$$

On the assumption that variations in C_p and in σ may be neglected Equation 41 reduces to:

$$\frac{1}{r}\frac{\partial}{\partial r}\left[(\epsilon_c+K)\,r\,\frac{\partial t}{\partial r}\right]+\frac{1}{r}\frac{\partial}{\partial y}\left[(\epsilon_c+K)\,r\,\frac{\partial t}{\partial y}\right] = u_r\frac{\partial t}{\partial r}+u_y\frac{\partial t}{\partial y} \tag{42}$$

Now K is small as compared with ϵ_o in the turbulent core. Also the transfer of energy by eddy conduction along the axis is small as compared with the transfer of energy by bulk velocity in this direction. Thus Equation 42 may be written as:

$$\frac{1}{r}\frac{\partial}{\partial r}\left(\epsilon_c\, r\,\frac{\partial t}{\partial r}\right) = u_r\frac{\partial t}{\partial r}+u_y\frac{\partial t}{\partial y} \tag{43}$$

Equation 43 may now be integrated as r goes from zero to r.

$$\epsilon_c = \frac{\int_o^r u_r\, r\,\frac{\partial t}{\partial r}\,dr + \int_o^r u_y\, r\,\frac{\partial t}{\partial y}\,dr}{r\,\frac{\partial t}{\partial r}} \tag{44}$$

The term in Equation 44 involving u_r may be evaluated by making a material balance over the annular element, or by carrying out an equivalent procedure, integrating Equation 36. Thus:

$$-\frac{\partial}{\partial y}\left[\int_o^r u_y\,\sigma\,2\pi\,r\,dr\right]dy = u_r\,\sigma\,2\pi\,r\,dy \tag{45}$$

If variations in specific weight are again neglected, Equation 45 simplifies to:

$$u_r\,r = -\frac{\partial}{\partial y}\int_o^r u_y\,r\,dr \tag{46}$$

Eddy conductivities were evaluated as a function of position in the flowing stream by means of Equations 44 and 46. These quantities are listed in Table IX.

Eddy diffusivities were calculated by means of the following relationship:

$$\epsilon_d = \frac{\int_0^r \frac{\partial}{\partial y}\left[u_y C r\right] dr - C\int_0^r \frac{\partial}{\partial y}\left[u_y r\right] dr}{r\,\frac{\partial C}{\partial r}} \qquad (47)$$

This equation may be derived by arguments analogous to those given above for eddy conductivity. The eddy diffusivity values are listed in Table IX beside the corresponding eddy conductivities.

Analysis of Results

The rate of evaporation of the nozzle water was found to be very great in the region immediately beneath the nozzle where the velocity of the drops relative to the gas phase was large. An enthalpy balance was utilized to calculate the final average temperature to be expected in the stream as a result of the evaporation of all the nozzle water. The general energy balance (13) reduces to an enthalpy balance in the situation under discussion when changes in elevation and in velocity, and heat losses through the pipe wall are neglected. The average temperature resulting from the calculation was 91.3°F. Table VIII shows that the average apparent temperature at 8 inches from the nozzle was 90.6°F. Assuming that this experimental result was reasonably close to the average temperature of the gas phase, it is concluded that almost all

the nozzle water had evaporated even at 8 inches from the nozzle. It is known that some liquid was still present from the results of the drop sampling experiments, and evaporation was still continuing since none of the water weight fractions listed in Table III are close to the saturation value of 0.03 at 90°F.

The drop sampling experiments afford further indications that a very large fraction of the liquid water had evaporated at a short distance from the nozzle. The integrated values of the weight rate of liquid water flow have been listed in Table VIII for distances of 12 and 24 inches from the nozzle. The average enthalpy of the gas phase at each of these nozzle distances also has been listed in Table VIII. From these data it was possible to calculate the average latent heat of evaporation of water in the part of the tube between 12 and 24 inches from the nozzle. A value of 34,995 B.T.U./lb. resulted. It seems probable that two causes combined to produce this obviously erroneous result. First, the average enthalpy of the gas phase decreased only very slightly down the tube between the two elevations. Small errors in the measurements of the enthalpy would therefore have resulted in very large errors in the enthalpy difference. Secondly, it is uncertain whether or not the drop sampling probe picked up all the liquid water which should have been intercepted by it in the flowing stream. Under the assumption that all the discrepancy in the latent heat value was the result of the second factor, it was calculated that the fraction

of the liquid water intercepted by the probe was 1/34 of the total amount which normally passed in a unit of time through the area occupied by the drop sample well. On the above basis the integrated weight rates of water flow given in Table VIII should be multiplied by 34, and using the resulting figures it was calculated that evaporation of the nozzle water was 98.5% complete 12 inches from the nozzle and 99.9% complete 24 inches from the nozzle. Considering both the temperature and drop sample measurements, it is estimated that evaporation was 98% complete at 8 inches from the nozzle.

It is interesting to note that the specific surface of the liquid was reasonably constant between the two levels at which drop samples were taken. From Table VII the average specific surface at 12 inches from the nozzle was 194.5 sq.ft./lb, and at 24 inches from the nozzle, 156.1 sq. ft./lb. As an approximation, therefore, it might be possible to neglect the variation of specific surface with distance, in making calculations relative to the evaporation of nozzle spray.

The eddy quantities listed in Table IX are of particular interest because of the marked nonuniformity of the flow below the nozzle. The data were not sufficiently complete to allow the determination of these quantities with a high degree of certainty. However the results indicate that on the average the eddy diffusivity was approximately double the eddy conductivity. The eddy diffusivities were on the average approximately 100 times larger than those reported by Towle and Sherwood (14) and by Sherwood and Woertz (15) for similar Reynolds

numbers. The eddy conductivities were 50 times larger than those reported in Part I of this thesis for approximately the same Reynolds number.

Towle and Sherwood studied the eddy diffusivity of carbon dioxide and the eddy diffusivity of hydrogen in turbulent air streams. The hydrogen and the carbon dioxide were introduced at the axis of a cylindrical duct at an average velocity equal to the point velocity at the center of the stream. Sherwood and Woertz, on the other hand, allowed water to diffuse from a water film on one plate to a film of calcium chloride solution on a second plate parallel to the first. Air, carbon dioxide, and hydrogen in turbulent flow were passed in turn between the plates. The eddy diffusivity values reported in the two papers mentioned above are, in turn, of the order of 2.5 times greater than those found by Dohlinger (10) in an experiment where natural gas was introduced into an air stream by a tube concentric with the pipe carrying the air. The natural gas was at the same gross velocity as the air stream.

It is noteworthy that in the three references mentioned above the normal turbulent velocity profile of the flowing stream was relatively undisturbed by the introduction of the diffusing component. In the work described in this thesis the velocity profile of the air stream suffered considerable distortion as the flow passed the nozzle. Comparison of the present results with those of the above authors, on the basis of Reynolds number, is therefore unsatisfactory. The high

level of turbulence in the stream below the nozzle resulted in correspondingly high values of the eddy quantities.

Assuming the correctness of the figure for the fraction of the liquid water evaporated at 8 inches from the nozzle, one would expect comparatively few water drops below this level, but some would be present. The drop samples show that water drops were present at 12 and 24 inches from the nozzle. It is therefore necessary to class both the eddy conductivity and the eddy diffusivity as apparent eddy quantities. They have been so listed in Table IX.

The fact that on the average the eddy diffusivities were approximately double the eddy conductivities for the case under consideration indicates that in nonuniform flow the transfer of material and the transfer of heat are not wholly analogous. The discrepancy is somewhat larger than that noted when the eddy conductivity and the eddy viscosity are compared for the uniform case. Such a comparison has been made in Part I of this paper.

Conclusion

The evaporation of water drops in a turbulent air stream is a situation intrinsically difficult to explore experimentally. In making temperature measurements in heterogeneous liquid-gas regions an instrument of as small heat capacity, and of as small size as possible should be used. In making drop size measurements difficulty is encountered because a probe disturbs the flow and causes drops to be deflected from their courses.

However, at the sacrifice of some of the accuracy which is attainable in simpler situations, considerable progress has been made in the study of the evaporation of nozzle spray. The evaporation appeared to be substantially complete at a short distance from the nozzle. The specific surface of the liquid phase was found to be approximately constant as a function of distance down the tube. Eddy diffusivities were found to be approximately twice as large as the eddy conductivities obtaining and both quantities were very much larger than those measured in previous experiments where the turbulent velocity profile was undisturbed by a stream from a nozzle.

Nomenclature

b	specific gas constant, ft./^{o}R.
C	concentration, lb/ft.^{3}
C_p	specific heat at constant pressure, B.T.U./lb.^{o}F.
D	molecular diffusivity, ft.^{2}/sec.
D_v	average volume diameter, microns.
E	specific internal energy, B.T.U./lb.
H	specific enthalpy, B.T.U./lb.
h	elevation above datum plane, ft.
j	an infinitesimal quantity of friction, B.T.U.
K	thermometric conductivity, ft.^{2}/sec.
M_g	geometric mean size, microns.
m	weight of a system, lb.
$\dot{m}$	weight rate of material transfer, lb./sec. ft.^{2}
$\dot{m}_G$	total weight rate of gas phase flow, lb./sec.
$\dot{m}_r$	weight rate of flow in radial direction, lb./sec. ft.^{2}
$\dot{m}_w$	total weight rate of water flow, lb./sec.
$\dot{m}_y$	weight rate of flow in axial direction, lb./sec. ft.^{2}
n	number of drops with diameter δ.
P	pressure, lb./ft.^{2}
P'	pressure of material being added to a system, lb./ft.^{2}
r	radial distance, ft.
r_o	radius of a pipe, ft.

T	time average point temperature, $^{\circ}R.$
t	time average point temperature, $^{\circ}F.$
$t_{ave.}$	average temperature, $^{\circ}F.$
u	time average point velocity, ft./sec.
u_r	time average point velocity in the radial direction, ft./sec.
u_y	time average point velocity in the axial direction, ft./sec.
V	specific volume, $ft.^3/lb.$
$\underline{V}$	total volume of a system, $ft.^3$
V'	specific volume of material being added to a system, $ft.^3/lb.$
$\underline{w}$	an infinitesimal amount of work, B.T.U.
X	weight fraction gaseous plus liquid water.
x	distance in direction in which material transfer is taking place, ft.
y	axial distance, ft.

Δ	average surface diameter, microns.
δ	diameter of a drop, microns.
ϵ_c	eddy conductivity, $ft.^2/sec.$
ϵ_d	eddy diffusivity, $ft.^2/sec.$
θ	time, seconds.
Σ	sum of
σ	specific weight, $lb./ft.^3$
σ_g	standard geometric deviation, dimensionless.
σ_{32}	specific weight of gas phase at $32^{\circ}F$, $lb./ft.^3$

References

(1) Gilliland, E. R., and Sherwood, T. K., Ind. Eng. Chem., 26, 516 (1934).

(2) Frössling, N., Gerlands Beitr. z Geophys., 52, 1-2, 170-216 (1938); Science Abstracts, 41, 257 (1938).

(3) Houghton, H. G., Physics, 4, 413-424 (1933).

(4) Ermilova, V. N., J. Experimental and Theoretical Physics (U.S.S.R.), 9, 1281 (1939); Chem. Zentr., 111, 3298 (1940); Chem. Abstracts, 36, 3721 (1942).

(5) Fisher, R. A., and Yates, F., Statistical Tables, Oliver and Boyd Ltd., Edinburgh (1943).

(6) Keenan and Keyes, Thermodynamic Properties of Steam, Wiley (1936).

(7) Keenan and Kaye, Thermodynamic Properties of Air, Wiley (1945).

(8) Austin, J. B., Ind. Eng. Chem., Analytical Edition, 11, 334-339 (1939).

(9) Green, H., J. Franklin Inst., 204, 713 (1927).

(10) Hatch, T., and Choate, S. P., J. Franklin Inst., 207, 369 (1929).

(11) Sage, B. H., Thermodynamics of Multicomponent Systems, California Institute of Technology (1946).

(12) Sage, B. H., Standart, G. C., and co-workers, Elementary Fluid Mechanics, California Institute of Technology (1948).

(13) Lacey, W. N., and Sage, B. H., Thermodynamics of One-Component Systems, California Institute of Technology (1947).

(14) Towle, W. L., and Sherwood, T. K., Ind. Eng. Chem., 31, 457 (1939).

(15) Sherwood, T. K., and Woertz, B. B., Trans. A.I.Ch.E., 35, 517 (1939).

(16) Schlinger, W. G., Ph.D. Thesis, California Institute of Technology, 1949.

List of Figures

1. The General Arrangement of the Apparatus.

2. The Pitot Tube and Thermocouple.

3. The Drop Sampling Probe.

4. A Comparison of Thermocouple Readings.

5. Smoothed Temperatures.

6. Temperature Contours.

7. Smoothed Compositions.

8. Smoothed Velocities.

9. Average Rate of Collecting Drops at Each Sample Point.

10. A Drop Size Distribution.

11. D_v as a Function of Radial Distance.

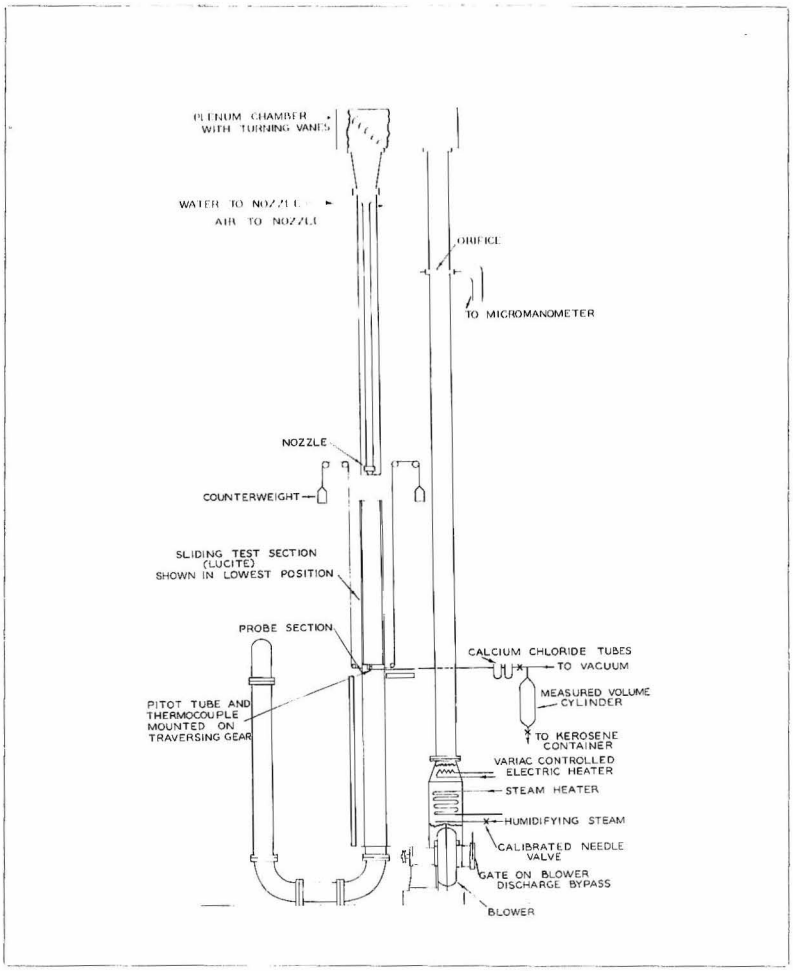

Figure 1. The General Arrangement of the Apparatus

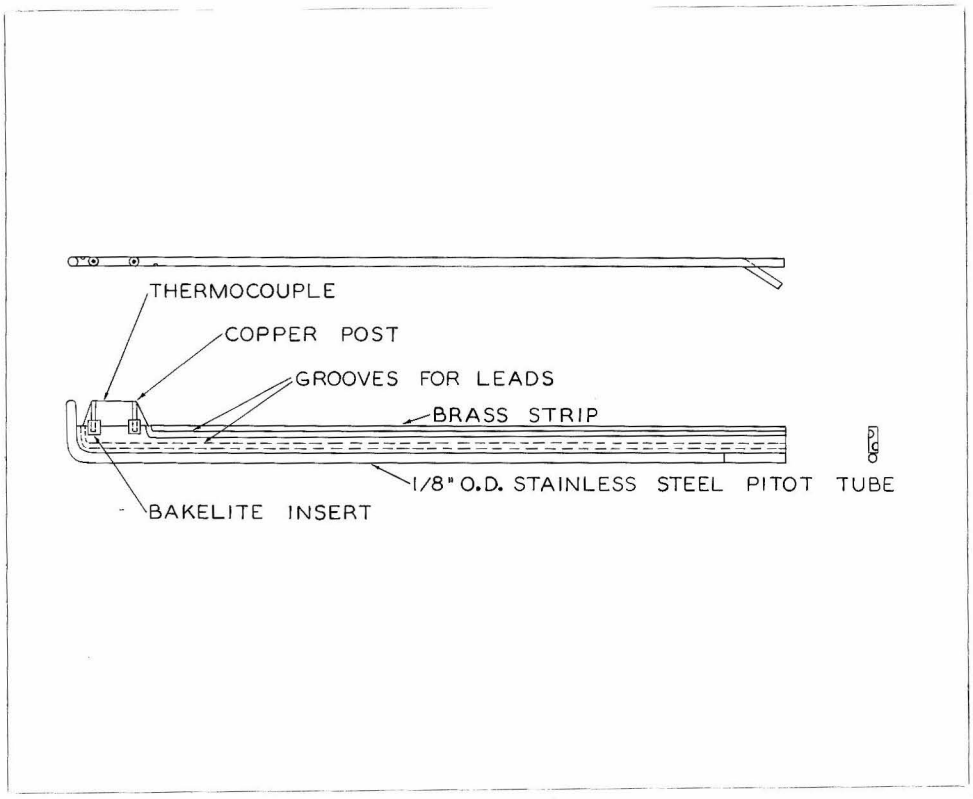

Figure 2. The Pitot Tube and Thermocouple

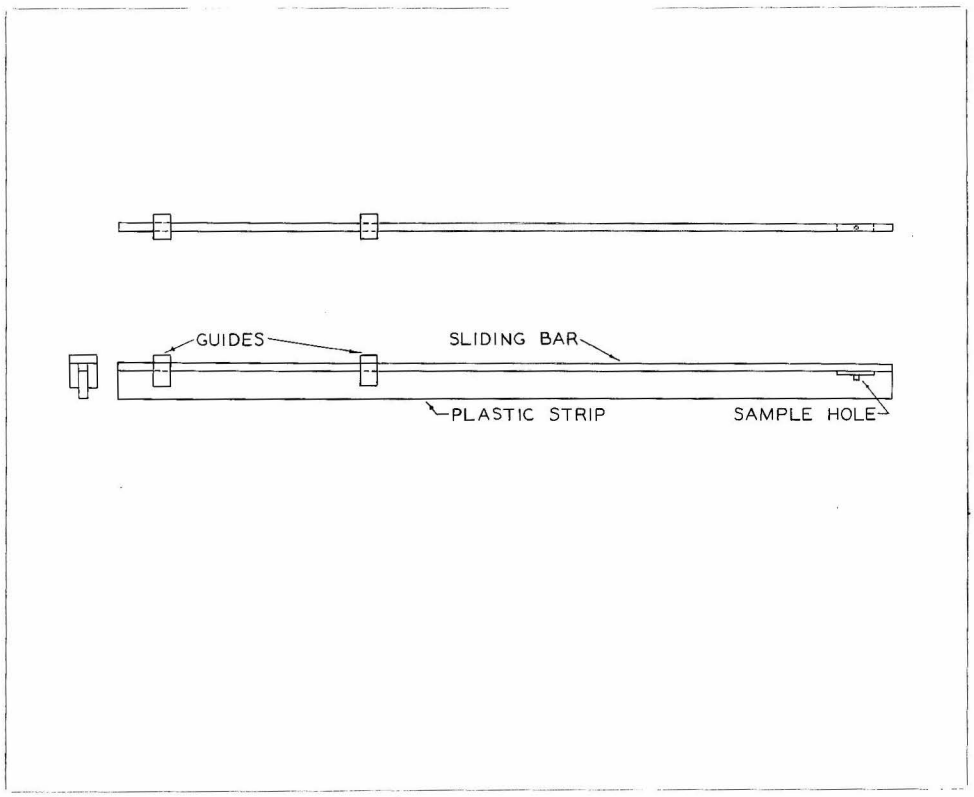

Figure 3. The Drop Sampling Probe

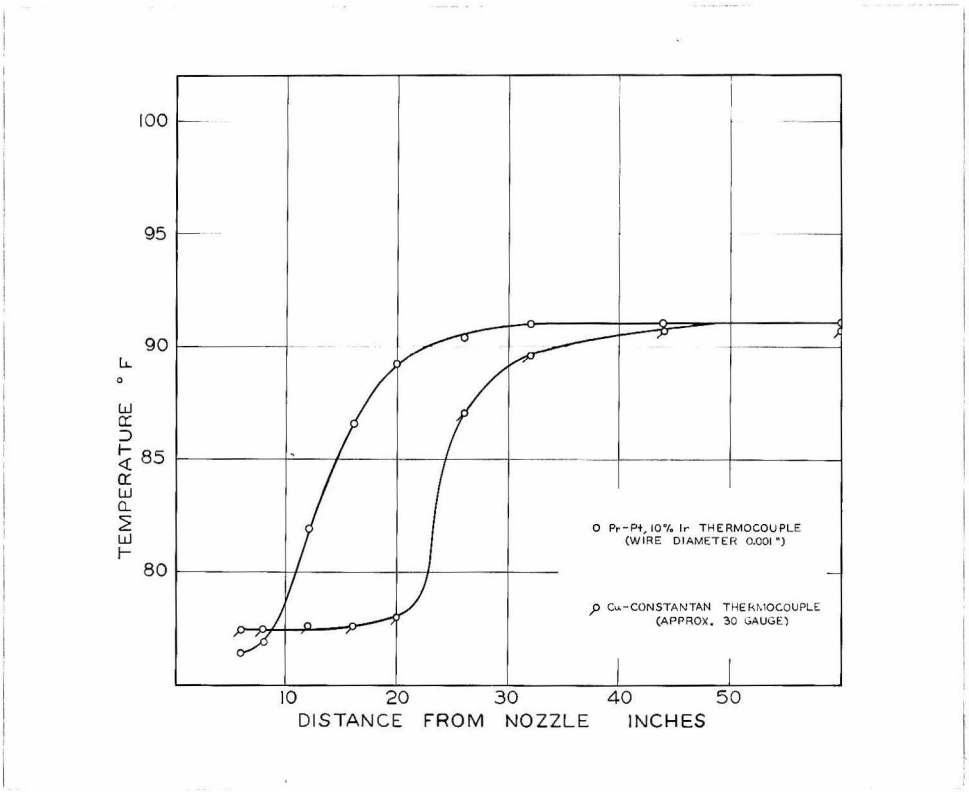

Figure 4. A Comparison of Thermocouple Readings

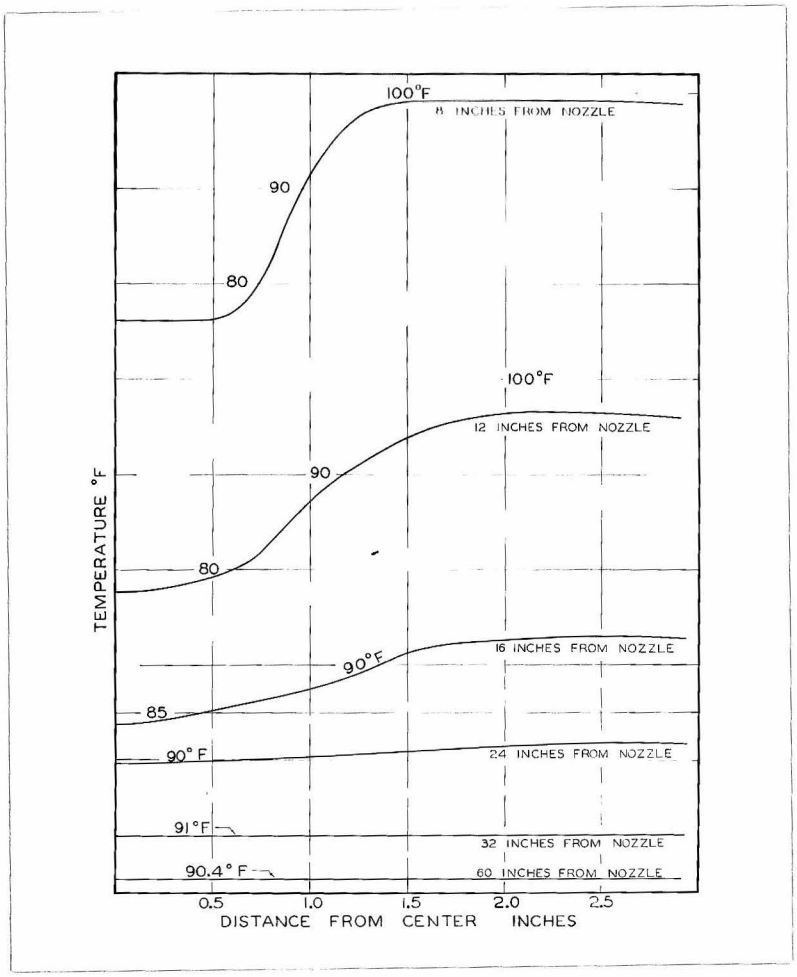

Figure 5. Smoothed Temperatures

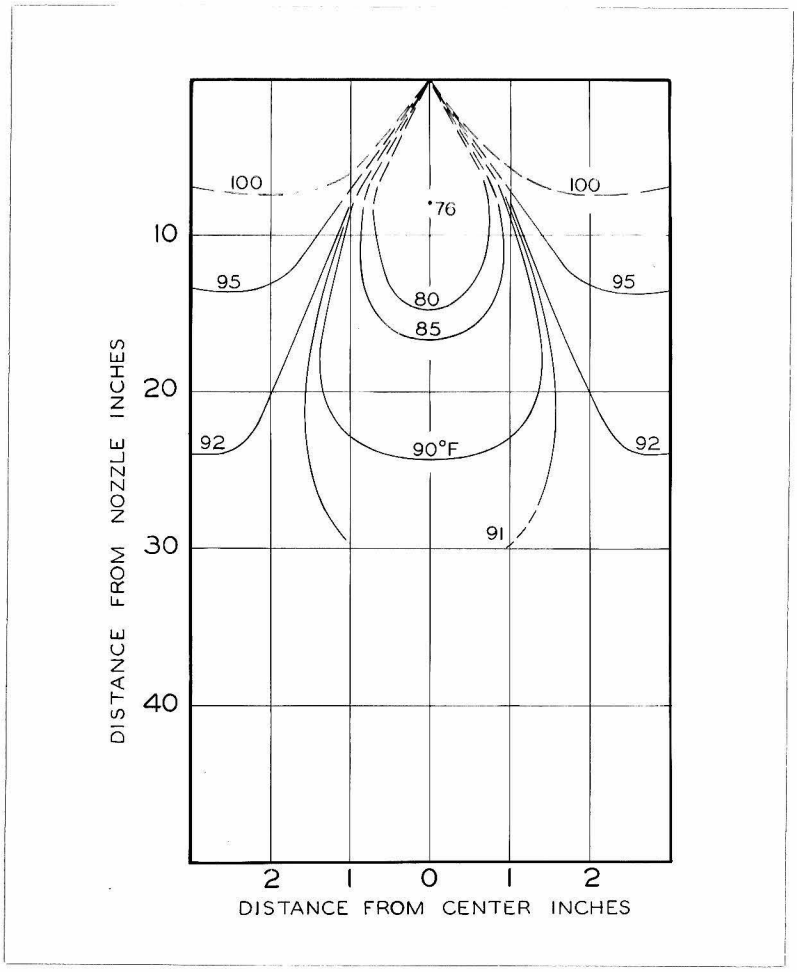

Figure 6. Temperature Contours

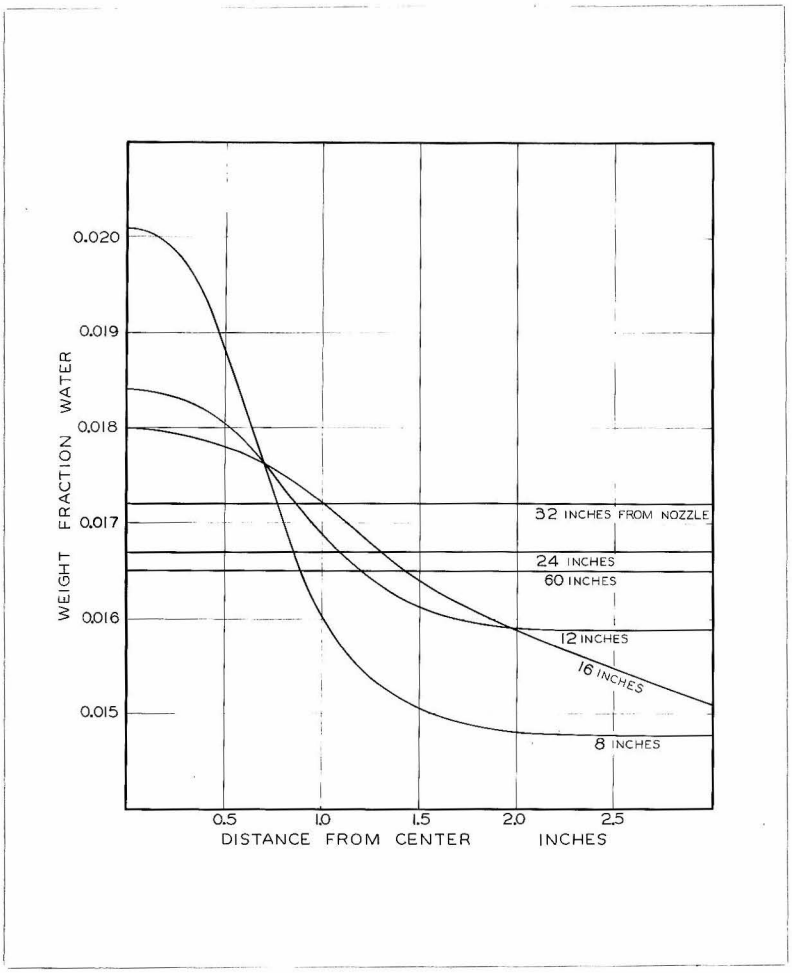

Figure 7. Smoothed Compositions

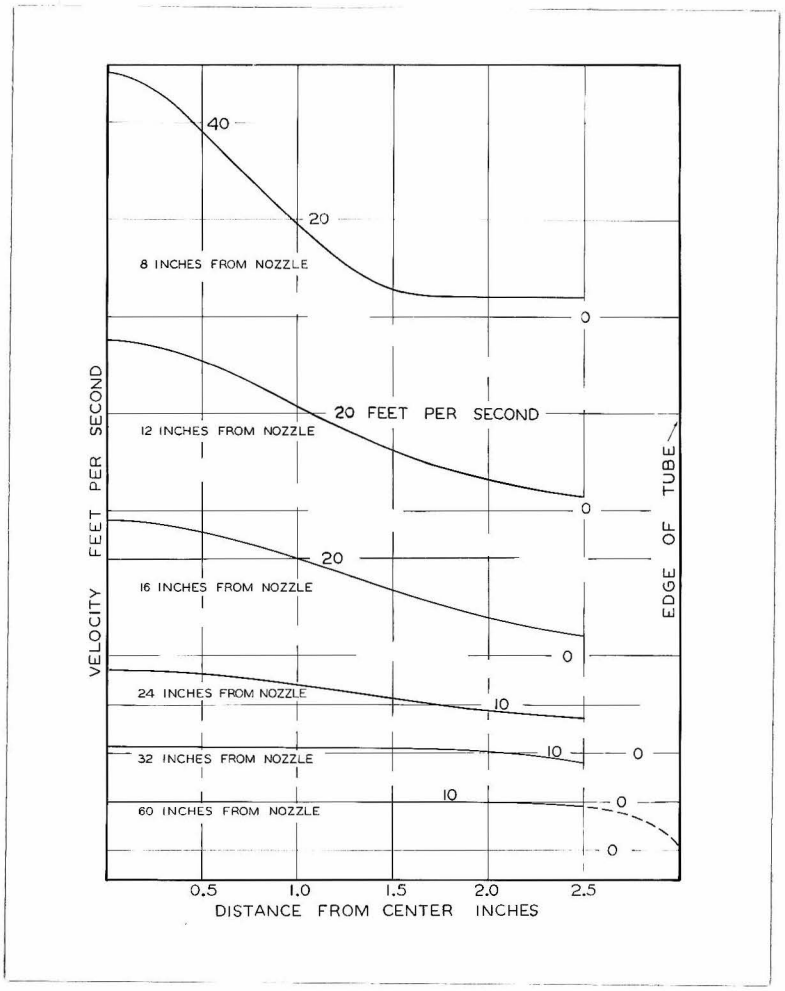

Figure 8. Smoothed Velocities

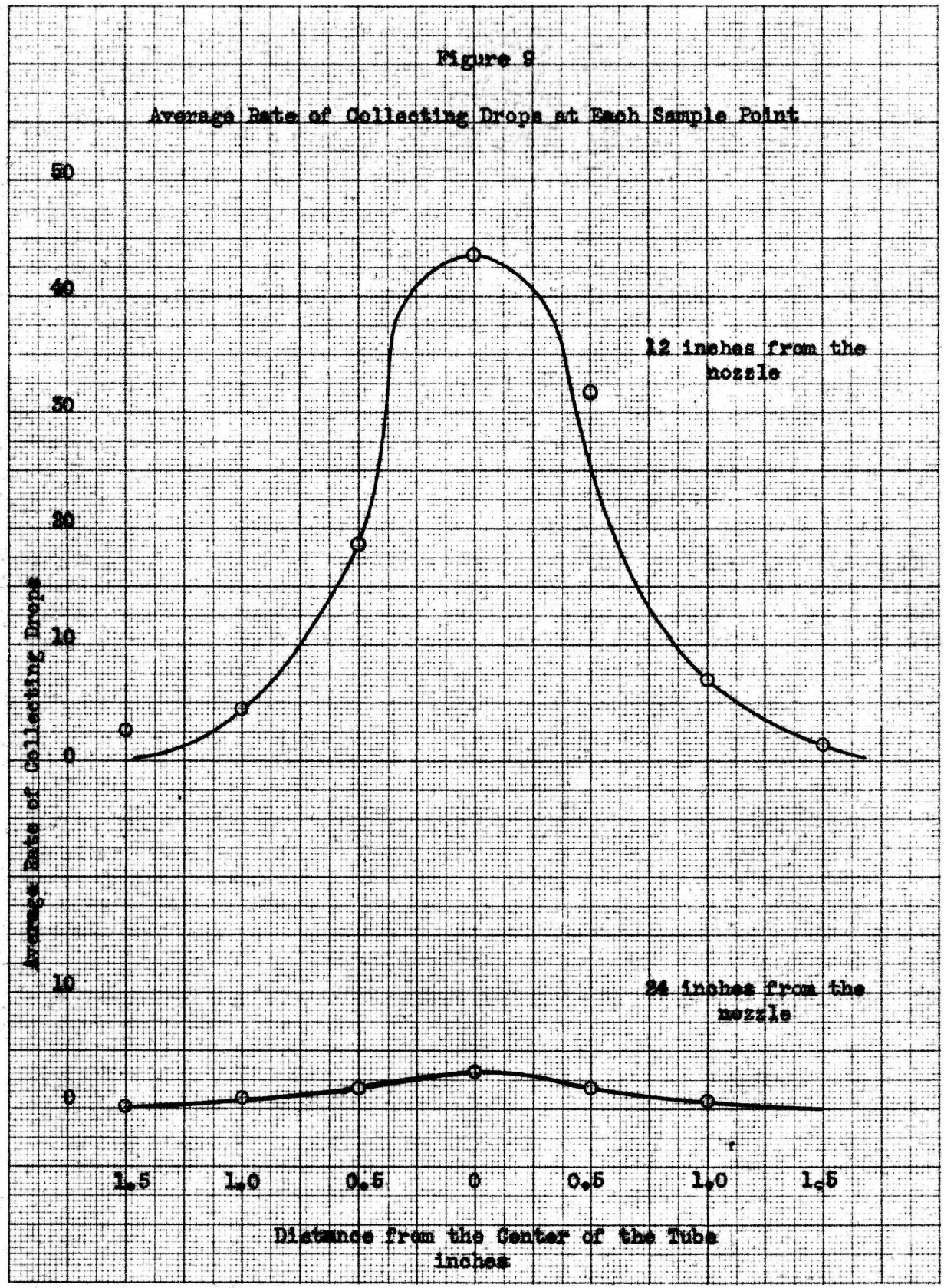

CLEARPRINT PAPER CO. 739 MILLIMETERS BOTH WAYS 180 X 250 DIVISIONS
PRINTED IN U.S.A. ON CLEARPRINT TECHNICAL PAPER NO. 1000H

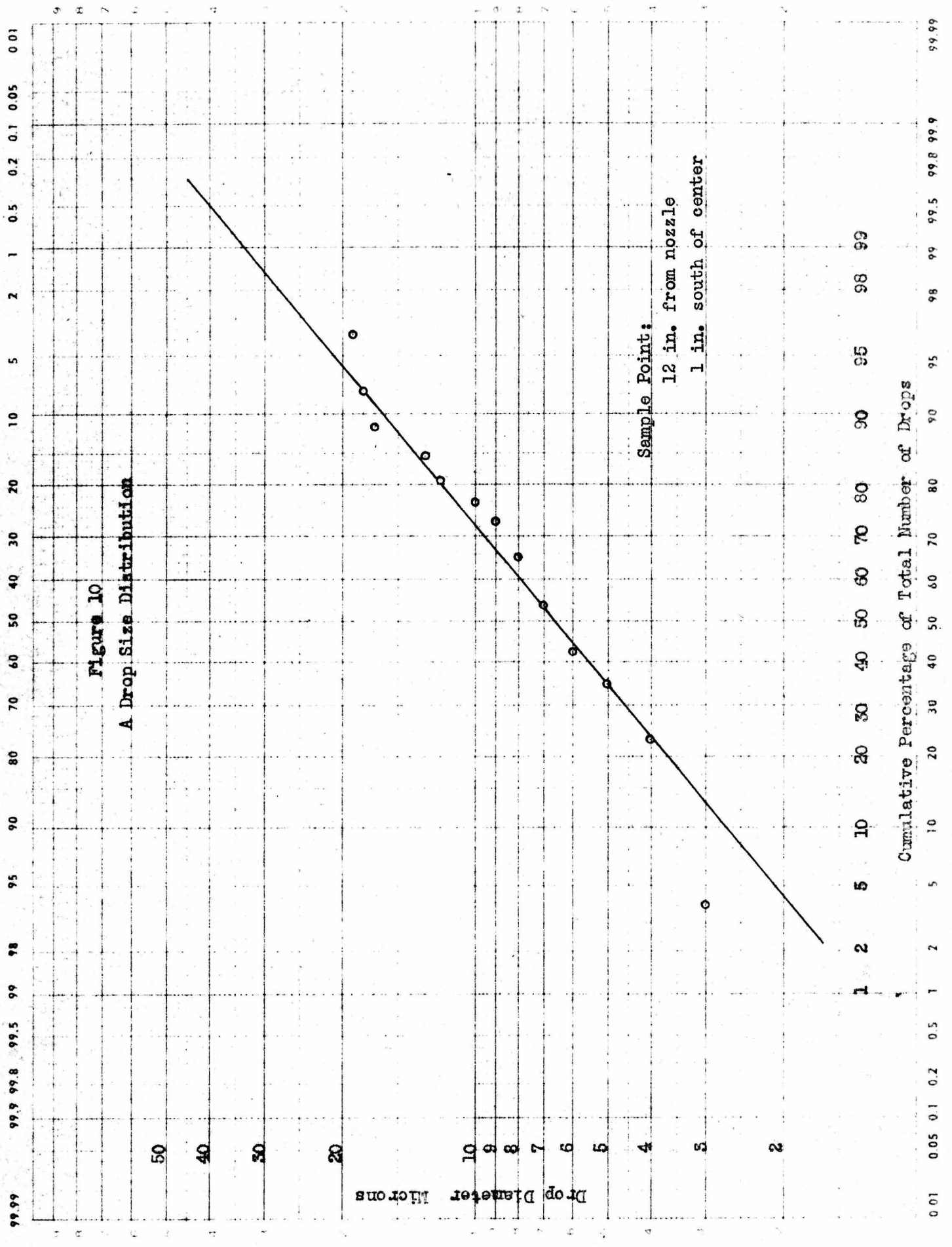

Figure 10
A Drop Size Distribution

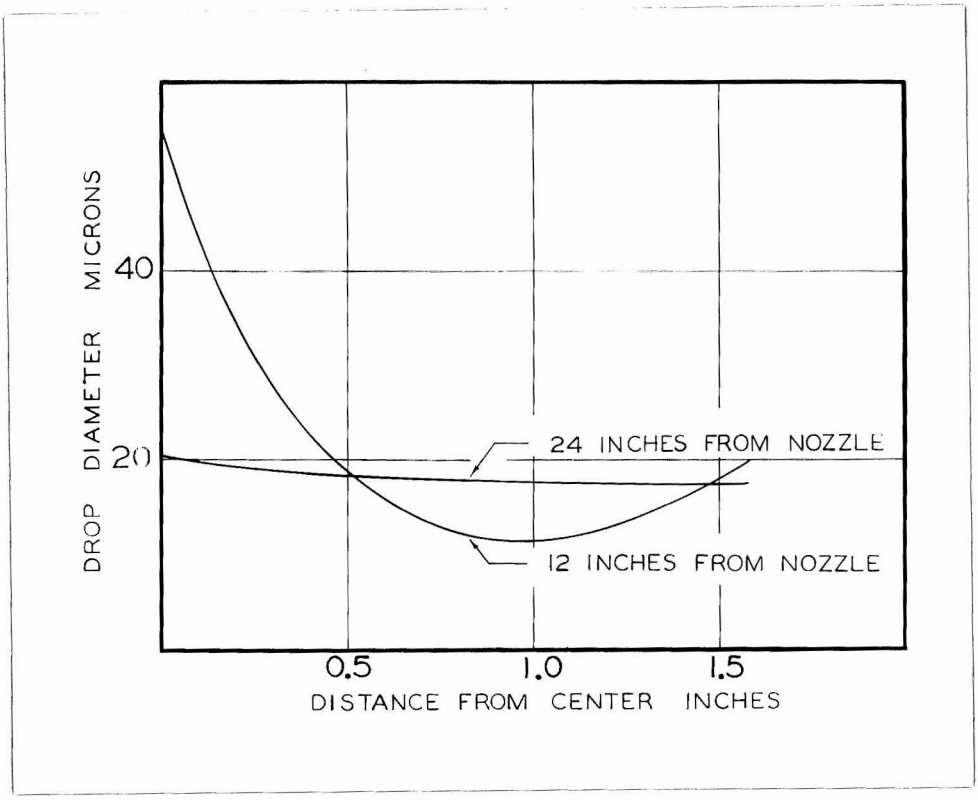

Figure 11. D_v as a Function of Radial Distance

List of Tables

I	Comparison of Thermocouple Readings.
II	Apparent Temperatures.
III	Weight Fractions of Water.
IV	Velocity Measurements.
V	Drop Size Distributions for Each Sample.
VI	Rate of Collecting Drops at Each Sample Point.
VII	Specific Surface and Average Volume and Average Surface Diameters of Drops.
VIII	Integrated Rates of Flow and Average Flow Characteristics.
IX	Apparent Eddy Diffusivities and Eddy Conductivities.

Table I. Comparison of Thermocouple Readings

Distance from Nozzle in.	Distance from Center of Tube in.	Reading of 0.001-inch Thermocouple °F	Reading of 30-Gauge Thermocouple °F
1	2	101.2	100.4
6	0	76.4	77.4
8	0	76.9	77.5
12	0	81.9	77.6
16	0	86.6	77.6
20	0	89.2	78.0
26	0	90.4	87.1
32	0	91.0	89.6
44	0	91.0	90.7
60	0	91.0	90.7

Table II. Apparent Temperatures[a]

Distance[b] from Center of Tube in.	Distance from Nozzle, in.					
	8	12	16	24	32	60
2.94						
2.5	99.3	95.9	93.1	92.4		
2.0	99.1	96.2	92.8	91.9	91.0	90.4
1.5	99.0	92.8	91.3	90.9		
1.0	89.2	86.4	86.6	90.4		
0.5	76.2	78.3	85.4	89.8		
0	76.1	77.6	83.7	90.2	91.0	90.4
0.5	76.1	79.9	84.8	89.8		
1.0	94.0	88.0	82.8	90.6		
1.5	99.3	94.2	91.4	90.8	91.0	
2.0		96.8	92.4	91.2		
2.5		96.8	93.1	91.4		

[a] Apparent temperatures expressed in °F.

[b] Distances are listed from north to south.

Table III. Weight Fractions of Water

Distance[a] from Center of Tube in.	Distance from Nozzle, in.					
	8	12	16	24	32	60
2.94	0.0152	0.0162	0.0160	0.0167		
2.5	0.0148	0.0160	0.0156	0.0165	0.0169	0.0165
2.0	0.0148	0.0152	0.0167	0.0166		
1.5	0.0147	0.0152	0.0148	0.0168		
1.0	0.0168	0.0168	0.0165	0.0180		
0.5	0.0187	0.0188	0.0176	0.0166	0.0173	0.0165
0	0.0201	0.0184	0.0180	0.0164		
0.5	0.0188	0.0172	0.0180	0.0155		
1.0	0.0153	0.0159	0.0180	0.0169	0.0176	
1.5		0.0168	0.0174	0.0170		
2.0		0.0159	0.0158	0.0174		
2.5						

[a] Distances are listed from north to south.

Table IV. Velocity Measurements[a]

Distance[b] from Center of Tube in.	Distance from Nozzle, in.					
	8	12	16	24	32[c]	60[c]
2.94						
2.5	4.9	3.1	5.1	7.6	8.2	9.3
2.0	5.4	6.6	9.3	9.3	10.5	9.5
1.5	7.6	13.7	15.0	12.2	10.9	9.7
1.0	21.4	22.9	21.1	14.3	11.2	9.8
0.5	40.3	31.9	26.3	16.8	11.5	10.0
0	50.3	35.2	28.0	17.0	11.6	10.1
0.5	35.7	30.0	25.1	15.9	11.5	9.9
1.0	17.3	20.2	18.9	13.3	11.2	9.7
1.5		11.2	12.6	10.5	10.9	9.4
2.0		6.2	7.3	8.2	10.5	9.1
2.5					8.2	8.3

[a] Velocity of flow expressed in ft./sec.

[b] Distances are listed from north to south.

[c] Smoothed data.

Table V. Drop Size* Distributions for Each Sample

1.5 in. north of center 12 in. from nozzle		1.0 in. north of center 12 in. from nozzle	
Size Microns	Number	Size Microns	Number
4	4	2	1
5	2	4	2
6	1	5	2
7	1	6	3
8	1	7	3
12	1	8	7
13	1	10	1
15	2	13	1
17	1	15	1
20	1	18	1
22	1	35	1
	Total 16		Total 23
Sampling time 6.08 sec.		Sampling time 5.19 sec.	

* In Table V size should be interpreted as diameter.

Table V. (Cont'd.) Drop Size Distributions for Each Sample

0.5 in. north of center

12 in. from nozzle

Size Microns	Number
1	3
2	5
3	5
4	5
5	10
6	6
7	3
8	2
9	1
10	3
15	1
17	1
18	1
Total	46

Sampling time 1.88 sec.

0.5 in. north of center

12 in. from nozzle

(1st count)

Size Microns	Number
3	1
4	3
5	2
6	3
7	2
8	6
9	1
10	1
12	1
15	4
16	2
18	6
20	3
21	1
22	1
25	1
40	1
60	2
Total	41

(2nd and 3rd counts next page)

Table V. (Cont'd.) Drop Size Distributions for Each Sample

0.5 in. north of center
12 in. from nozzle
(2nd count)

Size Microns	Number
6	2
7	2
8	4
10	6
12	1
13	1
15	1
17	3
18	7
20	4
22	1
50	1
60	2
	Total 35

0.5 in. north of center
12 in. from nozzle
(3rd count)

Size Microns	Number
4	2
5	2
6	4
7	3
8	3
9	2
13	1
15	1
16	2
17	2
18	4
19	3
50	1
60	2
	Total 32

Sampling time 2.77 sec.

Table V. (Cont'd.) Drop Size Distributions for Each Sample

On center line

12 in. from nozzle

(1st count)

Size Microns	Number
2	2
6	3
7	4
8	2
10	1
12	1
15	3
18	3
Total	19

(2nd count)

2	4
4	1
5	4
6	1
7	1
10	1
12	1
15	4
18	2
22	2
Total	21

Sampling time 0.6 sec.

On center line

12 in. from nozzle

Size Microns	Number
2	1
7	2
8	1
10	1
15	1
Total	6

Sampling time 0.52 sec.

Table V. (Cont'd.) Drop Size Distributions for Each Sample

On center line 12 in. from nozzle		On center line 12 in. from nozzle	
Size Microns	Number	Size Microns	Number
0.5	1	25	2
1	8	30	12
2	33	35	2
3	11	40	24
4	32	45	2
5	33	50	4
6	7	55	1
7	11	60	13
8	29	70	4
10	42	100	2
12	4	115	1
14	1	130	1
15	5	140	2
17	2	Total	335
18	25	Sampling time 3.9 sec.	
20	21		

Table V. (Cont'd.) Drop Size Distributions for Each Sample

0.5 in. south of center

12 in. from nozzle

Size Microns	Number
1	1
2	8
3	4
4	13
5	8
6	9
7	9
8	6
10	7
11	1
13	2
14	1
15	6
17	2
18	3
20	6
22	1
25	2
30	1
40	2
	Total 92

Sampling time 2.90 sec.

1.0 in. south of center

12 in. from nozzle

Size Microns	Number
3	1
4	5
5	3
6	2
7	3
8	3
9	2
10	1
12	1
13	1
17	1
18	1
19	1
20	1
	Total 26

Sampling time 3.5 sec.

Table V. (Cont'd.) Drop Size Distributions for Each Sample

1.0 in. south of center

12 in. from nozzle

Size Microns	Number
1	4
2	4
3	3
4	2
5	3
6	1
7	3
8	2
9	1
12	1
16	1
20	1
Total	26

Sampling time 3.47 sec.

1.5 in. south of center

12 in. from nozzle

Size Microns	Number
3	2
4	1
9	1
11	1
Total	5

Sampling time 3.87 sec.

Table V. (Cont'd.) Drop Size Distributions for Each Sample

1.5 in. north of center

24 in. from nozzle

Size Microns	Number
5	1
10	1
20	1
Total	3

Sampling time 34.81 sec.

1.0 in. north of center

24 in. from nozzle

Size Microns	Number
2	4
3	5
4	4
5	6
6	1
7	1
8	1
12	1
13	1
17	1
18	1
Total	26

Sampling time 24.0 sec.

Table V. (Cont'd.) Drop Size Distributions for Each Sample

1.0 in. north of center

24 in. from nozzle

Size Microns	Number
3	1
7	1
10	1
12	1
17	1
21	1
23	1
35	1
	Total 8

Sampling time 12.1 sec.

0.5 in. north of center

24 in. from nozzle

Size Microns	Number
2	1
6	2
7	1
8	1
10	1
13	2
14	1
15	1
16	1
17	1
18	2
19	2
20	1
	Total 17

Sampling time 9.8 sec.

Table V. (Cont'd.) Drop Size Distributions for Each Sample

On center line

24 in. from nozzle

Size Microns	Number
2	1
4	2
5	2
6	5
7	3
8	3
9	4
10	4
11	1
15	1
16	3
17	3
18	2
20	6
21	1
23	1
24	1
25	1
26	1
27	1
30	1
35	1

On center line

24 in. from nozzle

Size Microns	Number
40	3
50	1
60	2
75	1
85	1
Total	56

All drops could not be counted, time of no significance

1	1
3	1
4	2
6	1
7	1
8	1
9	1
10	1
15	2
17	2
18	2
20	2
30	1
Total	18

Sampling time 6.18 sec.

Table V. (Cont'd.) Drop Size Distributions for Each Sample

On center line
24 in. from nozzle

Size Microns	Number
1	3
2	11
3	5
4	10
5	5
6	4
7	4
8	2
9	3
10	2
11	2
13	1
14	1
15	1
16	1
17	1
18	1
19	2
22	1
Total	60

Sampling time 12.22 sec.

On center line
24 in. from nozzle

Size Microns	Number
2	1
3	4
4	3
5	4
6	3
7	6
8	9
9	4
10	5
11	2
12	1
13	2
14	2
15	5
16	1
17	4
18	2
19	2
20	3
21	1
22	1
30	1
50	1
Total	67

Sampling time 19.4 sec.

Table V. (Cont'd.) Drop Size Distributions for Each Sample

0.5 in. south of center

24 in. from nozzle

Size Microns	Number
1	1
2	2
3	6
4	1
5	1
6	2
8	2
9	2
10	2
11	1
22	2
Total	22

Sampling time 12.72 sec.

1.0 in. south of center

24 in. from nozzle

Size Microns	Number
4	1
7	2
9	1
13	1
25	1
27	1
Total	7

Sampling time 14.97 sec.

Table V. (Cont'd.) Drop Size Distributions for Each Sample

1.0 in. south of center

24 in. from nozzle

Size Microns	Number
5	1
6	2
7	1
8	2
9	3
10	1
12	2
14	1
15	1
18	1
19	2
23	1
25	1
	Total 19

Sampling time 30.0 sec.

Table VI. Average Rate of Collecting Drops at Each Sample Point

Distance from Nozzle in.	Distance[a] from Center in.	Average Rate of Collecting Drops drops/sec.
12	1.5	2.63
12	1.0	4.43
12	0.5	18.74
12	0.0	43.59
12	0.5	31.72
12	1.0	6.99
12	1.5	1.29
24	1.5	0.09
24	1.0	0.87
24	0.5	1.74
24	0.0	3.16
24	0.5	1.81
24	1.0	0.55

[a] Distances are listed from north to south.

Table VII. Specific Surface and Average Volume and Surface Diameters of Drops

Distance from Nozzle in.	Distance[a] from Center in.	Specific[b] Surface ft.^{2}/lb.	Average Volume Diameter microns	Average Surface Diameter microns
12	1.5	113.5	20.86	14.49
12	1.0	334.7	11.09	9.65
12	0.5	145.0	21.28	16.87
12	0.0	236.5	55.12	28.41
12	0.5	172.6	15.64	11.60
12	1.0	234.5	11.69	8.74
12	1.5	125.5	14.85	9.15
24	1.5	140.6	18.52	13.49
24	1.0	112.6	20.10	13.66
24	0.5	124.6	24.31	19.10
24	0.0	136.1	20.78	15.78
24	0.5	215.4	12.15	8.87
24	1.0	207.3	16.57	13.86

[a] Distances are listed from north to south.

[b] Average surface for a distance of 12 in. 194.6 ft.^{2}/lb.

24 in. 156.1 ft.^{2}/lb.

Table VIII. Integrated Rates of Flow and Average Flow Characteristics

Property	Distance from Nozzle, in.					
	8	12	16	24	32	55
Average Temperature, °F	90.6	90.4	90.7	89.5	90.5	[illegible]
Average Enthalpy B.T.U./lb.	-2.30	-2.33	-2.24	-2.54	-2.31	-2.4[illegible]
Total Weight Rate of Gas Phase Flow lb./sec.	0.1189	0.1187	0.1282	0.1243	0.1211	0.1190
Total Weight Rate of Water Flow lb./sec.	0.00198	0.00202	0.00211	0.00203	0.00200	0.00202
Total Weight Rate of Liquid Water Flow, lb./sec.		102.5×10^{-9}		10.2×10^{-9}		

Table IX. Apparent Eddy Diffusivities and Eddy Conductivities

Distance from Nozzle in.	Distance from Center in.	ϵ_c ft.^{2}/sec.	ϵ_d ft.^{2}/sec.	$\frac{\epsilon_d}{\epsilon_c}$
8	0.5	0.77	0.25	0.32
8	1.0		0.05	
8	1.5		0.70	
8	2.0		4.39	
12	0.5	0.20	0.52	2.66
12	1.0	0.07	0.15	2.22
12	1.5	0.07	0.32	4.54
12	2.0	0.08	3.99	50.49[a]
16	0.5	0.20	0.79	3.91
16	1.0	0.22	0.22	1.01
16	1.5	0.10	0.11	1.14
16	2.0	0.41	0.12	0.29
16	2.5	1.73	0.11	0.06

Average $\frac{\epsilon_d}{\epsilon_c} = 2.01$

[a] Omitted from average.

Propositions Submitted by Stuart Donald Cavers

Ph. D. Oral Examination, July 19, 1950, 1:00 P.M., Crellin Conference Room.
Committee: Professor Sage (Chairman), Professors Badger, Bates, Lacey, Liepmann, Swift.

Chemical Engineering

1. The equation:

$$\frac{hD}{k} = 0.023\,(Re)^{0.8}\,(Pr)^{0.4}$$

which was derived for nonuniform flow conditions (1) may be applied without undue error to the uniform case where heat is transferred between parallel plates across a turbulent gas stream.

2. The equation:

$$\frac{\epsilon_c}{\epsilon_m} = \frac{\phi(y^+)}{Pr}$$

where ϕ is a universal function of y^+, affords a ready means of predicting the extent to which Reynolds' analogy will obtain at a given y^+ value and for a fluid with a given Prandtl number.

3. The universal velocity distribution law (2) applies to flow between parallel plates as well as to flow in circular pipes.

4. Plots of $\log \left[\frac{\epsilon_m}{(\nu)_{y/y_o=0.5}}\right]\left[\frac{1}{1-2y_a/y_o}\right]$ versus $\log y^+$ are straight lines of different slopes in the laminar sublayer, in the buffer zone, and in the turbulent core. Extrapolation of these lines to their points of intersection shows the laminar sublayer and the buffer zone to have effective outer y^+ limits of 6 and 45 respectively.

5. When a hot wire anemometer is used to measure velocities in the laminar layer near a wall, erroneously large values of the measured velocity result because of conduction of heat to the wall. Attempts to correct for this inaccuracy under non-flow conditions have been unsatisfactory (3). It is suggested that hot wire measurements be made near a wall with the bulk flow in the laminar region where the velocity profiles can be calculated. It might be possible to correlate the corrections by means of the dimensionless distance parameter y^+.

6. A need exists for experimental study of rates of heat transfer by natural convection in enclosed spaces between parallel plates when there is no gross flow.

Chemistry

1. The pH range of 3 to 4.5 has been cited as a range to avoid in nickel plating (4) because within this range pitting is said to be more likely to be encountered. However if it is convenient to plate in this range satisfactory results may be obtained by keeping the bath free of sludge and by adding H_2O_2.

2. The contamination of electrolytic hydrogen cells with carbonate (5) could be further decreased by installing a small loosely packed plug of anion exchange resin in the distilled water feed line to each cell.

3. It has been found that the size distributions of various ground solids do not give linear relationships when plotted on arithmetic probability paper, but do on logarithmic probability paper (6). The size distribution of drops from a nozzle gives a linear relationship when plotted on logarithmic probability paper as the results reported in this thesis indicate. It is suggested that the quantitative treatment of foams and emulsions in colloid chemistry might be assisted by the use of such plots.

Mechanical Engineering

1. In the design of air conditioning equipment in which water is sprayed into a turbulent air stream, it may be assumed that the interfacial area per pound of liquid is approximately constant with distance from the nozzle.

2. It is proposed that the line carrying the lubricating oil to the vital parts of the automobile engine be connected in series with a small venturi meter, which would indicate that the engine was actually being lubricated, and that a large percentage of the oil was not simply returning to the crankcase through the pump bypass.

3. The present methods employed by manufacturers for describing spray nozzles are unsatisfactory. It is proposed that the specifications for such equipment include the size distribution of the drops produced under various operating conditions.

Nomenclature

D	diameter or equivalent diameter, ft.
h	heat transfer coefficient, B.T.U./sec. ft.^{2} $^\circ$F.
K	thermometric conductivity, ft.^{2}/sec.
k	thermal conductivity, B.T.U. ft./sec. ft.^{2} $^\circ$F.
P	pressure, lb./ft.^{2}
Pr	Prandtl number, dimensionless.
Re	Reynolds number, dimensionless.
x	longitudinal distance downstream from a reference point in a channel, ft.
y	distance above lower plate, ft.
y_d	distance from nearer wall, ft.
y_o	height of channel, ft.
y^+	dimensionless distance parameter, defined as follows: $\left[\frac{u^* y_o}{(\nu)_{y/y_o=0.5}}\right]\left[\frac{y_d}{y_o}\right]$
u^*	friction velocity, ft./sec., defined as follows: $\sqrt{\left(\frac{y_o}{2(\rho)_{\frac{y}{y_o}=0.5}}\right)\left(-\frac{dP}{dx}\right)}$
ϵ_m	eddy viscosity, ft.^{2}/sec.
$\underline{\epsilon}_m$	total viscosity or $\epsilon_m+\nu$, ft.^{2}/sec.
ϵ_c	eddy conductivity, ft.^{2}/sec.
$\underline{\epsilon}_c$	total conductivity or $\epsilon_c + K$, ft.^{2}/sec.
ν	kinematic viscosity, ft.^{2}/sec.
ρ	density, lb. sec.^{2}/ft.^{4}
$\phi(\ )$	a universal function of

References

(1) McAdams, W. H., Heat Transmission, 168, McGraw-Hill (1942).

(2) von Kármán, Th., Trans. A.S.M.E., 61, 705-710 (1939).

(3) Dryden, H. L., N.A.C.A. Technical Report No. 562 (1936).

(4) Pinner, W. L., Soderberg, G., Baker, E. M., Modern Electroplating, 235-274, The Electrochemical Society (1942).

(5) Sutherland, B. P., Trans. Electrochem. Soc., 85, 183-191 (1944).

(6) Austin, J. B., Ind. Eng. Chem., Analytical Edition 11, 335-339 (1939).